Marine coastal dynamics and primary production response in Golfo Dulce, Costa Rica

——A multi-sensor satellite approach

Zhang Lei
March 2002

Marine coastal dynamics and primary production response in Golfo Dulce, Costa Rica

——— A multi-sensor satellite approach

Zhang Lei

M.Sc. thesis submitted to the International Institute for Geoinformation Science and Earth Observation in partial fulfilment of the requirements for the degree of Master of Science in Application of Geoinformation to Coastal Zone Studies

Degree Assessment Board:

Chairman: Dr. N. Rengers (AGS)
Name Supervisor: Dr. Tjeerd Willem Hobma (AGS)
Dr. Chris Mannaerts (WRES)
External Supervisor: Dr. Steef Peters (IVM-VU)
Name other member: Drs. M.Damem (AGS)

INTERNATIONAL INSTITUTE FOR GEOINFORMATION SCIENCE AND EARTH OBSERVATION, ENSCHEDE, THE NETHERLANDS

DISCLAIMER

This document describes work undertaken as part of a programme of study at the International Institute for Geoinformation Science and Earth Observation. All views and opinions expressed therein remain the sole responsibility of the author, and do not necessarily represent those of the institute.

ABSTRACT

The tropical ocean labelled as “global heat engine” plays a major role in global physical processes; heat flux moderates seawater temperature and changes water momentum, thereby influencing global climate. Phytoplankton is often referred to as the “biological pump”, it constitutes the main marine primary production, fixes CO_2 from the air and mitigates the “greenhouse” effect. But so far, how much phytoplankton is produced annually and what kind of factors affect their growth remains unknown. The objectives of this case study are focused on the spatio-temporal marine physical processes and primary productivity, and physical process impacts on phytoplankton primary production.

AVHRR, SeaWIFS, TM, SeaWind and AMI data have been processed for the parameter extraction of sea surface temperature, phytoplankton pigment concentration, suspended sediment concentration, wind speed and direction. The 2 thermal bands of AVHRR at nighttime are applied for processing. A non-linear algorithm is used in the calculation, which has advantage of some atmosphere remove and satellite zenith angle correction, the other techniques are applied for quality improvement, such as temporal data match and cloud detection technique. An OC4 algorithm (Case 2 Water) is available approach for chlorophyll-a extraction, it concerns the suspended sediment impacts and chlorophyll spectrum shift when the concentration increases, and but the errors are larger than the errors of sea surface temperature and suspended sediment calculation. A simple linear formula is applied for the estimation of annual phytoplankton primary production. The parameter of Climate Integrate Factor is defined for estimation of potential primary production, it is composed of the variables of solar hours and rainfall. A Natural Logarithm algorithm is suitable for suspended sediment calculation in this study, TM band 3 is sensitive to the change of suspended sediment, and the band 3/5 removed the unexpected atmosphere impact.

There are four series of products: sea surface temperature, phytoplankton pigment, phytoplankton primary production and suspend sediment, and other annex data of wind map and SAR were processed for analysis. Annual sea surface temperature between 1991 and 2001 are analysed on spatio-temporal change, anomalous “hot pool” and “cold tongue” distribution and formation reason. The monthly sea surface temperature in 1998 focused on comparison of sea surface temperature with daily solar hours and rainfall. These results are compared to El-Niño sea surface temperature in 1998 for impact analysis. The monthly phytoplankton pigment concentration and primary production in 1998 are calculated, then potential yearly primary production was estimated based on the Climate Intergrate Factor in the passed decade. The analysis of primary production was concentrated on spatial distribution and its formation. The four maps of suspended sediment concentration were produced between 1998 and 2001, so as to analysis on spatio-temporal change. The tide and wave currents were analysed based on suspended sediment plumes and the wave textures on SAR image. The modelling of complex sea current was established for gulf physical analysis. The affections of sea surface temperature in 1998 and suspended sediment in 1998 on phytoplankton pigment in 1998 were analysed in the open sea.

The research in Golfo Dulce demonstrates that: (1) sea surface temperature in the gulf is controlled by the factors of extra-terrestrial solar radiance, but is highly affected by climate change and horizontal heat flux. A so-called “hot spot” and “cold tongue” of anomalous sea surface temperature have been detected in the gulf. The El-Niño event directly affects gulf sea surface temperature. SST has impact on phytoplankton growth speed, 30.01ºC is the critical temperature; (2) There are three types of complex sea currents appear in the gulf: flooding tide dominant, counter-clockwise and clockwise. The sea current model shows that the flooding current is stronger than the ebbing current. Counter-clockwise type is dominant in the gulf. It dilutes and shifts the phytoplankton population and distribution. The distribution and concentrations of suspended sediment are mainly dependent on the tidal cycle and river sand supply; (3) suspended sediment concentration has a light attenuation effect on the phytoplankton growth. High suspended sediment concentration with an impact of -0.25 mg/m^3_*ssc mg/l affects the pigment concentration larger than low suspended sediment concentration with impact of -0.02 mg/m^3_* ssc mg/l; (4) The observed phytoplankton pigment concentration “dome” shows that phytoplankton primary production is determined by the river nutrients during the rainy season, rather than by upwelling of the deep-water nutrient supply. The gulf primary production is estimated 1.4×10^5 ton in1998, potential primary production is 1.8×10^5 ton.

Remote sensing technique is available approach for researches on SST, SSC, PPC, PPP and wave current, especially on daily monitoring of SST, PPC, wave current at mesoscale. The gulf physical processes and biological processes are more complicate than in open sea, accurate calculation and correction are necessary for the parameter extraction.

Key words: gulf closeness; phytoplankton primary production; phytoplankton pigment concentration; suspended sediment concentration; sea surface temperature; climate integrate factor

ACKNOWLEDGEMENT

I would like to express my sincere gratitude to the Netherlands government for granting me the NFP scholarship to enable me to pursue my Master degree from ITC. Thanks to all staff members that contributed to my success in my course.

My heartiest gratitude to Professor Dr. Van Genderen, who gave me the opportunity for studying in the AGS division, and more thanks to him for his guidance, not only for scientific aspects but also project management skill during my study. My sincere thanks also go to Professor Dr. Wu Bingfang in IRSA for taking care of my individual skill development and supporting me to pursue the MSc study abroad.

I am highly indebted to my supervisors Dr. Tjeerd Willem Hobma, Dr. Chris Mannaerts for their guidance during my research and improvement of the structure and text of the thesis. Their contributions are of great input to the completion of my research. Without their contribution and guidance, this thesis would be of less quality.

My thanks to go also out to Prof. Jose A. Vargas At the Centre for Marine Research (CIMAR), of the University of Costa Rica, for providing the materials for sampling Golfo Dulce waters and analysing the data in the laboratory.

Kind thanks are also due to the ITC staff members, Dr. B.H.P. Maathuis, Dr.A. Gieske, Dr.G.N.Parody, Drs.J.P.G.Bakx, Mr. G.Rerinink, who gave me much useful advice on the parameter calculation theory and data processing methodology.

Many thanks also go to the people in DAAC SeaWIFS, JPL, USGS EROS data centre, NOAA Satellite Active Archive, SeaDas company, ERS company for giving me free data for this thesis work. Thanks to the professional experts in the Ocean Colour Data Support Team and SeaDas for their kind answering of my inquiries about parameter calculation and software installation.

To my family and relatives, I thank you for your steadfast understanding and patience. My whole-hearted special thanks go to my wife, for all her support and prayers for me during my studies. Her office is far away from home, and she takes care of my little son carefully everyday. I know life is hard for her, and I have left my son LeLe in his golden age. I know you missed your dad so long, but thank you for being patient and a loving son. My success is your success.

TABLE OF CONTENTS

LIST OF FIGURES

LIST OF TABLES

LIST OF ABBREVIATIONS

APPP	Annual phytoplankton primary production
CIF	Climate integrate factor
DPPP	Daily phytoplankton primary production
ENSO	El-Niño Southern Oscillation
GC	Gulf closeness
GCP	Ground control points
PPC	Phytoplankton pigment concentration
PPP	Phytoplankton primary production
RMS	Root mean square error
SSC	Suspended sediment concentration
SST	Sea surface temperature

Chapter 1: Introduction

1.1. Coastal environment and issues

Over the years, intense development pressure has resulted in rapid growth and accelerated economic development in coastal areas. Hurricanes, severe storms and flooding pose the greatest risks because these coastal hazards hold the greatest potential for destroying property and taking lives. Coastal land is particularly vulnerable to natural phenomena, such as flooding, erosion and subsidence. Shoreline erosion and subsidence destroy thousands of dollars in property each year. The phenomena of algae bloom and coral reef bleach due to over-discharge of nutrient and anomalous high sea surface temperature destroy the marine ecosystem and biodiversity. Marine environment protection, resource reasonable use and disaster mitigation have caused increasing concerns.

Earth's oceans form a complex web of physical processes, which change the marine and climate environment. The ocean is labelled as "global heat engine" possesses a vast capacity to absorb and store sunlight as heat, the top five meters of the ocean can store as much heat as the entire atmosphere, and contain fifty times more carbon than in the atmosphere. The tropical ocean plays a major role in global-scale physical (oceanographic and meteorological) and biological processes (Eileen Hofmann, 1999), they transport heat from the equator towards the poles, moderating the otherwise great extremes of temperature which would exist on our planet. The climate influences the ocean current direction with trade wind, cause ocean complex variability of the heat and momentum. The typical event is El-Niño Southern Oscillation, which is the result of a cyclic warming and cooling of the surface ocean of the central and eastern Pacific. This region of the ocean is normally colder than it's equatorial location would suggest, mainly due to the influence of north-easterly trade winds, a cold ocean current flowing up the coast of Chile, and to the up-welling of cold deep water off the coast of Peru. El-Niño results in heavy rainfall in South America, but severe droughts in eastern Australia. The more intense the El-Niño, the more intense and extensive the Australian droughts; contrast to El-Niño, La-Niña results in droughts in south America and heavy rainfall, even floods, in eastern Australia.

The ocean is also a large ecosystem with abundant marine life. Phytoplankton, which serve as the foundation of the marine food chain, account for approximately 50% of the photosynthesis on this planet, over 90% of all the carbon dioxide that has been incorporated into living things over geologic time is buried in marine sediments, indicating that phytoplankton play a very important role in regulating the amount of carbon in the atmosphere. The absolute magnitude of carbon fixation attributed to marine photosynthetic organisms accounts for approximately 40% of the global total, estimates of global oceanic primary production have been revised to about 50 Gt C/y (Martin 1992), oceanic photosynthetic organisms turn over far more rapidly than their terrestrial counterparts, and marine photosynthetic organisms, composed almost entirely of single-celled phytoplankton, account for less than 1% of the total global plant biomass. Thus, oceanic photosynthetic organisms are extremely efficient

in fixing carbon compared to terrestrial plants and they mediate a large flux of organic carbon into the ocean interior. This carbon flux sustains a steady-state air-sea gradient in inorganic carbon and is often referred to as the 'biological pump' (Volk and Hoffert, 1985). Phytoplankton biomass forms main marine primary production, which is influenced by solar irradiance, SST, CO_2 and O_2 in the water and atmosphere, up-welling nutrients supply and sea current (Figure 1.1).

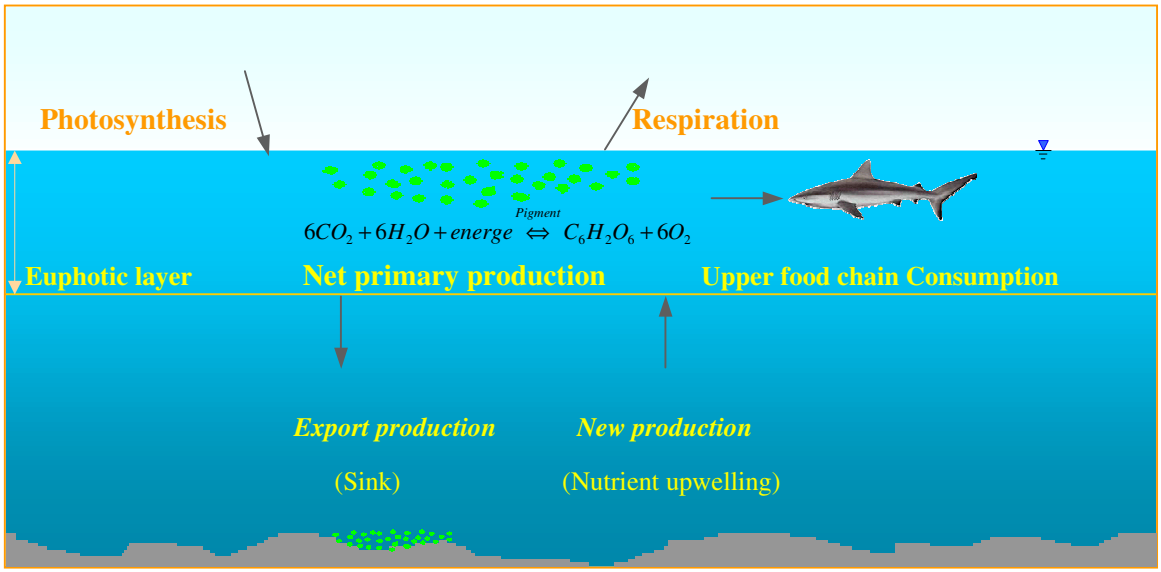

Figure 1.1 Ocean primary production formation and depletion

Because of its use of carbon dioxide, phytoplankton may play an important role in the Earth's climate. Carbon dioxide is continually emitted into the atmosphere from volcanic, biological, and anthropogenic (man-made) sources. This gas traps energy from the sun, warming the Earth's surface; a phenomena commonly known as the greenhouse effect. The collective mass of all the world's phytoplankton extracts a large quantity of the Earth's carbon dioxide, although the exact amount is unclear. Phytoplankton could affect and perhaps even moderate changes in the air temperature depending on the amount of carbon that is taken up by phytoplankton.

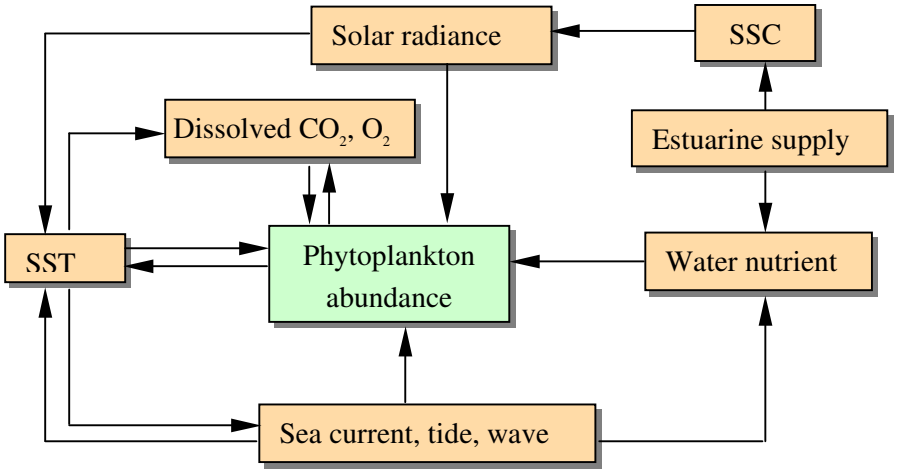

Figure 1.2 Ocean physical environment and its impact on phytoplankton growth

Physical and biological processes are linked and interacted (Figure 1.2). Ocean currents can affect the nutrient supply for phytoplankton consumption, the vertical flux of subsurface nutrients into the surface euphotic zone controls ocean primary production, this motion is caused by the global sea current transportation and sea surface temperature gradient variability seasonally, solar radiance budget in the water directly influence the phytoplankton abundance; meanwhile, solar radiance in the water cause the SST variability, and moderate the capacity of dissolved CO_2 and O_2 in the mixed layer, it influences the phytoplankton abundance; marine nutrients in the euphotic layer are controlled by river supply and upwelling current, which are main a component of phytoplankton formation; On the other hand, light attenuation by marine phytoplankton and suspended sediment concentration modulates the flux of visible light absorbed or scattering in the surface mixed layer and, therefore, may have significant feedbacks on sea surface temperature and air-sea heat flux; meanwhile, the growth speed and range of phytoplankton in the ocean moderate the carbon fixation in the water and air, which predominantly influence the global climate variability.

1.2. Aerospace technology for ocean application

An increasing number of ocean scientists recognize that the traditional sub-disciplines of ocean science no longer constitute a sufficient framework for advancing ocean scientific knowledge. It is necessary to study the dynamic mechanisms by which physical processes influence biological and population dynamic processes, their interactions and attendant feedbacks. These studies must attain a new level of understanding as to how mesoscale and smaller scale processes and interactions determine the distributions and variability of biological and chemical variables over a wide variety of temporal and spatial scales.

Oceanography based on remote sensing provides the only method to collect global data on a regular basis; it supplies the possibility to monitor ocean surface or sub-surface dynamic variability at the spatial extension with multiple spectral data, and calculate the global ocean energy transfer and balance, carbon fixation and cycling, impact on the climate quantitatively. The several sensors are now served or corresponded to the monitoring of marine environment and resources (Table 1.1). The SeaWiFS (Sea-viewing Wide-Field-of View Sensor) on board the SeaStar spacecraft is an advanced sensor designed for ocean monitoring. SeaWIFS satellite, launched in September 1997, is capable to detect sea-surface phytoplankton chlorophyll with ocean colour measurements for estimating total phytoplankton primary production in an effort to determine the role of the oceans in global climate change, These goals should become more tractable with the higher spectral resolution and more complete global coverage of SeaWiFS and other future satellites. Clearly the satellite sensors which measures SST best, the NOAA AVHRR and Terra MODIS which have a spatial resolution of 1.1 and 4 km, are suitable for measuring mesoscale and global scale thermal monitoring in the ocean, there are 3 thermal bands for AVHRR for measurement of brightness temperature and calculation of the SST, so as to 6 thermal bands for calculation of SST for MODIS, but NOAA has night time overpass mode, it can get more accurate result than daytime mode. The scientists have organized the validation team, using the ocean fixed buoy measurement to develop monthly algorithm coefficients for moderating the SST. Using thermal band of the sensor, it is possible to detect the anomalous thermal

"plume", "tongue", "dome", and "meander" in the ocean, such as the phenomena of "ENSO" and "Costa Rica

Table 1.1 Main operational sensors for ocean application

Satellite	Sensor	Spectrum (μm)	Spatial resolution (m)	Temporal resolution (day)	Detection	Modelling
SeaStar	SeaWIFS	0.40-0.88	1300	1	Chlorophyll-a, Turbidity	Primary production
NOAA	AVHRR-3	3.5-12.55	1100	0.5	Brightness temperature	SST
Terra	MODIS	0.4-0.87	1000	1-2	Chlorophyll-a, Turbidity	Primary production
Terra	MODIS	3.66-12.27	1000	1-2	Brightness temperature	SST
Terra	ASTER	0.52-0.86	15	16	Coral reef, Turbidity	
Landsat	TM-5, 7	0.45-1.75	30	16	Coral reef, Turbidity	
IRS-P4	OCM	0.40-0.88	360×236	2	Chlorophyll-a, Turbidity	Primary production
Radarsat	Radarsat	5.6 cm	12.5-100	24	Sea ice, Oil spill, wave	
ERS	AMI	5.6 cm	12.5, 30	3	Sea ice, Oil spill, wave	
ERS	RA			3	Wave roughness	Wind direction, Wind speed
QuickScan	SeaWind		25000	2	Wave roughness	Wind direction, Wind speed

dome", "Gulf Stream meander", "warm pool" and "cold tongue" in the ocean, it indicates the climate variability with air-water exchange, and the position and the season of nutrient upwelling. In 1999, NASA implemented the EOS satellite Terra programme to collect a new 15-year global data record on which to base future scientific investigations about our complex planet. The purpose of project is that they look at the earth as an integrated ecosystem to continuously monitor its energy and substance transfer at global scale, it is possible to acquire the information of SST, cloud extraction, air temperature profile, air pressure, relative humidity, water vapour and aerosol distribution, normalized water leaving radiance and chlorophyll, etc, This long-term, comprehensive study of the Earth answers important questions, such as: is it the beginning of an accelerating increase in global temperatures? How will this affect the weather and sea level? Are the number and size of clouds increasing, how will it affect the planet heat budget and human health? Scientists will make efforts on research of global carbon cycling, atmosphere impact on energy budget, air-water interaction and ocean productivity. At the small scale observation, the purpose of the sensors for land resource detection are also applied in the ocean detection, such as the sensors Landsat TM, IRS-D, Terra ASTER, they have high spatial resolution for analysis of coastal coral reef, sea grass, SSC distribution, and estimate the biomass and water quality assessment. The active sensors of SAR are powerful in cloudy tropical area, it is weather-free sensor, which is capable to detect wave height, velocity and direction vectors, estimate the sea current physical process, also are capable for ocean disaster monitoring, such as oil spill, sea ice motion.

1.3. Significance and objectives of researches

1.3.1. Study area

Costa Rica holds a privileged place in the world, located in the very centre of the isthmus of Central America (Figure 2.1). It is flanked to the east and northeast by the Caribbean, to the southeast by Panama and by Nicaragua to the north. Costa Rica's total surface area is only 51.100 sq. Km, the geographic coordinates are 8°03′ to 11°13′ N latitude and 82°32′ to 85°57′ W longitude, but it contains a wide variety of rivers, plains, mountains, valleys, volcanoes, beaches; a diversified flora and fauna

Figure 1.3 Costa Rica geographical map

in numerous nature and wildlife reserves, and many more attractions for the tourist, including a wide range of climates. The flat land is distributed on regular Caribbean coastline of 210 km in contrast strikingly with the very irregular and rocky Pacific coast. Four peninsulas, Santa Elena, Nicoya, Osa and Burica from north to south extend Costa Rica's Pacific coastline to 1,016 km. The Nicoya and Osa peninsulas shelter the deepwater gulfs of Nicoay and Golfo Dulce, respectively. The Pacific coast is characterized by rocky headlands interspersed with short, sandy beaches. Extensive mangroves occur on the deltas of major rivers draining to the Pacific. The Pacific coast is almost five times longer than the Caribbean coast and is also more complex, with a much larger tidal range, rocky coast, sandy beaches, deep-water bays and major estuaries. Yet the only coral reef occurs at Punta Cahuita on the

southern Caribbean coast. Although mangroves occur on both coasts, they are much more extensive on the Pacific coast where major estuaries and associated mangroves occupy 15% of the coastline.

The test site for this thesis is a small tropical bay called Golfo Dulce, which is located on the southern Pacific coast, between latitude 8°27′ N and 8°45′N; longitude 83°07′ W and 83°30′ W. it is oriented from NW to SE, is about 50 km long and 10 to 15 km wide, and covers an area of approximately 680 km2. The inner part of Golfo Dulce has a maximum depth of slightly over 200 m and there is a 60 m deep sill at the opening to the Pacific Ocean. It is similar to high latitude fjords both in bathymetry and the presence of anoxic deep waters.

1.3.2. Significance and objectives

This study focuses on an investigation of physical processes and biological response by means of satellite remote sensing techniques in Golfo Dulce, Costa Rica. Such studies on the ocean physical processes can assist one to understand the planet energy budget, heat transfer and predict future climate change, and sea level rise. The research on phytoplankton biomass can help us understand the ocean potential commercial fishing, reasonable exploration and protection of ocean resources, carbon cycling and global Greenhouse Effect.

The research program carried out attended to will attain the following goals:

(1) General objective:

- Assess coastal dynamical processes in Golfo Dulce, Costa Rica, and their impacts on carbon fixation using a multi-sensor approach

(2) Specific objectives to spatial analyses:

- Spatio-temporal change of sea surface temperature
- Tide and wave actions in the gulf
- Suspended sediments concentration and annual change
- Phytoplankton (potential) primary production estimate
- Physical process impacts on phytoplankton growth

1.3.3. Research structure

This M.Sc. Thesis is composed of seven chapters as follows:

Chapter 1: Introduction. This chapter provides an introduction to the general marine environment, ocean physical and biological processes; recent new earth observation detection techniques for application on ocean research, discussion of marine issues and its impact on planet climate and environment, and this research objectives and significances of this thesis.

Chapter 2: Marine physical and biological environment in Golfo Dulce. This chapter provides the background introduction of the marine and coastal environment, briefly introduced the type, distribution, and history of geology, geography, and biology in the test area.

Chapter 3: Methodology and Data. This chapter explains in detail scientific research methodology developed and used by author, as well as the work procedures adopted and data acquisition strat-

egy. The methodology is based on information extraction principles, approaches, algorithms and steps, mainly on the calculation of sea surface temperature, SSC, and PPC. Data quality is discussed in terms of what spatial data should be selected for the case study in relation to their advantage and quality.

Chapter 4: Spatio-temporal analyses of physical prosesses in Golfto Dulce. This chapter is related to the image products processed, and how to apply the result to analyse the SST annual and monthly variability, its relation to El Nino phenomena, to evaluate the action of tide and sea current processes in Gulfo Dulce, and to establish the relation between coastal erosion and the Gulf suspended sediment distribution.

Chapter 5: Chlorophyll-a analysis and ocean primary production estimate modelling in Golfo Dulce. This chapter describes the models developed for the spatial SST simulation and primary production estimate.

Chapter 6: Impacts of Physical processes on phytoplankton primary production in Golfo Dulce. This chapter analyses the impacts of the physical processes on the primary production and primary production in response to physical process action with statistical data, as well as the improvements made of the algorithm of primary production estimate.

Chapter 7: Conclusion and recommendation. This chapter summarize the above methodology, analysis, and evaluation. The chapter also presents the constructive suggestions for future coastal management and development in Golfo Dulce.

The thesis also contains the literature reference consulted during the research, as well as an appendix with level 1products.

Chapter 2: Marine physical and biological environment in Golfo Dulce

2.1. Introduction

Golfo Dulce has virtually been neglected due to its minor economic importance, very humid climate, and presumed remote location. Nevertheless, its geographical, oceanographic, and ecological features make it a unique and relatively pristine tropical estuary. A large part of the catchments of Golfo Dulce drains lowland tropical rain forests of Peninsula de Osa (Allen, 1956), the largest relatively undisturbed forests in Central America. The physiography of Golfo Dulce, with a deep inner basin and a shallow sill, restricts water circulation and creates deep stagnant waters similar to those of high-latitude fjords, a unique feature in the tropics (Richards, 1971). Although the fishery production of Golfo Dulce seems to be negligible, it contains diverse shallow water habitats, such as mangrove forests, coral reefs, rocky shores, inter-tidal flats and sand beaches, and deep-water habitats in the inner basin. Such a variety of habitats allow a high diversity of fishes and the presence of resident reptile, seabird, and cetacean populations.

2.2. Climate

The Golfo Dulce area receives 4,000 -5,000 mm of rain per year. Data from two stations within the Gulf area, Playa Blanca (8°40′ N; 83°25′ W) and Esquinas (8°44′ N; 83°20′ W), and from two nearby stations, Palmar Sur (8°57′ N; 83°28′ W) and Coto 47 (8°36′ N; 82°59′ W), demonstrate that rainy season last from April through December with an average annual peak of 610 mm in October (Figure 2.1), precipitation exceeds evaporation during at least 8 months of the year (generally April to December) and soil are permanently water saturated during at least 7 months, except at Esquinas where there is excess precipitation year around (Herrera, 1985). The high degree of water saturation of soil gives rise to frequent river flooding that rapidly erodes exposed, steep-slope soil. The driest months are December through March, with 100 mm or less per month, except at Esquinas where the minimum was 160 mm. The air temperature vary little year round, rainfall reduces the air temperature, maximum temperatures are registered during the dry season along with a seasonal increase in the hours of daily sunshine (3-5 hours per day during the rainy season to 9-11 hours per day during the dry season). Daily temperature maximum typically range from 28°C to 33°C at Palmar Sur and from

30°C to 35°C at Coto 47, with peak values recorded during the dry season, mean monthly temperature is 27.6°C in April at Palmar Sur. Temperature minimum range from 21°C to 23°C at Palmar Sur, and from 16°C to 23°C at Coto 47 .

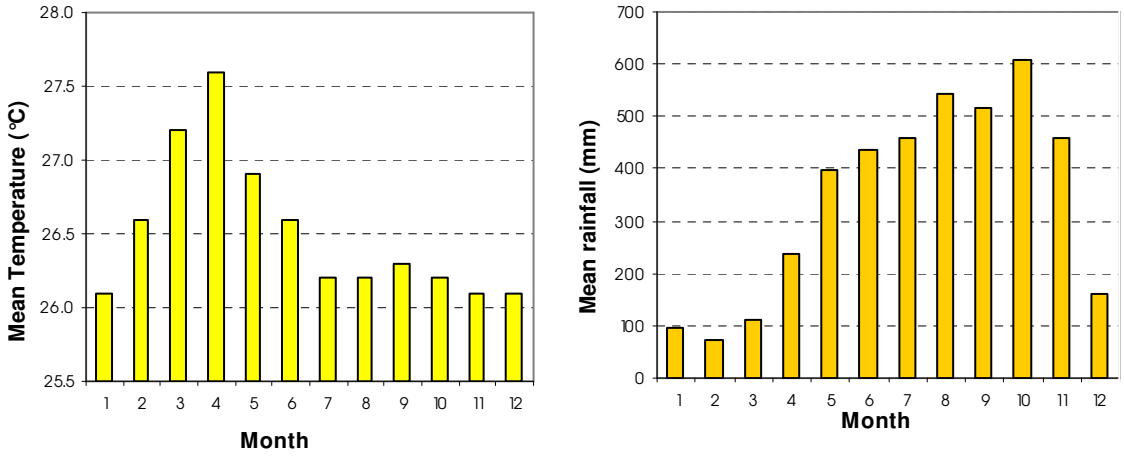

Figure 2.1 Mean monthly temperature and rainfall at station Parmar Sur (N08 57, W83 28)

The climate of the Golfo Dulce catchments is defined as humid to very humid and warm to hot. It rains year round with the rainy season determined by the seasonal north-southward movement of the inter Tropical Convergence Zone (ITCZ). From May to December the ITCZ moves north of the equator past 6° N and the northward-flowing Costa Rica Coastal Current is fully developed, the humid south westerly equatorial trade winds bring torrential rains to the south Pacific coast. From January to March the ITCZ moves the south and the Costa Rica Coastal Current bends westward form the North Equatorial current off Panama, thus the NE Caribbean trade winds dominate. The NE Caribbean trade winds are strongly developed off NW Costa Rica and SW Nicaragua and further south to the Golfo of Panama producing strong coastal upwelling in those areas. However, off SE Costa Rica and NW Panama, the NE Caribbean trade winds are weakened by the Cordilleara Central Mountain and upwelling is reduced or absent (Glynn et al., 1983). Local marine breezes bring regular rains to the Golfo Dulce catchments basin even during the dry season.

2.3. Geology and bathymetry

Due to the subsiding of the oceanic Cocos and Nazca Plates beneath the Caribbean and South American plates, the Pacific coast of Costa Rica has been uplifted through the last 80 million years (Weyl 1980). Golfo Dulce is presently considered as a “pull-apart” basin, which opened about 1-2 million years ago by the displacement of the Burica peninsula to the south (Figure 2.2)(Berange and Thorpe, 1989). Although tectonic activity and uplifting are still going on (Fischer 1980), the inner part of Golfo Dulce is currently subsiding, due to local tectonic adjustment (Fischer 1980, lews 1983). The subsidence of the inner part of Golfo Dulce and the relative stability of the sill region results in its fjord-like structure. The tectonic activity in the whole region results in a complex tectonic pattern, where major tectonic faults can be traced as the Panama fracture zone as far out as the East Pacific

Rise (Berrange 1989). The Panama fracture zone is connected to the two major faults that dominate the shape of Golfo Dulce, the Golfo Dulce oriental fault along its northeast slope and the Golfo Dulce occidental fault along its coastal lowlands in the southwest. These two faults strongly dominate the morphology of the Golfo Dulce region. Geologically, the western and northern sides of Golfo Dulce, known as the Fila Golfito, are formed by the Golfito Terrane, which is deeply weathered and covered by a thick, reddish-brown latosol. The far eastern side of the Gulf consists of low lands of Quaternary alluvial origin, dominated by the Coto-Colorado River and the northern section of the Burica

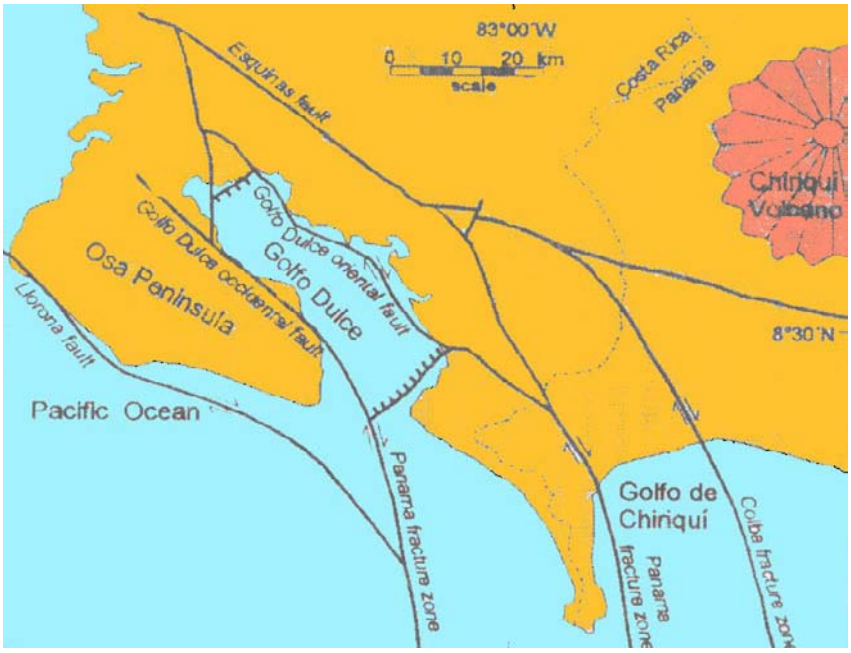

Figure 2.2 Tectonic fault systems in Golfo Dulce (simplified from Berrange 1989)

Peninsula, which is made up mainly of the Burica Terrane. On the southern side, Golfo Dulce is bounded by the Osa Peninsula consisting of ophiolitic lavas of the Nicoya Complex, the Osa Group conglomerates, and the Puerto Jimenez Group, which contains alluvial sediments.

Golfo Dulce is an unique fjord with a 60 m underwater sill (Figure 2.3), general morphology of Golfo Dulce looks as a basin with the flat bottom, but a narrow semi-open mouth at the north. The deepest bottom is in the northwest, to reach 210 m water depth, the north offshore slope is more steep than south due to the active fault in the north, the slope is steeper at the north than at the north. The total area of Gulf is approximate 7500 km^2, 15 km wide and 50 km long, but the Gulf mouth open to the Pacific ocean is only 12 km wide and 60 m deep, the sea current and tide current are incoming and out going from this narrow mouth. Due to its the special morphology, it formes a nearly enclosed and anoxic basin, it has both ocean and lake features different from other tropical bays.

2.4. Coastal land cover and land use

The Golfo Dulce is distributed in a remote and undeveloped bay; land cover is mainly composed of forest, grass and farmland. Among them, the forest accounts for 50%, the grassland accounts for 16% and the farmland accounts for 27% of total area.

The vegetation around the Golfo Dulce area corresponds to the Tropical Wet Forest type in the Holdridge Life Zone System, which have a great floristic affinity with the southern American forest, which today constitute in one of the best forestry representation with a high diversity of trees in Costa Rica (Quesada *et al.*, 1997). There are near to 10,000 flora species with orchids (1,500 species), palms (100 species), ferns (1,100 species) and trees (1,500 species). The rest of the vegetation correspond to lianas, herbs and shrubs are all are very abundant (Jimenez and Poveda, 1996). Golfito has a tropical rain forest in transition (Nubn, 1978). The "Wild life conservation area in Golfito was created in 1985 to protect near to 1,304 ha. of primary forest (Boza, 1996), has a total of 3,200 ha. Of tropical rain forest (always green) with dense and high trees, near to 200 kinds of trees and shrubs (MINAE and

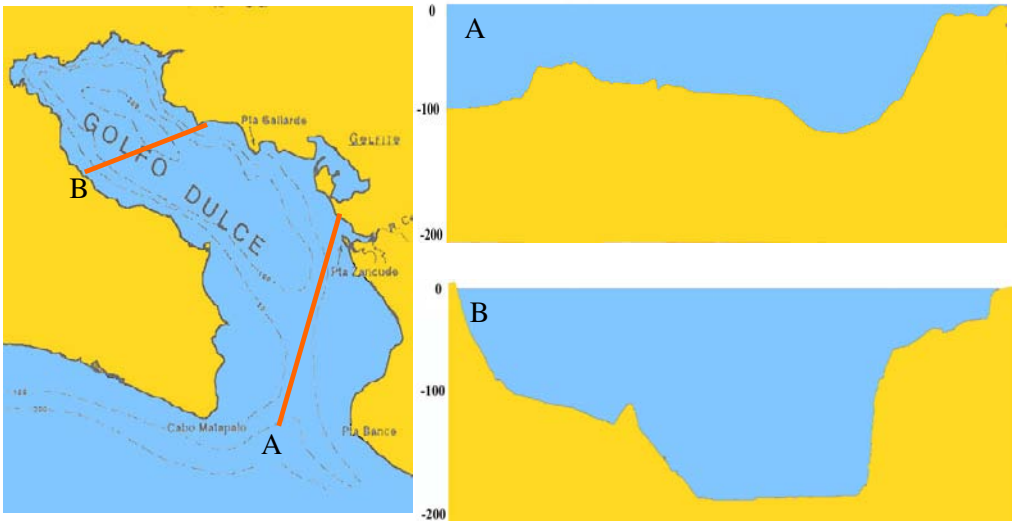

Figure 2.3 Transect maps of gulf underwater geomorphology

SINACOSA, year not specified).

In the northern part of the Golfo Dulce, there are dense vegetation, primary forest with trees of more than 60 m in height and closed canopy. Beside the typical forest there is a special group of vegetation called beach vegetation or “berma” vegetation. It is located parallel to the coastline with an active interaction in the tidal zone. There is material of all kind of calibres, from ravines or by erosion of formations that appear on the surface in the coast (ECOPLAN, 1998). There is vegetation in the sandy soil, well drained, located between the high tide limit. The coastal lagoon or internal channels is resulted from the alluvial and marine deposition in the estuaries or coastal lagoons. The level is higher than the terrains on both sides of this area. It is called “coastal association” and is dominated by gramine or creeping plants and some shrubs. The sea side is dominated by coconut trees *Cocos nucifera* (Arecaceae), almendro de playa *Terminalia catappa* (Combretaceae), marañon *Anacardium occidentale*, tamarindo *Uribea tamarindoides* (Fabaceae) and herbs as *Heliconia latisphata* (Heliconiaceae) (Soto and Jimenez, 1992; ECOPLAN, 1998). The composition and the association of spatial and temporal change in each place, is related with deposition and erosion of sand along the coast (Soto and Jimenez, 1992).

The savannah pasture is the result of cutting and burning forest, leaving only a few trees in the pasture area. In these communities it is possible to find savannah trees that are fire resistant and some

ants-tree association (*Acacia*). Generally, the areas are dominated by only gramines or littler shrubs species and they are maintained indefinitely (Janzen, 1991).

Since 1983 there has been a considerable increase in deforestation that corresponds with the opening of a road connecting the Osa Peninsula with the Inter-American Highway. In the past 50 years road construction in different parts of Costa Rica has led to extensive deforestation.

Farmland is distributed on Coto-Colorado river catchment. The banana plantation is now replaced partially by oil palm, and rice. The principle products are rice (mechanized sowing), except in some small areas in which the rice is sown by hand (for family consumption), corn and beans that are commercialised through of the National Production Consel and Intermediaries; African palm that is commercialised through of Palmatica and Coopeagropal with industrial plants; banana that is exported by Dole and Chiquita; vanilla that is commercialised in external and internal commerce; plantain, advocado and mamon chino that are commercialised by intermediaries and roots and tubercles that are mainly for export.

2.5. Tide and wave currents

The physical activities in the Golfo Dulce are weaker compared to the other gulf, It is composed of tide, wave, river action; the tide action is dominated inside of Golfo Dulce.

The tides are semidiurnal, the tidal range in the inner basin varies from about 2 to 4 meters, mean range of 2.35 m and spring range of 2.89 m. Tidal currents are strong over the sill, attenuating rapidly in the inner basin, where currents are weak and water transport minimal. Through a two-dimensional tidal circulation model, three major current zones are characterized in the Gulf: (1) Inner basin, with sluggish tidal currents (<0.5 cm/s); (2) Mid-Gulf, between Puerto Jimenez and Golfito, where large current eddies develop during rising tides; (3) Outer basin, including the mouth, where current are strong and reversing in phase with external tidal forcing. Tidal flow is not homogeneous across the mouth. Rather, a strong tidal flow dominates over the deep centre of the channel, while the current over the shallow edges are weaker and out of phase.

The currents of Golfo Dulce have not been studied, but field observations demonstrate that water circulation is similar during both ebbing and flooding tides. Apparently there is a counter-clockwise flow of water into the Gulf along the eastern and northern shores and out along the western and southern shores. There are prevail southwest wind year round in the gulf, cause the surface current move to the shore, so the current-caused the upwelling is very little in the gulf; during the dry season, there are strong southeast winds during the afternoons that create a moderate mess in the inner part of the Gulf.

2.6. Off shore sediment

The Gulfo Dulce is a clean gulf, the sediment in Gulfo Dulce is limited to the estuarine region, tide action is stronger than river force. Mean tidal water transport was estimated to average around 45,000 m^3/s (Quiros, 1991). Average annual freshwater transport is low compared to the tidal transport. The largest river, Coto-Colorado, has an estimated mean annual transport of 177 m^3/s. altogether the total freshwater advective flow probably does not exceed 500 m^3/s. direct input from rain, assuming an an-

nual precipitation of 4000 mm, would average around 100 m^3/s. the main sediment is distributed by the rivers Coto-Colorado, Esquinas, Rincom, and Tigre, which are main sources of sediment, other sediment is distribution along the Sabaios beach, at the east of the sill, but these sediment come from the outer gulf. Due to the counter-clockwise current flow, the sediment move according to the current direction, a large sediment spits is formed along the Coto-Colorado River and the gulf of Golfto, which is a small gulf inside the Gulfo Dulce.

2.7. Water nutrients

The distribution of nutrients in Golfo Dulce allows the identification of prevailing oxidation-reduction events in the water column that are typically associated with anoxic conditions. Data from the early 1970's show low nutrient concentrations, near the surface, a typical non-upwelling tropical shelf waters. PO_4 and SO_4 increase with depth and are, on average, 1.5 to 3 times more concentrated in the anoxic zone below 120 m that at corresponding depths outside the Gulf. The vertical distribution of NO_2 shows an intermediate peak typically associated with oxyclines above the anoxic water of deep basins. Concentrations of NO_3 increase from <1 µgat/L at the surface to a maximum of 20-25 µgat/L around the sill-depth, decreasing steadily thereafter and down to zero in the anoxic deep basin. Concentrations of NH_3 near the surface are as low as those of NO_3 and increase moderately with depth; however they show relatively important inter-annual variations at the bottom.

The accumulation of PO_4 and NH_3 at depth, the absence of NO_3 at depth, and the formation of NO_2 above the anoxic zone demonstrate that denitrification takes place, producing variable amounts of NH_3, molecular N_2, and oxidative PO_3 (Richards et al., 1971), and that by-products of organic decomposition accumulate in the deep Gulf. The variable accumulation of NH_3 at depth indicates qualitative and quantitative inter-annual changes in oxidation-reduction processes. Thus, it may be hypothesized that in years with high NH_4 levels not all NH_3 released during denitrification was oxidized to NO_3 (Richards, 1971), more NH_3 was produced during SO_4 reduction, and less NH_3 was used for biological assimilation reactions (Anderson and Devol, 1987). Inter-annual variations in these parameters will also depend on the annual rate of deep-water renewal and on organic matter input from river runoff, coastal pollution, and surface productivity.

2.8. Mangrove and coral reef

Environmental conditions favour growth of coral reefs up to the recent past. There are three main reef areas described in Golfo Dulce, two off the northern shore and the other off the southern shore. Most of the reefs in Golfo Dulce are paucispecific, dominated by *Porites lobata* Dana (Jorge Cortes, 1990). The largest reef off the northern shore at Punta Islotes covers several hectares, and has a well-developed reef-flat (0.5 m deep) composed, for the most part, of dead *Pocillopora damicornis Linnaeus*, and small dead or live hemispherical colonies or large micro-atolls of *Porites lobata*. The edges, slope and base of these reefs are composed totally of large, live partly dead or dead massive colonies of *Porites lobata*, with a few isolated colonies of *Pavona gigantean Verrill* and *Psammocora stellata*. The reef slope is very step, 45° or more, vertical in some places and extending to 10-13 m depth.

Outer Golfo Dulce reefs (Sandalo and Punta El Bajo), characterized by a relatively high live coral coverage, high species diversity and low relief, at Sandalo, a low profile Pocillopora-Porites reef is located on the south shore of the Golfo Dulce; *Porites lobata* predominates on the shore-side with *Pacillopora damicornis* and three other species of corals covering most the seaward side. The reef at Puanta Ei Bajo is a low profile Psammocora reef located on the north shore of the Gulf, east of the Punta Isolates reef. Most reefs in the inner basin are now deteriorating as a result of increased sediment loads due to deforestation, near-shore road construction, agriculture in the lowlands, and gold mining in the mountains of the Osa peninsula (Cortes, 1993).

The Golfito area is situated in the south Pacific zone with 5 typical mangrove species: *Rhizophora mangle, R. racemosa, Pelliciera rhizophorae, Laguncularia racemosa* and *Avicennia germinans.* Due to the high precipitation, these mangroves have more diversity of epiphyte species and marginal vegetation than the others in the rest of the country. Besides the number of others groups associated as birds, invertebrates and mammals is large. Species as the donkey “cara blanca” and donkey “ardilla” looking for insects or larvae inside the mangrove, form a special group associated (Soto and Jimenez, 1992).

There are three kinds of vegetation according to distribution, biological characteristics, soil salinity and tide. Nuclear vegetation: mangrove species with typical adaptation (viviparity, high range tolerance to salinity, aerial roots, excretory salinity glands). The distribution is linked to the tidal zone. This area is characterized by*: R. mangle* that growths mainly in places with recent depositions and loose consolidation of the soil. *R. racemosa* is situated on the rivers and estuaries where there is a 90 degrees escarpment and the sediments are consolidated. *P. rhizophorae* growth near to internal channels, in consolidated soils, soils highly sandy and in the principal channels. Some times it forms patches or it grows mixed with *R. racemosa*, but does not have a specific pattern. *A. germinans* grow at the backside. Marginal vegetation: composed by adjacent species of nuclear vegetation. The distribution is on high land, irrigated by estuarine waters and in low salinity conditions, could be mixed with the nuclear vegetation, contains the species list of each kind of vegetation. *Mora oleifera* and *Pterocarpus officinalis* are part of the transitional vegetation between mangrove and forest (Soto and Jimenez, 1992). Facultative marginal vegetation: generally without mangrove species, which is distributed on soil with low salinity (3.5 ppm) and composed of trees, shrubs, herbs, palms and lianas.

2.9. Pelagic environment

Plankton in Golfo Dulce shows typical features of tropical coastal plankton systems: abundance of diatoms and dinoflagellates in the net plankton, potential for development of red tides, diverse zooplankton with some preponderance of small *calanoid copepods*, and presence of *detritivores* (Hartmam, H.J, 1996). Seasonal differences in abundance and species composition were observed. Total net-plankton volume, including zooplankton, peak in June and in November and is lowest from mid-February to April, Some diatom taxa appear mostly during the rainy season, while others are restricted to the dry season, Among the species that are present year around, *Chaetoceros spp.* is more abundant during the rainy season, while *Rhizosolenia spp. Coscinodiscus spp.* And *dinoflagellates* as a group has no clear seasonal preference. The net plankton is more than twice as abundant offshore than inshore. Red tide is Golfo Dulce marine disaster once occurred in rainy season, there were 52 red tide patches recorded from September 1991 through December 1992 and their size ranged from tens

to hundreds for meters. The large amount of nutrients is brought from river runoff, and lead to the abundance of *dinoflagellates*.

Cell counts and size-specific measurements of respiration activity demonstrate that pico-to-microplankton organisms should play an important role in energy and nutrient turnover in Golfo Dulce. Primary productivity appears moderate, likely comparable to mesotrophic tropical shelf conditions. Daily net primary production in Golfo Dulce is estimated about 0.7 gc/m2·d, total annual production is 93075 t·c/y. Productivity appears to be fuelled by a terrestrial nutrient supply that is filtered through the mangroves, which use a large part of these nutrients and then export some of it to the Gulf in form of detritus, and by internal nutrient recycling through the activity of *detritivores* and microbial-loop organisms. An additional fuel source of productivity is the annual entrainment of enriched subsurface coastal water into the lower part of the euphotic zone. Given these fuel sources for productivity and recent increases in terrestrial erosion, agricultural runoff, and human pollution, primary productivity should have increased dramatically from the early 1970's.

Chapter 3: Methodology and data

3.1. The steps and stages of research work

3.1.1. Inventory and preparation

The inventory stage started with formulation of a prelimary research proposal and preparation of the fieldwork in ITC. The work was conducted at ITC between April 30 and June 5, 2001; the following research tasks were carried out:

- Review and reading the ocean literature in library and internet;
- Review and reading the remote sensing and ocean literature in the library and on the internet;
- Data check and collection in ITC;
- Thesis topic selection;
- Processing and interpretation of satellite images;
- Samples of SST and SSC made on the image;
- Scanning and geo-reference of topographic map for fieldwork use;
- Schedule for fieldwork;
- Collection of equipment for fieldwork use.

3.1.2. Fieldwork

The purpose of this stage is to collect data, visit experts on oceanography and local government, sampling, image validation. The fieldwork lasted 40 days from June 5th until July 15th, 2001. ITC organized the CZS students and Carribean students to work in Golfto, Costa Rica, for baseline of coastal environment.

- Schedule for fieldwork;
- Date collection (climate, image, statistics);
- Visit to the SeaWIFS ground station, National University, Heredia, Costa Rica, to understand the use of SeaDas software, chlorophyll-a calculation;
- Visit to school of geography, national university for water and soil erosion and geomorphology maps;
- Visit to CIMAR to collect the data of phytoplankton and other data;
- Visit to the Golfo port to collect tide data;
- Field reconnaissance for coastal erosion and land use;
- Suspended sediment and chlorophyll-a sampling;
- Re-processing satellite image in SSC and classification of SSC.

3.1.3. Data processing and result analyses

This stage includes

- Lab analysis of SSC samples which were taken in the field;
- Order and download of images from internet: including: NOAA, Seawifs, ASTER and MODIS;
- Processing of images on geo-reference, atmosphere correction, time match;
- Information extraction of SST, SSC, chlorophyll-a;
- Statistical analysis and comparison on SST, SSC, chlorophyll-a;
- Modeling of the primary production and SST.

3.1.4. Thesis reporting

This stage includes:

- Thesis report writing;
- Consulting with supervisors;
- Modifying and editing of thesis report;
- Presentation preparing;
- Thesis defense;
- Thesis poster editing.

3.2. Data acquisition

3.2.1. Sensor and data quality

Sensors are designed for some specific purposes, because there are limitations of data recording capacity and detection techniques; therefore, the evaluation of sensor quality is necessary for special purposes, in this case, the direct purposes extracted from image are the SST, PPC, SSC, and wave current.

Normally, SST changes slowly, it varies less than 1 ˚C in 10 days in the study area, and smoothly at spatial extension, it varies less than 3 ˚C at the distance of 100 km, it is sensitive to the thermal spectrum between 3-12 μm. 90% phytoplankton chlorophyll-a is distributed above the depth 15 meter of sea water, it reflects the spectrum between 480 nm and 650 nm, absorbs the spectrum in 420-430 nm and 670-680 nm, and emit the chlorophyll fluorescence, phytoplankton live last 1-2 days, its distributed patch extent more than 0.5 km, shape of the patch is depended on the sea current. Suspended sediment is distribute along the coast and estuary, its plume extent from 10 meter to 5 km, but SSC varies quickly, it can be changed to form a new plume in a few hours, it is depended on the river discharge and tide current. It reflects strongly on the spectrum between 500 and 600 nm; sea wind and wave vary more quickly and irregularly than any other objects, normally, it changes velocity and direction in an hour, sea wave varies between 20-200 m, its spatial unchanged can extent at last 5×5 km in ocean.

The Advanced Very High Resolution Radiometer (AVHRR) is a broad band, four or five channel (depending on the model) scanner, sensing in the visible, near infrared, and thermal infrared portions of the electromagnetic spectrum. This sensor is carried on NOAA Polar Orbiting Environmental Satellites (POES), beginning with TIROS_N in 1978. The mission of the AVHRR data provides opportunities for studying and monitoring vegetation conditions in ecosystems, various geophysical pa-

rameters (SST) and energy budget data. It has three thermal bands available for detection of the surface thermal radiance (3.6 µm, 11µm, 12µm), and two times revisit in same place each day (one in daytime and another in night time), it is powerful to apply to extract SST (Figure 3.1).

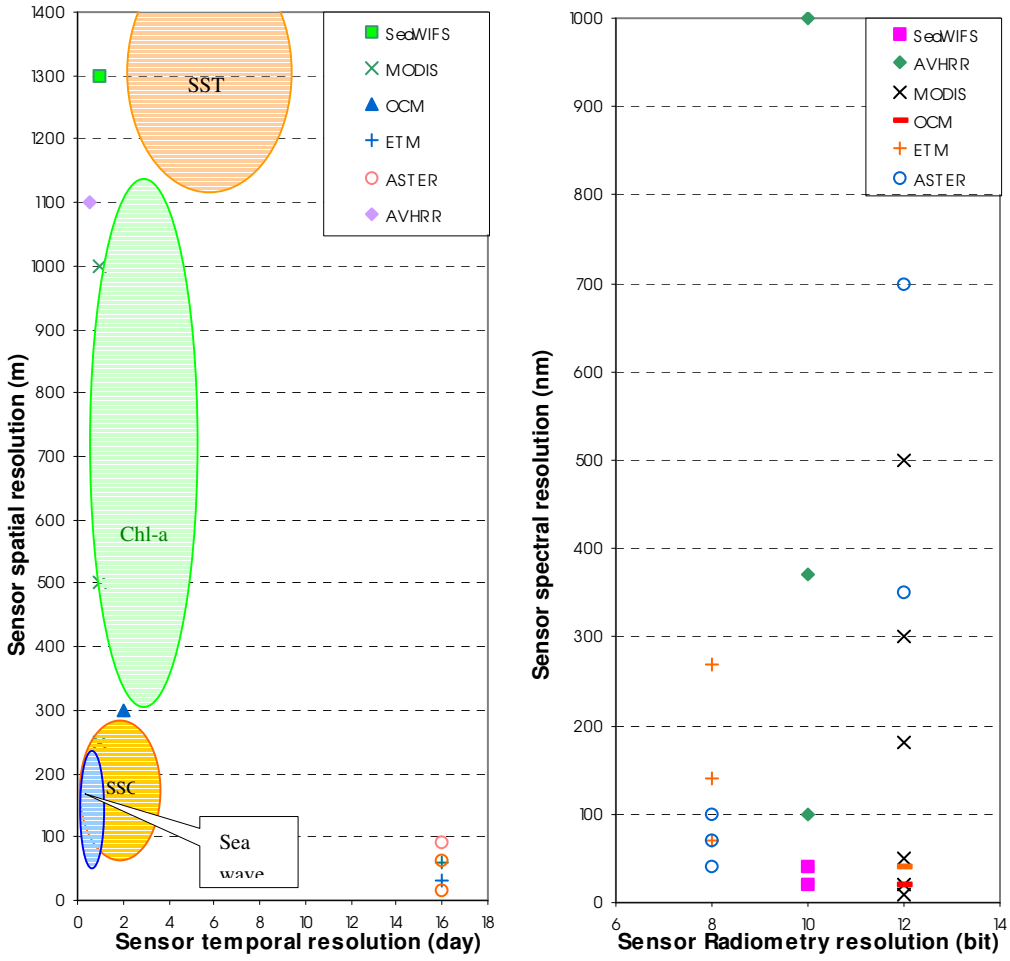

Figure 3.1 Ocean sensor's data quality comparison

The Sea-Viewing Wide Field-of-view Sensor (SeaWiFS) is a Spectroradiometer, which means that it measures radiance in specific bands of the visible light spectrum (402-885 nm). It has high accurate spectral resolution of 20 nm between 402 and 680 nm, strong absorption of chlorophyll-a is within spectrum width of 20 nm, It is possible to detect the free-floating photosynthetic organisms (phytoplankton) and inorganic particulates which contain the pigment influencing the visible spectrum.

Moderate Resolution Imaging Spectroradiometer (MODIS) is a powerful instrument, it is designed 36 spectral bands cover all the visible, near infrared and thermal band, and has high radiometry resolution of 12 bits, it record atmosphere parameters for atmosphere correction, it has all advantages of SeaWIFS and AVHRR, problem is image quality is not perfect due to first launch of satellite series, some stripes occur on image, which will influence the quantitative calculation of ocean parameters, also it misses spectrum between 500-520 nm of sensing, which is one important band of chlorophyll absorption.

ASTER and ETM have high spatial resolution, they have the same distributed spectrum in visible and near infrared band, ETM has more stable quality on image than ASTER, ASTER has high radiometry resolution of 12 bits in spectrum 3-12 μm and better spatial resolution of 15 m in visible band, there are both available for detection of SSC.

According to sensor's advantage and disadvantage, and primary data accessible acquisition and suitable software for processing, the AVHRR data is selected for calculated for SST, SeaWIFS data is selected for extracting PPC, TM and ASTER are both selected for detection of SSC alternatively.

3.2.2. Data collection

Data was collected from four sources: 1) ITC-CIMAR Joint project cooperation; 2) fieldwork sampling; 3) local university and research organization; 4) internet download. The data used for this research is given as follows (Table 3.1).

Table 3.1 Data list of ocean environment monitoring in Golfo Dulce

Information source	Processing Software	Description	Expected result
NOAA AVHRR	Chips, Erdas	1.1 km LAC 1b image, 1990-2001 in January 1-15, every day in 1998	SST 1998 monthly map
			SST annual map 1991-2001
Seastar SeaWIFS	Seadas	1.13 km LAC 1b image, every day in 1998 and Jan., 2000	PPC monthly map 1998
Landsat TM	Erdas	2/16/1998 TM 5	SSC map
		15:41:21/2/14/2000 TM 7	
		15:39:07/1/31/2001 TM 7	
		16:18:06/1/31/2001 ASTER	
		Sept.9, 2000 ASTER	
ERS-1 AMI	Erdas	Jan. 02, 1999(North); Feb. 26, 1999 (South); 12.5 meter resolution	Direction vector
Quickscan-SeaWind	Internet	25 km grid, Each month in 2000	Wind velocity, direction vector
In situ measurement	Excel	12 samples in depth of 5 meter	PPC
	Excel	10 samples in 5 meter depth and 15 samples in depth of 1 meter	SSC
Climate statistical data (Palmar Sur climate station, 8.57 N, 83.28 W)	Ilwis	100m, 10m interval Contour line map	Analysis
	Ilwis	Point Bathymetry, unit: meter	Analysis
	Excel	Tide gauge daily record 2000-2001	Analysis
	Excel	Monthly mean Air temperature 1961-1993	Analysis
	Excel	Monthly mean Solar hours 1973-1994	Analysis
	Excel	Monthly mean Evaporation 1979-1989	Analysis
	Excel	Monthly mean Wind velocity, direction vector 1974-1992	Analysis

	Excel	Monthly mean Humid 1975-1991	Analysis
	Excel	Monthly mean Rainfall 1941-1986	Analysis
	Excel	Monthly mean Radiation 1974-1992	Analysis

3.2.3. Field samples collection

The sampling data is made to calibrate the algorithm coefficients and validate the image calculation results. The samples distribution design is according the following the principles: (1) different concentration of SSC and chlorophyll-a; (2) different types of physical process; (3) underwater geomorphology; (4) different coastal landform.

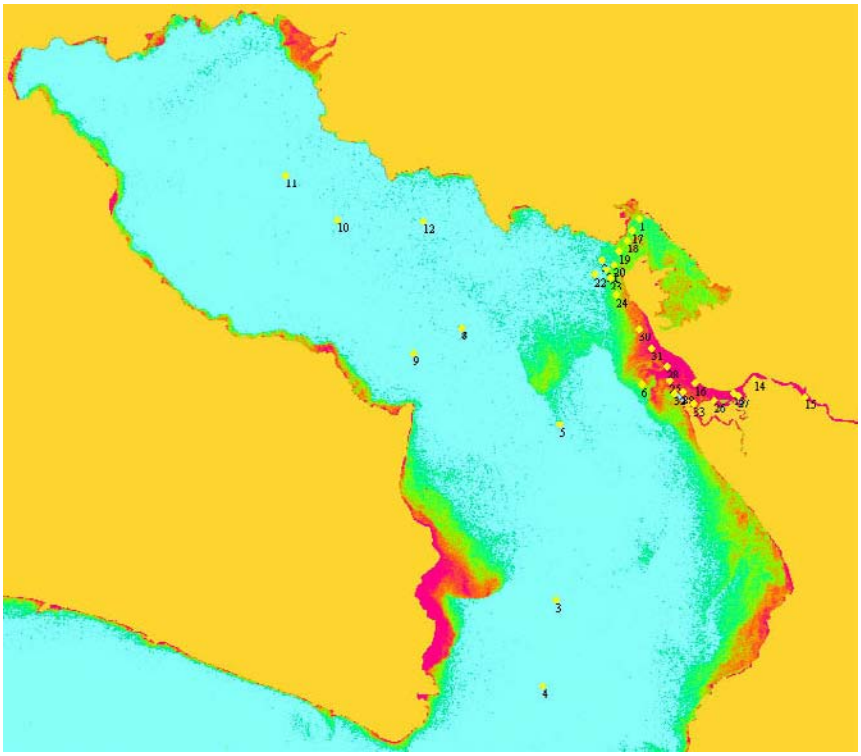

Figure 3.2 33 Samples distribution in Golfo Dulce (background is TM B2 of Jan. 2001)

33 sampling spots were selected in Golfo Dulce (Figure 3.2), and 45 samples were collected, 33 SSC samples, 12 chlorophyll-a samples, but only 28 SSC and 10 concentration results are available due to analysis errors or sampling errors. Of the 45 samples, 28 samples were taken along the course of the major stream of the Coto-Colorado River, its river mouth, and the Gulf of Golfito, the remaining 17 samples were distributed from the gulf mouth to inner gulf. Each SSC sample contains 1 litre water weight in the plastic bottles, each chlorophyll-a sample weighs 0.5 litre water stored in brown colour bottle, GPS was used to obtain the coordinates.

3.2.4. Sample analysis in the laboratory

The analysis process of the water SSC samples was carried out in the ITC lab and chlorophyll-a was processed in CIMAR lab in Costa Rica. First the needed equipment for the SSC filtering was prepared. The water samples were pumped and filtered through a GFC/C Whatmon filter paper of 0.45-micron pore size using a Millipore filter assembly in the laboratory to determine the total suspended sediments. After the filtering the samples were dried by using the oven for almost one hour. Finally weighted the suspended sediment with the filter and to get the pure amount of SSC, the filter paper weight is subtracted from the filter paper weight with the suspended sediment. The SSC for the 28 samples are given (Table 3.2).

Table 3.2 The concentration of SSC and pigments analyses in lab

ID	X-axle *	Y-axle	Sediment (mg/l)	Chlorophyll (mg/m^3)	Phaeo pigment (mg/m^3)	Depth (m)	Date	Area
1	591254	954582	73.67	1.11	0.54	5	06/22/01	Golfo Dulce
2	589212	952342		0.52	0.35	5	06/22/01	Golfo Dulce
3	586629	933537	68.33	0.32	0.18	5	06/22/01	Golfo Dulce
4	585949	928805	68.67	0.2	0.06	5	06/22/01	Golfo Dulce
5	586889	943254	73.00	0.39	0.13	5	06/22/01	Golfo Dulce
6	591435	945420	68.00	0.34	0.02	5	06/22/01	Golfo Dulce
7	581432	948615	75.00	0.2	0.06	5	06/22/01	Golfo Dulce
8	581432	948615	67.33	0.8	NST (-0.29)	10	06/22/01	Golfo Dulce
9	578757	947155		0.2	0.34	5	06/22/01	Golfo Dulce
10	574581	954520	66.33	0.31	NST (-0.14)	5	06/22/01	Golfo Dulce
11	571646	957044				5	06/22/01	Golfo Dulce
12	579309	954481				5	06/22/01	Golfo Dulce
13	596502	944985				1	06/12/01	Golfto
14	597324	945700	75.00			2	06/12/01	Golfto
15	600420	944769	92.00			1.2	06/12/01	Golfto
16	594374	945516	85.00			0.5	06/12/01	Golfto
17	590858	953907	48.00			1	6/16/01 8:23 AM	Golfto
18	590632	953404	50.00			1	6/16/01 8:26 AM	Golfto
19	590115	952805	45.00			1	6/16/01 8:30 AM	Golfto
20	589888	952093	40.00			1	6/16/01 8:36 AM	Golfto
21	589462	951799	58.00			1	6/16/01 8:41 AM	Golfto
22	588820	951506	35.00			1	6/16/01 8:48 AM	Golfto
23	589668	951351	67.00			1	6/16/01 9:00 AM	Golfto
24	590009	950389	40.00			1	6/16/01 9:05 AM	Golfto
25	592964	945672	65.00			1	6/16/01 9:29 AM	Golfto
26	595452	944548	68.00			1	6/16/01 9:40 AM	Golfto
27	596751	944831	72.00			1	6/16/01 9:47 AM	Golfto
28	592783	946480	69.00			1	06/20/01	Golfto
29	593671	945047	55.00			1	06/21/01	Golfto
30	591294	948534	60.00			1	06/22/01	Golfto
31	591946	947424	70.00			1	06/23/01	Golfto

* Coordinate system is adopted in Transverse Mercator, Ellipsoed WGS 84

32	593226	944973	54.00			1	06/24/01	Golfto
33	594283	944403	60.00			1	06/25/01	Golfto

3.3. Sea surface temperature calculation

3.3.1. Sea surface temperature calculation framework

At IR wavelengths, the ocean surface emits radiation almost as a blackbody (of 0.98). In principle, without an absorbing and emitting atmosphere between the sea surface and the satellite, it would be possible to estimate SST using a single thermal channel measurement. NOAA AVHRR, an instrument with three infrared (IR) channels, is suitable for estimating SST (Schwalb, 1978). These channels are

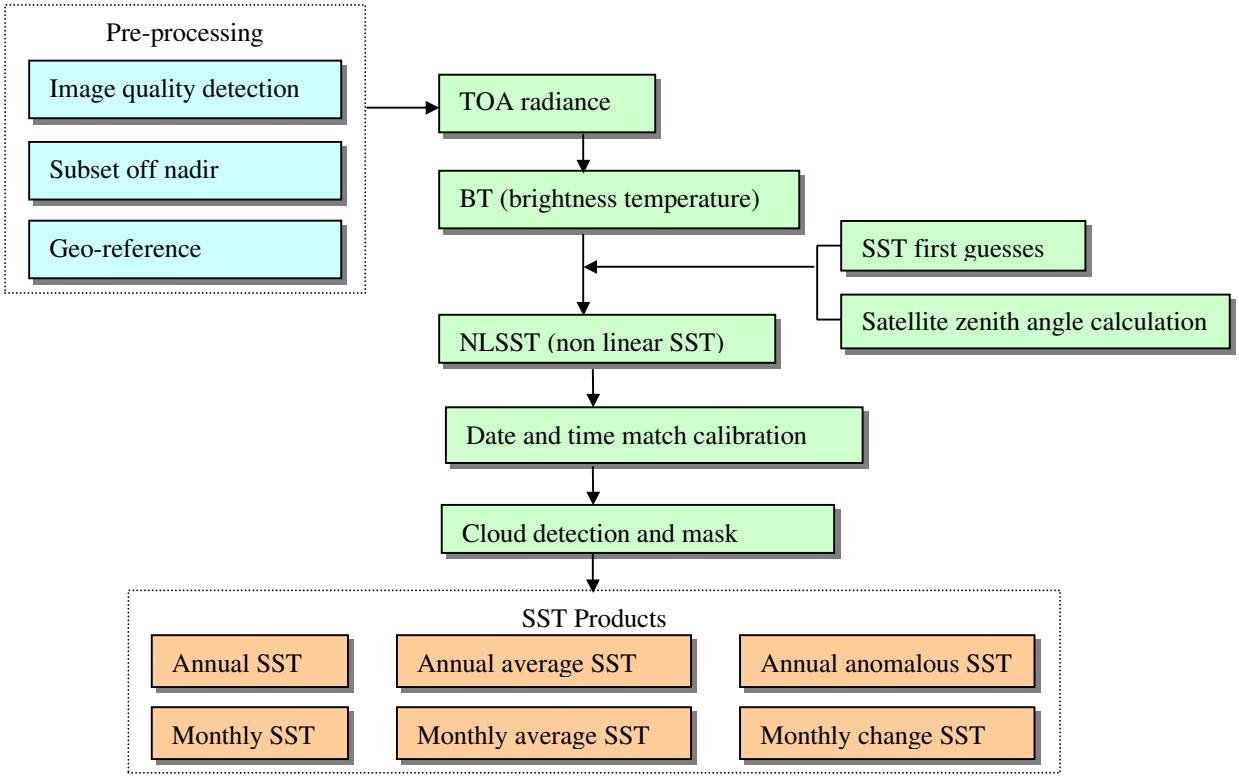

Figure 3.3 NOAA AVHRR image processing and sea surface temperature calculation

located in the wavelength regions in 3.5μm—4μm and 10μm—12.5μm, where the atmosphere is comparatively transparent. In reality, surface-leaving infrared radiance is attenuated by the atmosphere before it reaches a satellite sensor. Therefore, it is necessary to make corrections for atmospheric effects. Water vapour, CO_2, CH_4, NO_2 and aerosols are the major constituents that determine the atmospheric extinction of IR radiance (Minnett, 1990). The Split Window technique and non-linear algorithm are applied to remove water vapour influence in thermal band (Figure 3.3).

3.3.2. Pre-processing of NOAA AVHRR images

The raw images of NOAA AVHRR LAC with 1 km spatial resolution are downloaded from the internet http://www.saa.noaa.gov/, they have some data quality problems need to be solved before SST calculation, which are off-nadir distortion, cloud coverage and image shift.

NOAA satellite overpass same place two times each day, and shift east each day, 9.5 days return to same place, the place of interest on the image is not always the nadir recorded, the further away from nadir, the more distortion will occur due to the earth curve and the sensor FOV, pixel size is 1.1×1.1 km under the nadir, and 6×3 km at the limb (Figure 3.4),

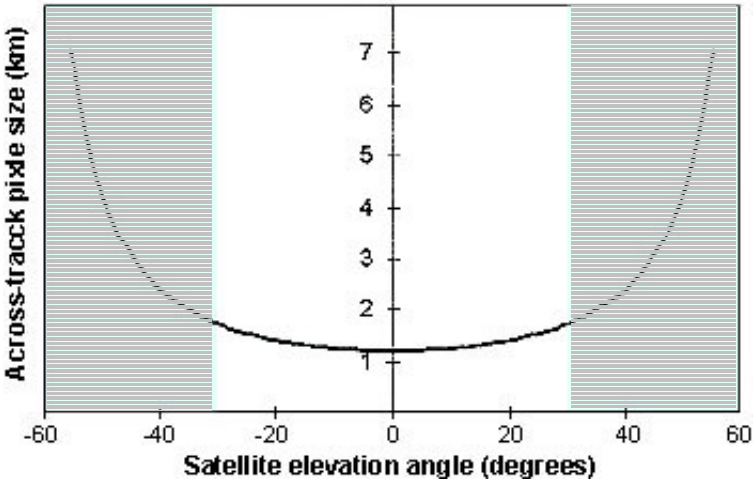

Figure 3.4 NOAA AVHRR image across-track distortion (Wim H.B. 2001)

In this case study, the 30 degrees image limit two side of nadir is selected to ensure the pixel size less than 1.5 ×1.5 km, out of this threshold spatial resolution is low and will be cut off.

The cloud coverage in this tropical region is popular, normally, the days of cloud coverage account for 50% in dry season, and account for 90% in the rainy season when NOAA satellite overpass the region, no any cloud coverage cover whole region is impossible, therefore, the mosaic technique is used for eliminate cloud, this will be later discussed. But first step is that AVHRR band 2 is applied to detect the cloud, this band is suitable to distinguished land and water, the spectral difference between land and water is more higher than other band, the coastline is clearly displayed on image if without cloud, if there are cloud appear, the coastline will disappear, so we can skip most cloud-covered scenes, if fog or thin cloud cover on the image, the coastline will be not clear, at this moment, it is

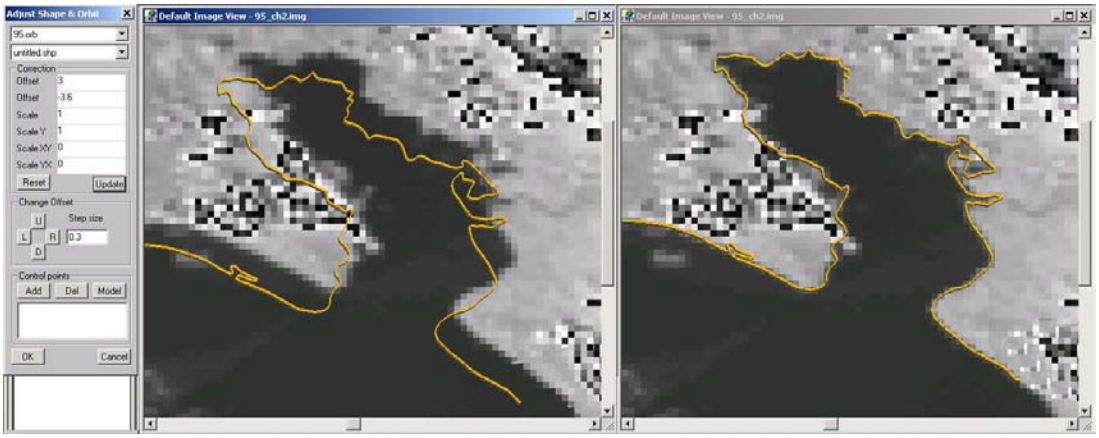

Figure3.5 Geometrical rectification for NOAA AVHRR image

quite difficult to determine if it is selected or not, because it will influence the SST value, it makes the low SST.

The images of NOAA HRPT have embed the geographical coordinate system, but it is pre-launched designed coordinate system, there are 0-4 pixels (0-6 km) distortion on image acquired from ground station. Geometrical rectification is necessary to eliminate the distortion; the gulf coastline .Shp file is input to match the image (Figure 3.5), we use "Adjust shape" tool in Chips software to fit coastline to image, normally, 0-0.5 pixel error is possible appeared in the rectification. Then the projection of normal cylindrical equal-area (Behrmann) is applied to geo-code image.

3.3.3. Brightness temperature calculation

AVHRR thermal data values (channels 3, 4, 5 before NOAA 15) may be converted to temperature values. The radiance measured by the sensor band i is computed as a linear function of the input data values as follows (Equation 3.1):

$$E_i = S_i \cdot C + I_i \tag{3.1}$$

Where E_i is the radiance value in mW/(m^2-sr-cm^{-1}), C is the input data value (ranging from 0 to 1023 counts), and S_i and I_i are respectively the scaled slope and intercept values which derived from image calculation through Chips software or other software. The scaled thermal channel slope values are in units of mW/(m^2-sr-cm^{-1}) per count and the intercept is in mW/(m^2-sr-cm^{-1}).

The conversion to brightness temperature from radiance is performed using the inverse of Planck's radiation (Equation 3.2):

$$T_{(E)} = \frac{C_2 v}{\ln\left(1 + \frac{C_1 v^3}{E_i}\right)} \tag{3.2}$$

Where $T_{(E)}$ is the brightness temperature (K) for the radiance value E, ν is the central wave number of the channel (cm^{-1}), and C_1 and C_2 are constants (C_1 = 1.1910659 x 10^{-5} $mW/(m^2\text{-}sr\text{-}cm^{-4})$ and C_2 = 1.438833 cm-K). Note that the temperatures obtained by this procedure are not corrected for atmospheric attenuation, etc. The central wave numbers (cm^{-1}) for Channels 3, 4, and 5 as a function of temperature can be found in http://www2.ncdc.noaa.gov/docs/podug/ html/c1/sec1-4.htm. in this case studies, NOAA 11 and NOAA 14 data are used for calculation, for NOAA 11, V_4= 927.75, V_5= 842.14; for NOAA 14, V_4=929.5878, V_5=835.374

3.3.4. Satellite zenith angle calculation and first guess SST acquisition

The most of thermal energy reach the sensor come from water emission, the sun reflection of thermal energy nearly equal to zero, sun angle correction is not necessary, but satellite zenith angle cannot be neglected, large satellite zenith angle lead to long distance transmit through the atmosphere, which attenuate the thermal energy, and make the SST lower. The satellite zenith angle map can be obtained from image calculation, but it is always same (Figure 3.6).

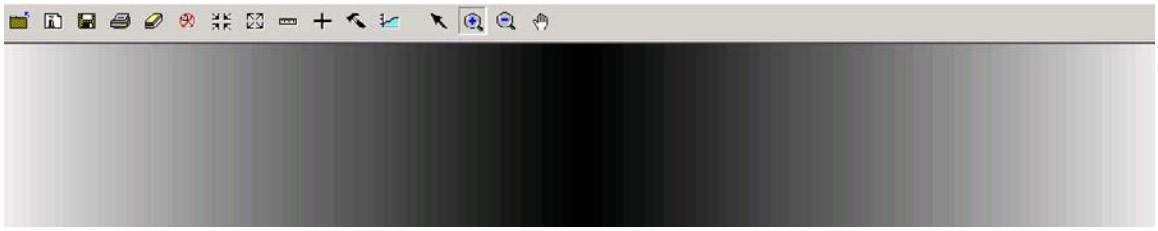

Figure 3.6 NOAA AVHRR satellite zenith angle (degree) map

The NCEP (National Centres for Environmental Prediction) Reynolds Optimally Interpolated (OI) Sea Surface Temperature product consists of weekly and monthly global sea surface temperature fields on a 1° by 1° grid. The analysis uses both in-situ SSTs and satellite derived SSTs from the NOAA Advanced Very High Resolution Radiometer (AVHRR). The in *situ* data were obtained from buoy data measurement (Figure 3.6), which send radio messages through the Global Telecommunication System, then the data interpolate to the global sea surface temperature. This product is available from 1981 to the present on Internet: ftp://podaac.jpl.nasa.gov/pub/sea_surface_temperature/reynolds/oisst/browse/oiweek/.

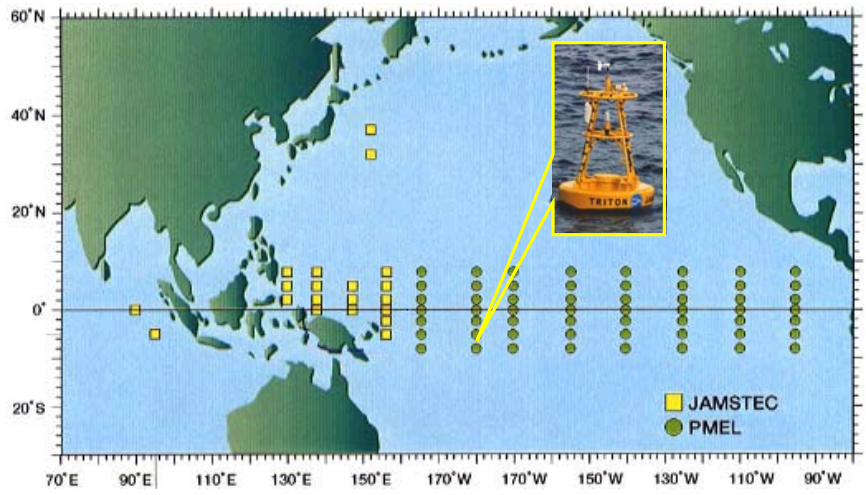

Figure 3.7 Fixed buoy location distribution map on the Pacific Ocean

3.3.5. Multi-channel and non-linear sea surface temperature calculation

(1) Multi-channel sea surface temperature (MCSST). The MCSST algorithm was NOAA's operational procedure for several years (McClain et al., 1985), which may be written as:

$$SST = \alpha \cdot T_i + \gamma \cdot (T_i - T_j) + c \tag{3.3}$$

Where T_i and T_j are brightness temperature measurements in channels i and j, and a and c are constants. The gamma term is defined as:

$$\gamma = \frac{(1 - t_i)}{(t_i - t_j)} \tag{3.4}$$

where t is the transmittance through the atmosphere from the surface to the satellite. In cases of weak absorption, the transmittance can be approximated by (1 - *ku*), where *k* is the mass absorption coefficient of the atmospheric absorbers and *u* is the path length.

There are several models for estimating the SST (P.Cracknell, 1997), here is NOAA-7 SST model expressed as follows:

(A) Day-time:

$$SST = 1.035T_{B4} + 3.046(T_{B4} - T_{B5}) - 283.93 \tag{3.5}$$

(B) Night-time:

- Split window:

$$SST = 1.0527T_{B4} + 2.6272(T_{B4} - T_{B5}) - 288.23 \quad (3.6)$$

- Triple window:

$$SST = 1.0239T_{B4} + 0.9936(T_{B4} - T_{B5}) - 278.46 \quad (3.7)$$

- Dual window:

$$SST = 1.0636T_{B4} + 1.4544(T_{B4} - T_{B5}) - 278.47 \quad (3.8)$$

This so-called MCSST algorithm assumed a constant gamma. It doesn't consider the satellite zenith angle and sensor parameter impacts on SST.

(2) Non-linear sea surface temperature. Subsequent improvements incorporated a correction for increased path lengths at larger satellite zenith angles (Cornillon et al., 1987). Other improvements in the atmospheric correction involved non-linear formulations, in which gamma was proportional to the brightness temperatures, as in the CPSST (cross-product SST) algorithm described by Walton (1988) and Walton et al. (1990). The latest version of the operational NOAA algorithm is the NLSST (non-linear SST), in which gamma is assumed to be proportional to a first-guess SST value (ftp://podaac.jpl.nasa.gov/pub/ seasurfacetemperature/reynolds/oisst/browse/oiweek/). The NLSST algorithm has the following form (Equation 3.9):

$$SST = a + b \cdot T_{B4} + c \cdot (T_{B4} - T_{B5}) \cdot SST_{guess} + d \cdot (T_{B4} - T_{B5}) \cdot (Sec_{(sza)} - 1) \quad (3.9)$$

Where SST is the satellite-derived SST estimate, T_{B4} and T_{B5} are brightness temperatures in AVHRR channels 4 and 5 respectively, SST_{guess} is a first-guess SST value, and $Sec_{(sza)}$ is the satellite zenith angle calculated from image in Chips software. Coefficients a, b, c, and d are estimated from regression analyses using co-located in situ and satellite measurements (or "matchups"). Typically, NOAA produced a set of coefficients using matchups for a certain period (http://www.rsmas.miami.edu/groups/rrsl/pathfinder/ Algorithm/algo_coeffs.html#N7%20coefficients%20-%20V4)

NLSST algorithm is more accurate than MCSST algorithm, it updates coefficients a, b, c, d each month and SST_{guess} each week, efficiently eliminate the impact of water vapour, which is applied in this case studies.

3.3.6. Time match correction and cloud detection and elimination

Multiple temporal SST comparisons should be carried out at the same time, the image acquired exhibit temporal variations, and therefore it is necessary to match each multiple data before the production of the annual and monthly SST. We are interested the January SST between 1991-2001, and

monthly SST in 1998 when El Niño event occurred. SST in January change a little from the beginning of month to 15 January (Figure 3.8), SST residual characterizes SST each day menus average monthly

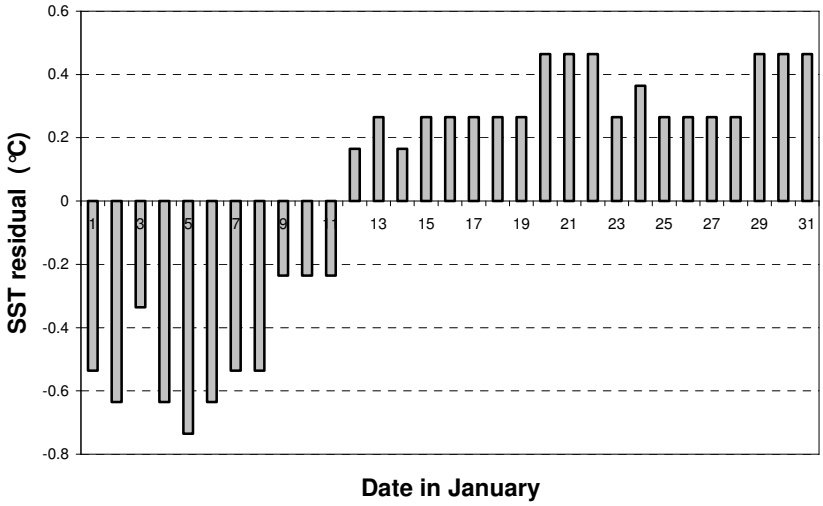

Figure 3.8 Average daily SST change in January (in *situ* buoy measurement)

SST, SST residual shows an increased trend from 1 to 31 in January, the increased rate is nearly 0.04 °C/d, that means image with early a day will plus 0.04 °C to compare with other image. Each day SST has been corrected to SST in 10th January.

The SST among one-day changes according to a Sine curve cycle (Figure 3.9), the highest SST occurs at 9:00 PM, and the lowest SST occurs at 1:00 PM, SST change one-hour lag of air temperature, and change more smoothly. The most of data acquired between 19:00 and 22:00, in this period, SST increasing rate is at 0.1 °C/h, and each time SST have been corrected to SST at 20:00 O'clock.

Cloud detection is quite difficult work according to the acquired data, acquired time is just after sunset, visible band is not efficient to detect the cloud quantitatively, especially on the thin cloud coverage, which leads to unclear border between cloud and sea surface, so the thermal bands are applied

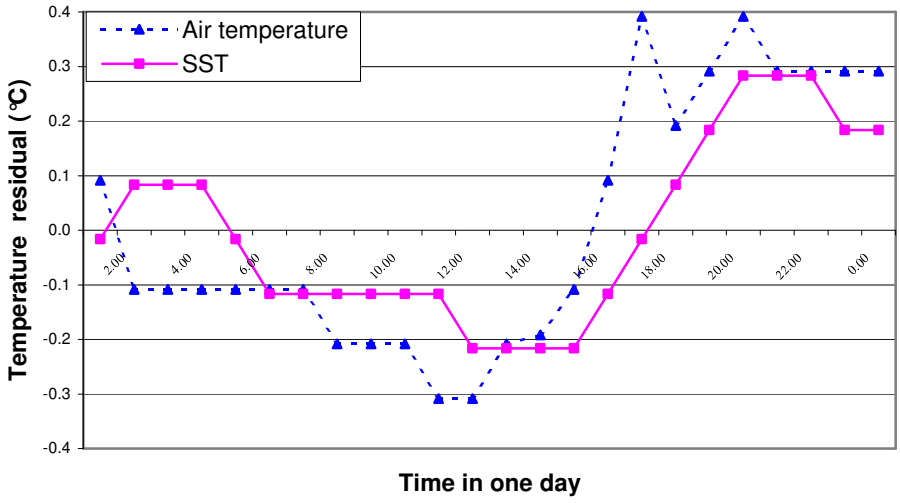

Figure 3.9 Average SST change in one day (in *situ* buoy measurement)

to distinguish the cloud. At nighttimes, sea surface emit the energy to the sensor, so does the cloud, both of them reach the sensor, but sea surface emit the much higher radiance than cloud due to their surface temperature, normally, cloud surface temperature is less than 5 ˚C at night, and SST is between 25-32 ˚C in study area, So it looks simple to identify the cloud and sea with the surface temperature calculation map, but problem is that the radiance coming from fog or thin cloud and reaching the sensor is mixed with the radiance coming from sea surface, when the radiance from the sea surface go through fog, one part of radiance is attenuated and scattered by cloud, another part directly go through to the sensor, therefore, the radiance reached the sensor compose of sea surface radiance, cloud scatter radiance, cloud radiance, this part of image will cause the error SST between 5-22 ˚C. SST changes less than 5 ˚C at spatial gradient in study area, in this moment, SST map below SST_{max} - 5 ˚C is masked as cloud or land (Equation 3.10).

$$T = T_{max} - \Delta T \tag{3.10}$$

Where T = Cloud top temperature

T_{max} = Maximum SST on image

ΔT = Thresholds, which is depended on cloud thickness. The more cloud thickness has, the larger threshold has

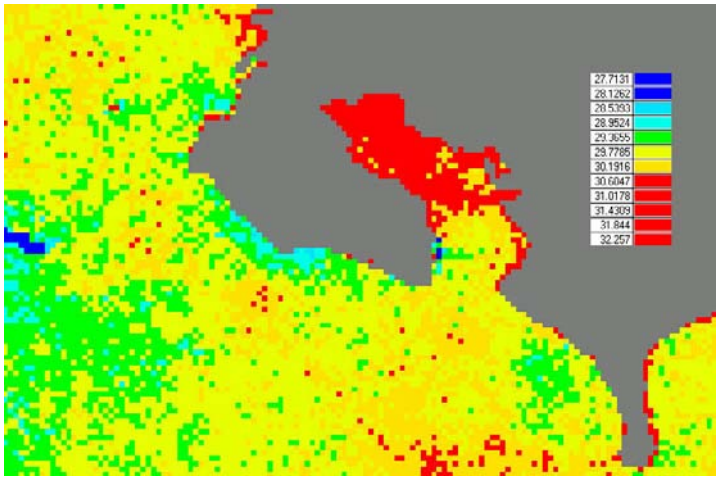

Figure 3.10 Sea surface temperature in January 1995 in Golfo Dulce

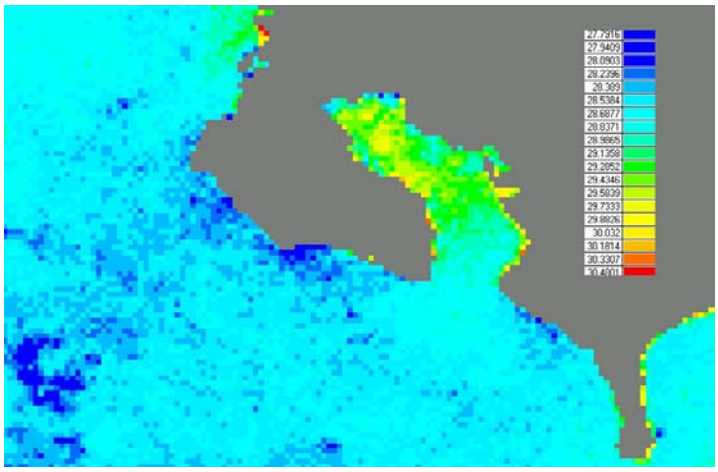

Figure 3.11 Annual average sea surface temperature in January in Golfo Dulce

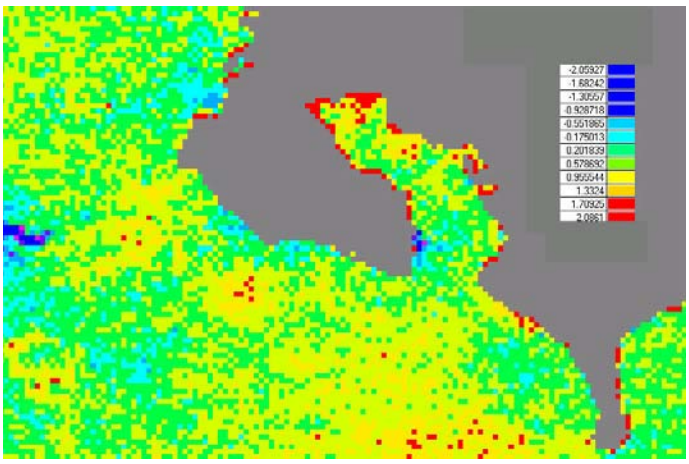

Figure 3.12 Anomalous sea surface temperature in January 1995 in Golfo Dulce

There are several factors affecting the SST when we use AVHRR thermal bands to calculate, they are water vapour, aerosols, CO_2, CH_4, NO_2, satellite zenith angle and time match, among them, absorption

To form average SST of January, there are two steps to operate, the first step is SST map mosaic to eliminate the cloud and fog coverage, the Condition Models in Erdas is applied to select cloud free patches to form the new SST map; the second step is generation of average SST map to eliminate the occasionally oscillated SST.

There are three series of products: monthly SST and multi-annual; annual average SST and annual anomalous SST; monthly change SST and annual change SST (Figure 3.10, 3.11, 3.12).

3.3.7. SST calculation relative error evaluation

due to water vapour accounts for most of the needed correction (Barton *et al.*, 1989). Now some statistic are carried out to display the errors that factor caused. If there are no atmosphere impact, AVHRR band 4 or band 5 brightness temperature could represent the SST, the atmosphere, especially

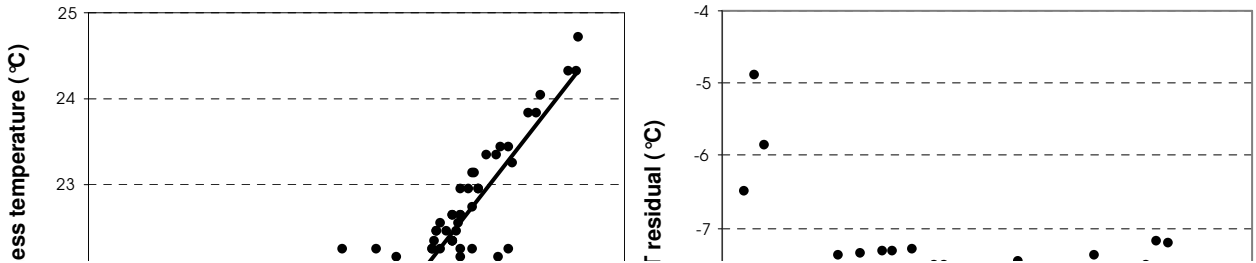

(a) **(b)**

Figure 3.13 Band 4 brightness temperature relative error analyses. (a) NLSST and B4 comparison; (b) relative errors between NLSST and B4

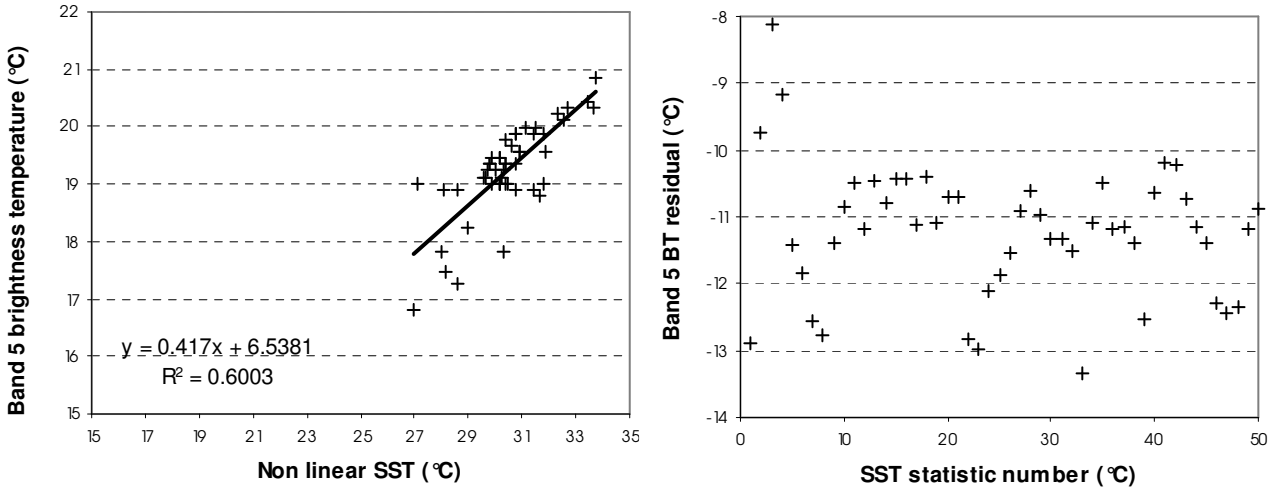

(a) **(b)**

Figure 3.14 Band 5 brightness temperature relative error analysis. (a) NLSST and B5 comparison; (b) relative errors between NLSST and B5

for water vapour, absorbs and scatters most of the radiance coming from water surface, makes the low value of SST calculation (Figure 3.13), band 4 brightness temperature has 7 °C lower than non-linear SST, and two SST have bad relation, relative coefficient is 0.7 at 50 statistic samples, the AVHRR band 5 brightness temperature has average 11.22 °C lower than non-linear SST (Figure 3.14), also has bad relativity between two temperatures, relative coefficient is 0.6 at 50 statistic samples, that means the atmosphere has large impact on the SST, which can not be neglected. The difference between MCSST and NLSST is that MCSST algorithm neglects the satellite zenith angle influence and in *situ* measurement correction, the "split window night-time" algorithm represents MCSST algorithm for

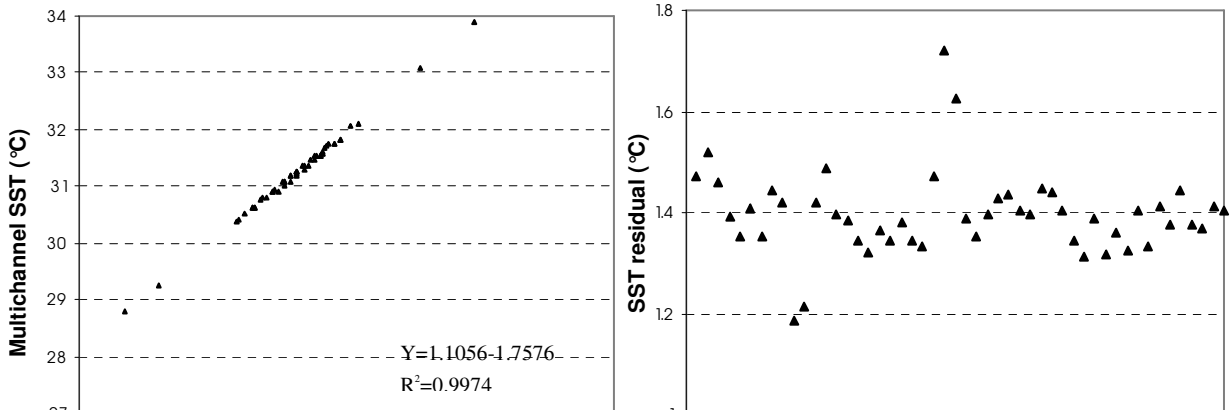

(a) **(b)**

Figure 3.15 MCSST relative error analysis. (a) NLSST and MCSST comparison; (b) relative errors between NLSST and MCSST

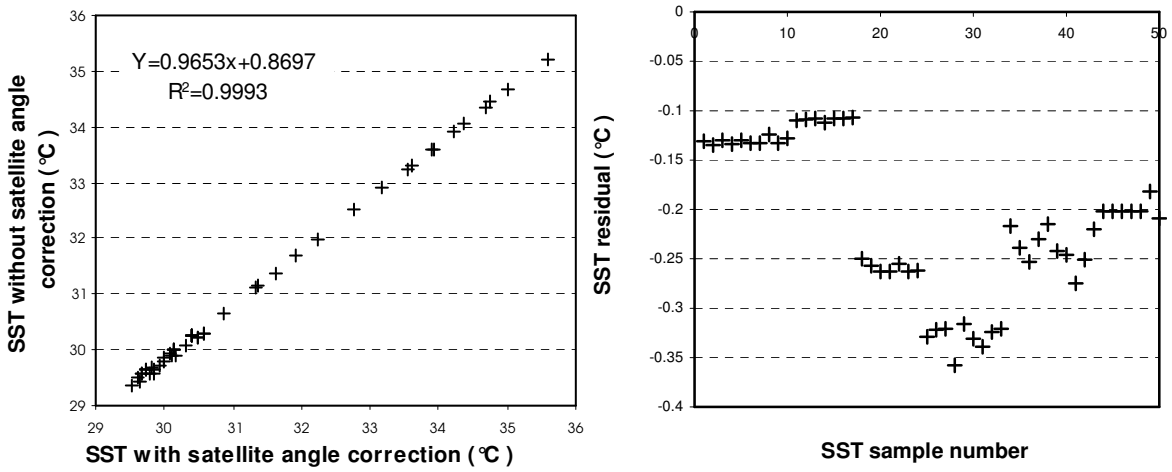

(a) **(b)**

Figure 3.16 Satellite zenith angle correction errors for SST (between 15-30 °). (a) Satellite zenith angle correction SST compared with uncorrected SST; (b) relative errors between satellite zenith angle correction and uncorrected SST.

the comparison at this moment, the result leads to the SST average 1.4 °C higher than NLSST (Figure 3.15), but MCSST has good relativity to NLSST, R is 0.99 at 50 statistic samples, that means the in *situ* measurement and satellite zenith angle only make a little adjustment for SST. We also consider how is only factor of the satellite zenith angle impact on SST, it makes SST average 0.2 °C lower than standard NLSST at 50 statistic samples (Figure 3.16)**.** Aerosol in the atmosphere in this area is very low when we check the MODIS aerosol product, so the factor aerosol is considered no impact on SST.

Compared to the factors above, the each factor average error and total RMS* have calculated (Table 3.2), the atmosphere factor (mainly water vapour) accounts for 98.6 % total error, satellite zenith angle factor accounts for 0.6 %, date match factor accounts for 0.5 %, time match factor accounts for 0.4 %. So the calculation of SST is mainly depended on the atmosphere condition.

Table 3.3 Average relative errors for SST

* $RMS = \sqrt{(X_1 - \overline{X})^2 + (X_2 - \overline{X})^2 + \cdots + (X_n - \overline{X})^2}$

Relative Errors	SST (℃)	Spatial resolution (km)
Without geometric correction		0-6
Band 4 brightness temperature	- 7.88	
Band 5 brightness temperature	- 11.22	
MCSST	1.39	
Satellite zenith angle effect (15-30°)	- 0.21	
Date match calibration (5 days)	± 0.2	
Time match calibration (1.5 hours)	± 0.15	
Aerosol impact	0	
RMS for B4 brightness temperature, satellite zenith angle, date match, time match	7.887	

3.4. Phytoplankton pigment concentration generation

3.4.1. Phytoplankton pigment detection principle

Chlorophyll is one of three basic pigments stored in plant leaf on the land, or Phytoplankton and marine species in the ocean. There are different chlorophylls, Chlorophyll-a is more popular than chlorophyll-b and-c, it plays an important role to capture energy from the sun and through the process known as photosynthesis convert water and carbon dioxide into organism and oxygen. This green pigment are chemical compounds which reflect only certain wavelengths of visible light. This makes them appear "colourful". More important than their reflection of light is the ability of pigments to absorb certain wavelengths (Figure 3.17). The chloroplast containing the chlorophyll also emit the radiance called fluorescence. Light energy absorbed by the chloroplast excites pigment molecules of the light harvesting chlorophyll proteins (LHC) and release the energy. Approximately 3%-9% of the light energy absorbed by chlorophyll pigments is re-emitted from the first excited state as fluorescence.

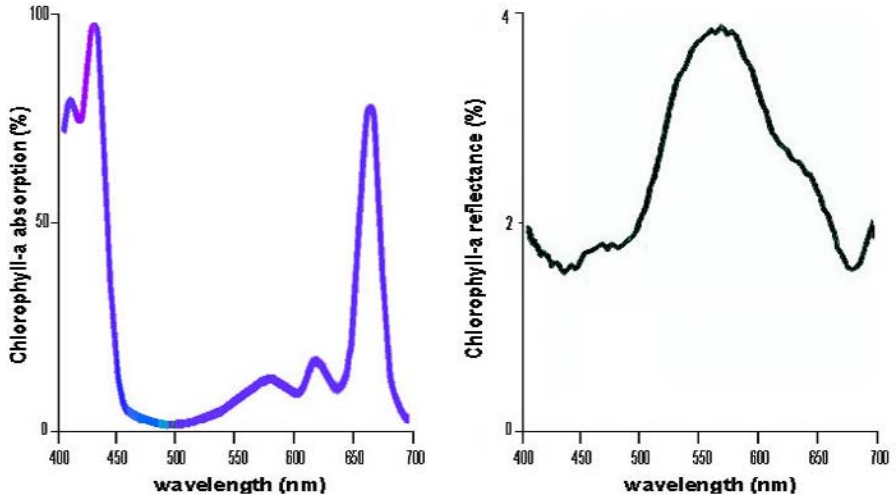

Figure 3.17 Chlorophyll-a absorption spectrum and reflectance spectrum (Internet, 2002)

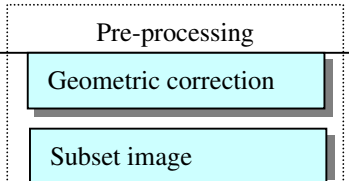

Figure 3.18 Phytoplankton pigment concentration calculation flowchart

Seawifs sensor is designed for ocean colour detection, which provides the top of atmosphere radiance data (L_t) that allows estimation of water leaving radiance in eight spectral bands, centred at wavelengths 412, 443, 490, 510, 555, 670, 765 and 865 nm, and measures PPC. There are four parts of work for total chlorophyll-a calculation (Figure 3.18): pre-processing, atmosphere correction, ocean physical factors correction, and calculation of chlorophyll-a.

3.4.2. Data pre-processing

The Seawifs L1A data are collected from internet http://daac.gsfc.nasa.gov/data/dataset/SEAWIFS/index.html, and ancillary file .MET and .OZONE attached to each image file are also downloaded from the same website address, which are applied to correct the atmosphere impact on the image. But these files can't be read by general software, the special software Seadas 4.1 is designed for calculated Seawifs image and ancillary data. So Seadas 4.1 is installed in SGI with IRIX 6.5 operation system, installation files include 4 files which are seadas_data1.tar; seadas_data2.tar; seadas_idl_rt.tar; seadas_irix6.5.tar which are not completely installed for all the functions, otherwise it need more files and space to install. Before processing the data, it is necessary to prepare the data, it includes four things: geometric correction; subset target area; land mask; cloud mask; last three steps could be done with calculation of water leaving radiance.

Geometric correction is done at first, which includes geo-reference and geo-code correction two steps. For low-resolution image, normally "screen image shift" method is a option for geo-reference correction (Figure 3.19), Seadas has embed global coastline database, it can match image with navigation information (lat/Lon data) stored in the image header, but some time it has ± 1or 2 pixel errors,

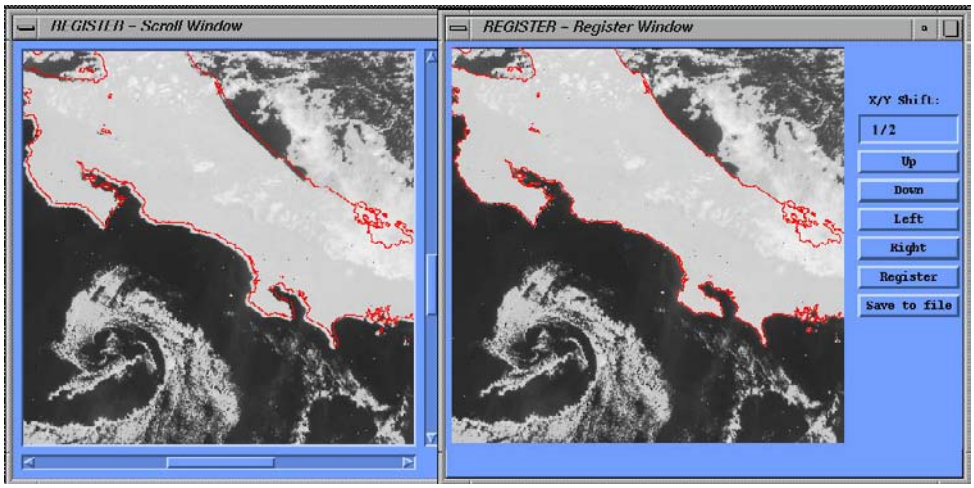

Figure 3.19 Seawifs data geometric correction in Seadas

Seadas has a module of "Register" for geo-reference correction, the band 8 (845-885 nm) is suitable to distinguish coastline and applied to shift image. Considering different distortion on different part of image, horizontal shift operation is focused on only coastline match in study area. The geo-code operation is delivered after geo-reference. Cylindrical projection is selected for re-sampling and transformation (Figure 3.20).

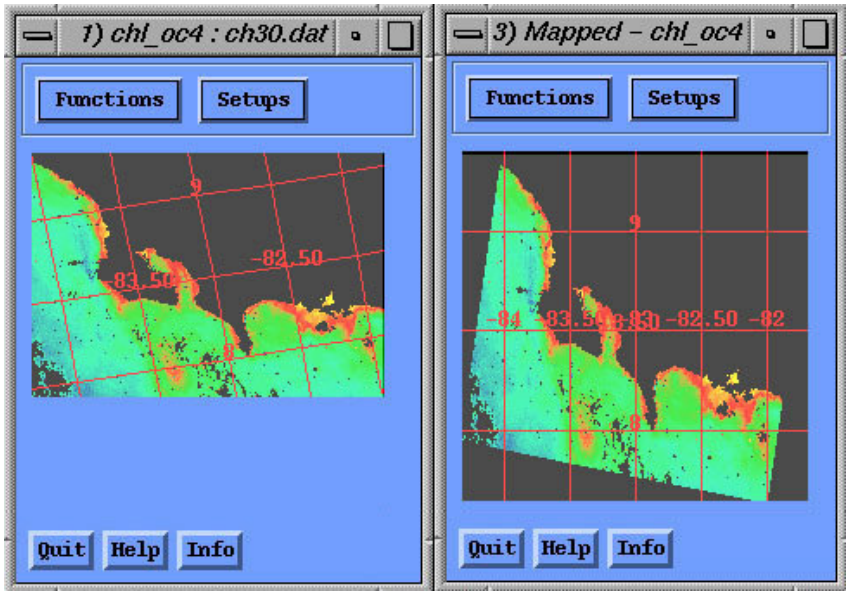

Figure 3.20 Seawifs data projection transfer in Seadas

3.4.3. Atmosphere correction on water leaving radiance

The atmosphere influences the water leaving radiance on atmosphere absorption and scattering. The radiance reach sensor include most components of atmosphere radiance (Equation 3.11) (Gordon,H.R,

$$L_t(\lambda_i) = L_p(\lambda_i) + T \cdot L_g(\lambda_i) + t \cdot L_w(\lambda_i) \tag{3.11}$$

$L_t(\lambda_i)$ = Total radiance received by the sensor;

$L_p(\lambda_i)$ = Scattering and specular reflection from atmosphere;

$L_g(\lambda_i)$ = Specular reflection of direct sunlight from sea surface;

$L_w(\lambda_i)$ = Water-leaving Radiance;

T, t = Direct and diffuse transmittance of the atmosphere;

λ_i = Sensor band.

1996), but what we are interested is the water-leaving radiance which is related to chlorophyll-a. Water-leaving radiance $L_w(\lambda_i)$ is the radiance exiting the sea surface, solar irradiance backscattered into the atmosphere from beneath the sea surface. This radiance carries information regarding the concentration of marine species. For typical marine atmospheres, $L_w(\lambda_i)$ accounts for approximately 10% of L_t in the first three bands, 4% of L_t in the green bands. The rest of the radiance is backscattered from the atmosphere and the sea surface. The water-leaving radiance is extracted from L_t through a process referred to as atmospheric correction. Clearly, atmospheric correction is particularly challenging in the green and red portions of the spectrum. A 1% error in calibration in the blue, green and red spectral regions is equivalent to an approximately 10%, 25% and 250% in $L_w(\lambda_i)$ error, respectively. The atmosphere is assumed to be composed of three layers. The top is the Ozone layer and is non-scattering, the second is a molecular scattering layer, this layer contributes most scatter radiance to the sensor, Rayleigh scatters strongly in blue region; and the third is the aerosol layer, it has both absorption and scattering characteristics. The atmosphere absorption in visible band is mainly composed of O_2, O_3, and water vapour (Figure 3.21), the Seawifs band 2, 3, 4, 5 are used for calculation of chlorophyll-a, therefore, only Ozone absorption influences on the accuracy of chlorophyll-a calculation (transmittance ρ>0.9, τ_{oz} <0.035), other factors O_2, water vapour have no impact on the four bands.

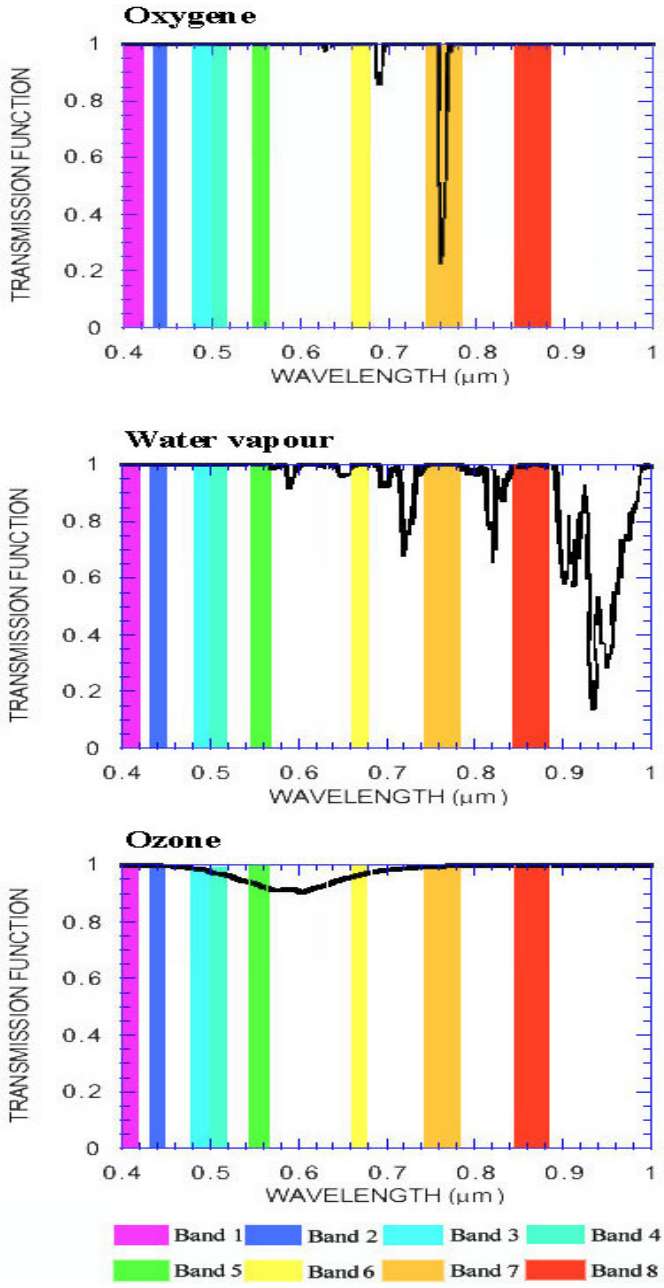

Figure 3.21 Transmissions and absorption of atmosphere in 8 SeaWifs bands (MODIS technique report)

Ozone absorption and Rayleigh scattering correction are necessary for calculation of chlorophyll-a (Figure 3.22), The Ozone optical thickness τ_{oz} and Rayleigh-aerosol optical thickness τ_r representing atmosphere impact are used in calculation algorithm of chlorophyll-a, and atmosphere optical thickness is related to the atmosphere transmittances ρ (Equation 3.12).

$$\rho = e^{-\tau} \tag{3.12}$$

Where ρ is atmosphere transmittance; τ is atmosphere optical thickness

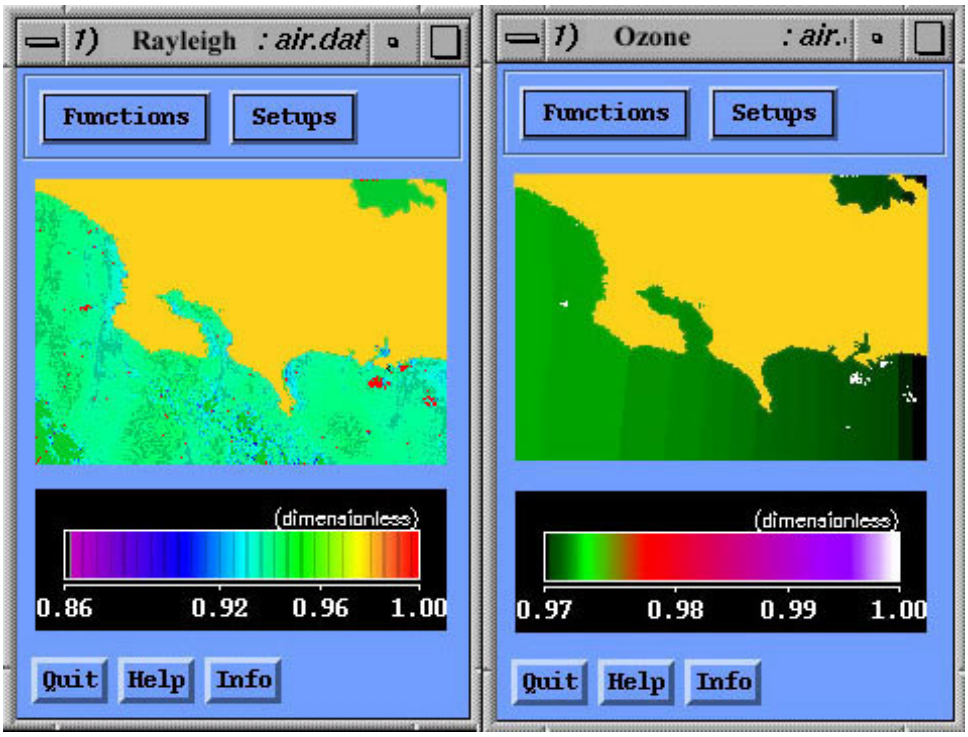

Figure 3.22 Transmittances of Rayleigh-aerosol and ozone from ground to the sensor at 555 nm

3.4.4. Suspended sediment impact correction on water leaving radiance

It is important to study the impact of suspended particulates on the phytoplankton pigment signal. In the natural world, sediments and phytoplankton interact and the upwelling radiance from water represents a composite signal corresponding to those components. Determining precisely what portion of the signal is attributed to chlorophyll alone is a complex undertaking (Alfoldi, 1980). The suspended sediment reflect more radiance than chlorophyll-a, normally, suspended sediment reflectance is between 3% and 8% at 500 µm (Figure 3.23), the class of "no sed." in the legend is corresponded to the chlorophyll and dissolved organism in the water, and chlorophyll-a reflectance is between 2% and 4% at 550 µm (Figure 3.17), so SSC contribute more information on image in single SeaWIFS band, but calculation of chlorophyll-a uses ratio of SeaWIFS band 2/5, band 3/5 and band 4/5, these process remove most impacts of SSC and dissolved organism, the spectral curve in figure 3.23 demonstrates that suspended sediments do not eliminate the prominent spectral patterns of chlorophyll-a, even as SSC reached 1000mg/l (L.HAN, 1994), but there is little change at spectral increase between spectrum 400-600 µm, the spectral increased rate in 500 µm is higher than in shorter Spectrum when SSC increase, so in this case, reflectance of SSC should be removed from the SeaWIFS band 2,3,4,5 which used to calculate the PPC.

The table of SSC reflectance at each SeaWIFS band is established from standard SSC reflectance (Figure 3.23; Table 3.4); then it is transferred to the remote sensing reflectance which is subsurface irradiance reflectance that later it will be compared to chlorophyll remote sensing reflectance. SeaWIFS have 8 visible bands, the band 6 with spectrum 660-680 µm is suitable to detect SSC, for

correction of SSC, TM band 3 is replaced by SeaWIFS band 6 because SeaWIFS data acquired time in June 26, 2001 is close to sampling time *in situ* in June 22, 2001, so we can evaluate the correction accuracy.

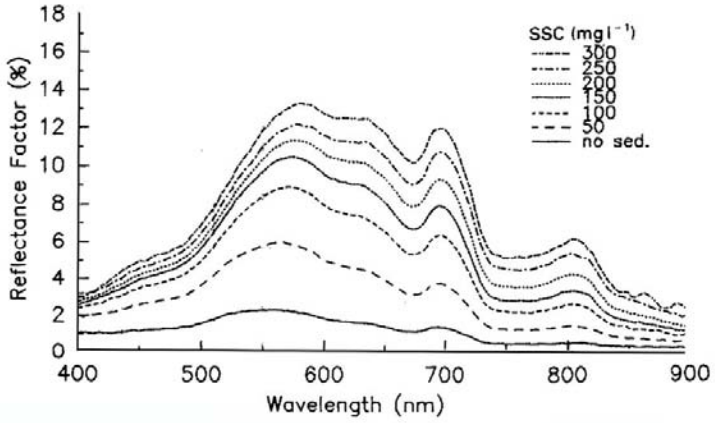

Figure 3.23 Suspended sediment spectral reflectance at varied SSC level (L.HAN, 1994)

Table 3.4 Water surface reflectance of varied SSC on chlorophyll related SeaWIFS bands

Seawifs spectrum	Surface Reflectance (SSC 0-45)	Surface Reflectance (SSC 45-55)	Surface Reflectance (SSC 55-65)	Surface Reflectance (SSC 65-75)	Surface Reflectance (SSC 75-85)	Surface Reflectance (SSC 85-95)	Surface Reflectance (SSC 95-99)
Band 440	0.0106	0.012	0.0134	0.0148	0.0162	0.0176	0.019
Band 490	0.0164	0.019	0.0216	0.0242	0.0268	0.0294	0.032
Band 510	0.0186	0.022	0.0254	0.0288	0.0322	0.0356	0.039
Band 555	0.0298	0.035	0.0402	0.0454	0.0506	0.0558	0.061

The SSC calculated from SeaWFIS band 6 will be transferred to the surface standard reflectance of SSC according to table 3.4, then surface standard reflectance of SSC is transferred to remote sensing reflectance, which is subsurface irradiance reflectance, true PPC reflectance's in band 2, 3, 4, 5 are generated from calculation of total remote sensing reflectance minus surface standard reflectance of SSC, these PPC are what I required to calculate PPC in coming section (Equation 3.15, Equation 3.16).

The evaluation of correction of SSC for PPC is made to assess the correction quality, the *in situ* samples of chlorophyll-a are compared with un-corrected chlorophyll-a map and corrected chlorophyll-a map, generally, the SSC correction for chlorophyll-a has improved 5% of accuracy of PPC

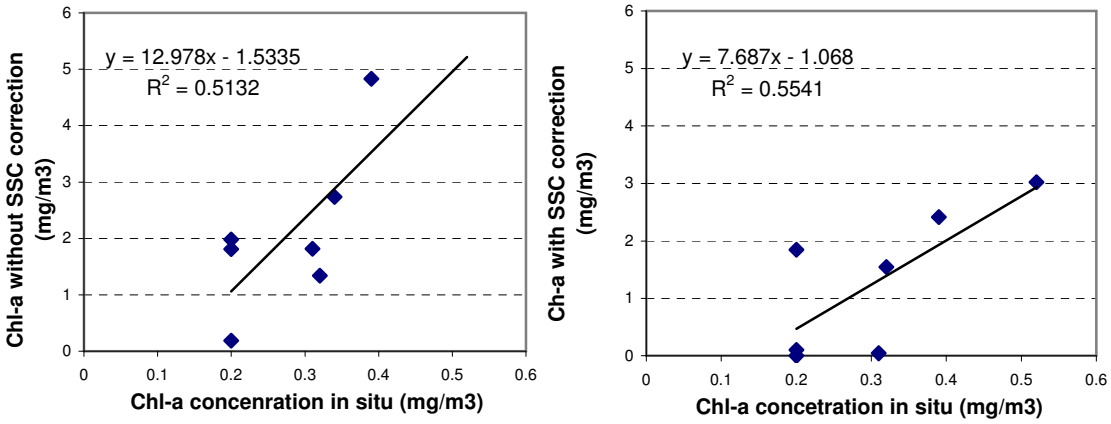

Figure 3.24 Correlation of in situ samples with corrected and un-corrected chlorophyll-a

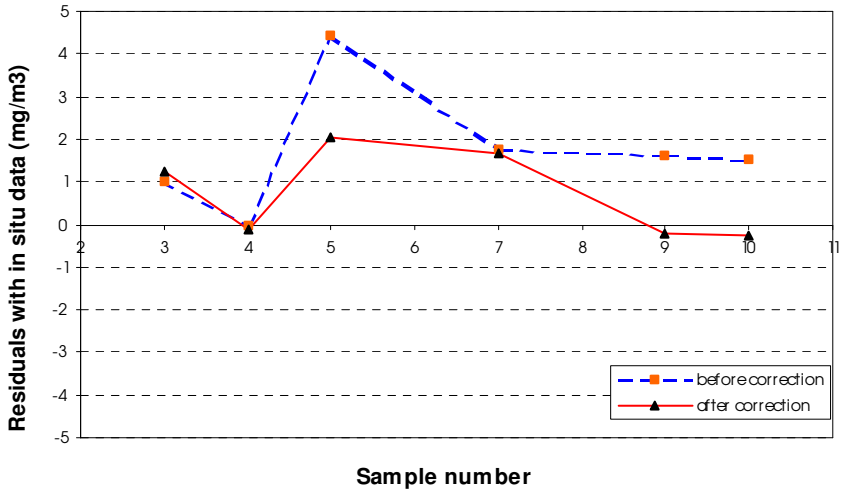

Figure 3.25 Residuals of corrected and un-corrected chlorophyll-a to *in situ* data

map (Figure 3.24), the PPC less than 2 mg/m^3 keeps unchanged or a little high after correction of SSC (Figure 3.25), the PPC more than 2 mg/ m^3 are lowered 0.5 to 15 mg/m^3, the high PPC there is, the more PPC is reduced.

3.4.5. Normalized water leaving radiance calculation

Water-leaving radiance is needed to transfer to normalized water leaving radiance to removes most of the effects of variations of the solar zenith angle. PPC is calculated from the normalized water leaving radiance. Normalized water-leaving radiance $[L_w(\lambda)]_N$, was defined according to the following equation 3.13 (Gordon and Clark, 1981).

$$L_w(\lambda) = [L_w(\lambda)]_N \cdot \cos\theta_0 \cdot \exp\left[-\left(\frac{\tau_r(\lambda)}{2} + \tau_{oz}(\lambda)\right)\cdot\left(\frac{1}{\cos\theta_0}\right)\right] \quad (3.13)$$

where $L_w(\lambda)$ is the radiance ($mw \cdot cm^{-2} \cdot \mu m^{-1} \cdot sr^{-1}$) backscattered out of the water at a wavelength λ, $\tau_r(\lambda)$ and $\tau_{oz}(\lambda)$ are the optical thickness of the atmosphere associated with molecular (Rayleigh) scattering and ozone absorption, respectively. θ_0 is the solar zenith angle.

Seadas has the function to calculate the water leaving radiance and normal leaving radiance water (Figure 3.26), normally, $[L_w(\lambda)]_N$ is larger than $L_w(\lambda)$.

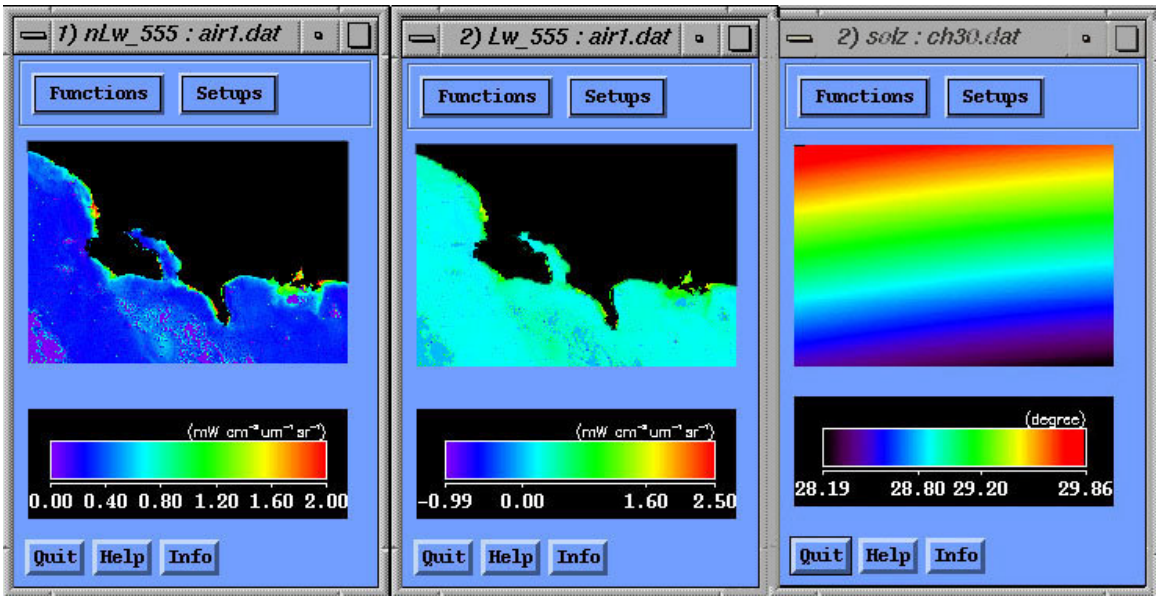

Figure 3.26 Water leaving radiance (middle), normalized leaving radiance (left) and solar zenith angle generation in Seadas (right)

3.4.6. Phytoplankton pigment concentration calculation

SeaWiFS has developed the 4-band OC4.v4 algorithm, which was parameterized with a large (n= 2,804) data set of coincident chlorophyll and spectral reflectance measurements (NASA TM 2000-206892, Vol. 11). The result of PPC is as close as possible to the in situ samples. The chlorophyll-*a* absorbs strongly in the blue-green (400-430 nm) and red regions (660-690 nm) of the light spectrum, average 50-60% absorption, and reflected on green spectrum formed the peak between 480-580 nm, reflectance is about 15-20%. These characters have responded on SeaWIFS bands 2, 3, 4, 5. The remote sensing reflectance of SeaWIFS data is calculated from $[L_w(\lambda)]_N$ (Equation 3.14).

$$R_w(\lambda_i) = \frac{\pi \cdot [L_w(\lambda)]_N}{K(\lambda_i)} \tag{3.14}$$

Where, $R_w(\lambda_i)$ is band i remote sensing reflectance; $[L_w(\lambda)]_N$ is normalized water leaving radiance; $K(\lambda_i)$ is the extraterrestrial solar irradiance;

Ratio of SeaWIFS color bands reflectance is calculated to search for the largest the reflectance of chlorophyll-a (Equation 3.15), which is suitable to all the water quality suituation. There is different reflectance or PPC in the open sea or clear sea (ocean colour Case 1) and coastal area or turbid or high concentration of chlorophyll (ocean colour Case 2) in different bands, that means any one ratio of bands can't represent PPC.

$$R_{555}^{443} = \frac{R_w(\lambda_{443})}{R_w(\lambda_{555})} = \frac{[L_w(\lambda_{443})]_N}{[L_w(\lambda_{555})]_N}, R_{555}^{490} = \frac{[L_w(\lambda_{490})]_N}{[L_w(\lambda_{555})]_N}, R_{555}^{510} = \frac{[L_w(\lambda_{510})]_N}{[L_w(\lambda_{555})]_N} \quad (3.15)$$

SeaWIFS post-launch technique report presents a corrected algorithm OC4 of chlorophyll (Jamdes L. Mueller, 2000), which have a log relation to subsurface irradiance reflectance (Equation 16). This

$$C_a = 10^{(0.366-3.067R_{4s}+1.930R_{4s}^2+0.649R_{4s}^3-1.532R_{4s}^4)} \quad (3.16)$$

Where $R_{4s} = \log_{10} Max\left(R_{555}^{443}, R_{555}^{490}, R_{555}^{510}\right)$, C_a = PPC (mg m^{-3}).

equation uses a maximum reflectance ratio. The 443-555 ratio is always the maximum in low-chlorophyll (blue) waters, but as the PPC increases, reflectance in the 443-nm band diminishes due to the strong absorption of chlorophyll at that wavelength. Eventually, the 490-555 ratio or 510-555 becomes larger. This algorithm has an advantage over previous switching algorithms (e.g., the CZCS algorithm) in that there is no inherent discontinuity between chlorophyll values at the point where the switch occurs. But this equation is designed for global ocean monitoring, it is high accurate in open

Table 3.5 Parameter threshold of chlorophyll-a calculation

Parameter	Threshold
Cloud albedo	1.1
Sun zenith angle	75
Satellite zenith angle	50
Minimum epsilon	0.85
Minimum epsilon	1.35
Minimum nlw (555)	0.15
Wind speed limit	8
Maximum 865 aerosol optical depth	0.3
Absorbing aerosol threshold	0.5
Lt 865 for stray-light correction	0.25
Number of pixel for stray light correction (-1 for default, 0 for no correction)	-1

sea, but there is some errors occur around coastal zone, especially in shallow water with SSC. In our case studies, the in situ samples are used to calibrate the algorithm.

Seadas is the capable function with algorithm OC4 to calculate the chlorophyll-a, and it contains the land mask and cloud mask file, the parameter threshold is needed to set up by users before the calculation, in this case, the thresholds are filled in according to table 3.5, and subset studied area on image calculation.

3.4.7. PPC mosaic and mean PPC calculation

The mean monthly PPC in 1998 is expected for estimation of phytoplankton primary production, so each day of every month chlorophyll-a is averaged to generate mean monthly PPC, but chlorophyll-a changes stable, normally, it can keep unchanged volume for one week, for our case study, we select image data each 10-15 day, 2-3 scenes for each month, and average them to form mean monthly PPC, but in the rainy season, cloud is common covering the test site, the more images are selected for mosaic of the image to eliminate the cloud on image. When mosaic operation is conducted, time match should be considered, some factors are concerned, one is variety of chlorophyll-a, and another is sensor's radiometry parameter change, and other factors influences the PPC are SST, sea current, nutrient. SST change more than one week, tide current is change quickly, normally less than one day, but in study area, tide current is weak due to the unique Gulf shape, so we consider chlorophyll-a unchanged in 3 days, the date of images selected less than 3 days for mosaic if a lot of cloud coverage occur. For sensor radiometric match, the approach of image mean difference offset is used, the mean of image DN values are calculated for obtaining the average difference value of two time images, this value is offset for one of image to keep two time images the same the mean DN values.

3.5. Suspended sediment concentration extraction

Confined by operation conditions, conventional investigation involves hard fieldwork to located many sites for the accurate mapping of the distribution of suspended sediment in a large water area. Since satellite remote sensing has a great advantage in a quantitative approach of SSC many efforts have been made in the study of relevant wave bands and models. As the radiation transfer processes in water are very complicated, many models have been proposed to obtain the relation between remote sensing data and SSC. The linear relevant relation was the earliest model used to estimate SSC from remote sensing data. Munday and Alfoldi (1979) proved that the logarithm relation is better than the linear relation for remote sensing of SSC. Philpot (1981) presented the radiative transfer model for remote sensing of vertically inhomogeneous water. Those models are:

- The linear model

$$R = A + B \cdot S \tag{3.17}$$

Where R is the reflectance, S is the suspended sediment concentration, and A, B are relevant coefficients

Because it is of its limited form and its tendency to be highly erroneous, its use is usually limited in the early stage of remote sensing application.

- The logarithm model

$$R = A + B \cdot \log S \tag{3.18}$$

This formula can only depict the relation between SSC and remote sensing data well when the concentration is not too high within a small range of concentration distribution. It should be noted that great discordance may appear in high concentrations when the distribution range is large, since it is applied extensively.

- The Gordon model

$$R = C + \frac{S}{A + B \cdot S} \tag{3.19}$$

A, B, C are parameters. This is based on a quasi-single-scattering radiative approximate model (Gordon, 1973) that is used less popularly than the logarithm formula.

- The negative index model

$$R = A + B \cdot (1 - e^{-D \cdot S}) \tag{3.20}$$

This model is developed by Li Jing (1986) makes some improvement for high concentration but discrepancy still exists because of adopting some approximate condition.

- The united model

$$L = A + B \cdot (\frac{S}{G + S}) + C \cdot (\frac{S}{G + S}) \cdot e^{-D \cdot S} \tag{3.21}$$

in this case study, remote sensing data will be compared to SSC samples *in situ*, and establish the correlation formula to calculate SSC. The procedures include the pre-processing and SSC extraction (Figure 3.27).

Geometric correction is conducted at first for five images, 15 GCP points are selected for each slave image, most points are selected on unchanged points, but no coastlines selected for GCPs due to tidal change modification of the coastline, GCPs are collected as accurate as possible to keep each RMS error of GCP less than 1.0 (30 m), total RMS of GCPs are less than 1.5 (45 m) (Figure 3.28).

Considering the changes on sensor's sensibility and atmosphere condition on images, multi-temporal data of images are required radiometric match before comparison of multi-temporal data, in this case is SSC comparison, all the geometric images are matched to TM image in January 31, 2001 which is closed to sampling data, the method of histogram is used for image match, then comparing the image January 31 to sample measurement *in situ*.

Land part on image should be masked before calculation of the SSC, otherwise, water SSC map will be confused with land part The TM band 4 is suitable band for detection of the border of land and sea water due to its large different DN values between land and sea along coastline, the DN

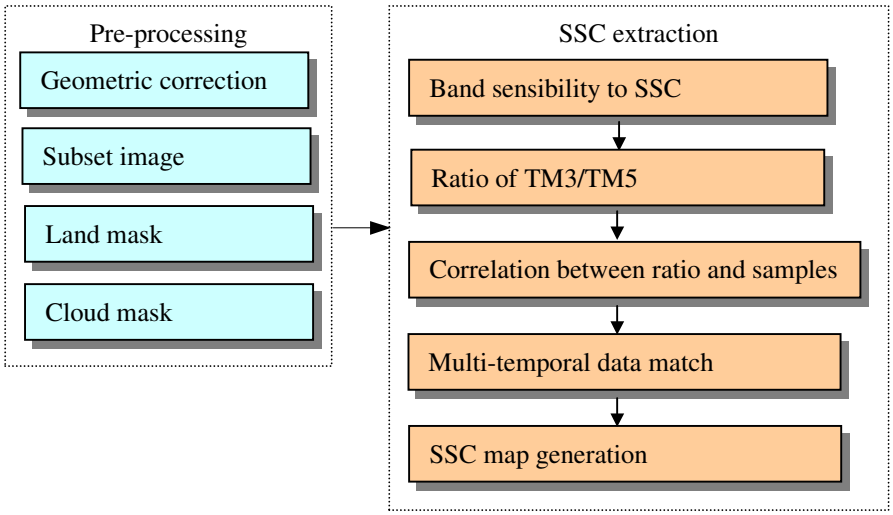

Figure 3.27 Suspended sediment concentration processing flowchart

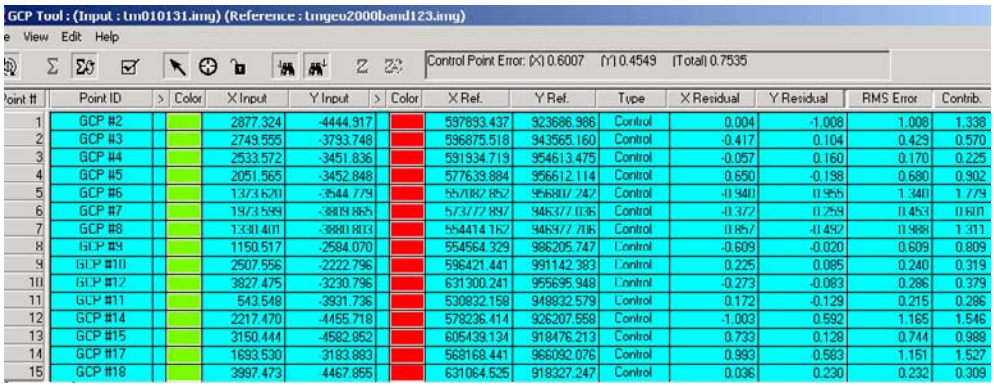

Point #	Point ID	Color	X Input	Y Input	Color	X Ref.	Y Ref.	Type	X Residual	Y Residual	RMS Error	Contrib.
1	GCP #2		2877.324	-4444.917		597893.437	923686.986	Control	0.004	-1.008	1.008	1.338
2	GCP #3		2749.555	-3793.748		596875.518	943565.160	Control	-0.417	0.104	0.429	0.570
3	GCP #4		2533.572	-3451.836		591934.719	954613.475	Control	-0.057	0.160	0.170	0.225
4	GCP #5		2051.565	-3452.848		577639.884	956612.114	Control	0.650	-0.198	0.680	0.902
5	GCP #6		1373.620	-3544.779		557082.857	956807.747	Control	-0.940	0.965	1.348	1.779
6	GCP #7		1973.599	-3819.865		573772.897	946377.036	Control	-0.372	0.259	0.453	0.600
7	GCP #8		1331.401	-3880.813		554414.162	948977.706	Control	0.857	-0.492	0.988	1.311
8	GCP #9		1150.517	-2584.070		554564.329	986205.747	Control	-0.609	-0.020	0.609	0.809
9	GCP #10		2507.556	-2222.796		596421.441	991142.383	Control	0.225	0.085	0.240	0.319
10	GCP #12		3827.475	-3230.796		631300.241	955695.948	Control	-0.273	-0.083	0.286	0.379
11	GCP #11		543.548	-3931.736		530832.158	948932.579	Control	0.172	-0.129	0.215	0.286
12	GCP #14		2217.470	-4455.718		578236.414	926207.558	Control	-1.003	0.592	1.165	1.546
13	GCP #15		3150.444	-4582.852		605439.134	918476.213	Control	0.733	0.128	0.744	0.988
14	GCP #17		1693.530	-3183.883		568168.441	966092.076	Control	0.993	0.583	1.151	1.527
15	GCP #18		3997.473	-4467.855		631064.525	918327.247	Control	0.036	0.230	0.232	0.309

Figure 3.28 Geometric correction for TM images and ASTER

value measured on image along coastline indicates that most land has DN value large than 70, and sea water is less than 25, but the close value between land and sea appears on the estuary, which high SSC in water made DN a little bit high, so the DN value 49 is can separate the most of land and water, the DN more than this value is land, other part is sea water. When the 5 mask files from each original image are generated, land is defined DN as 2, seawater is defined as 1. We find result is not

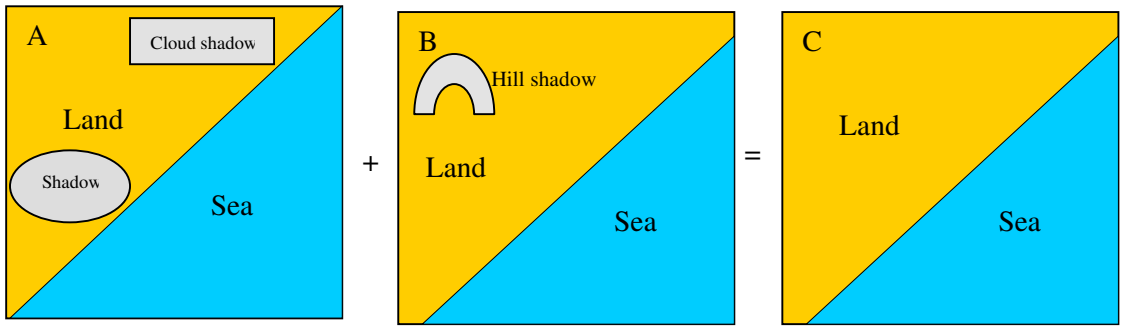

Figure 3.29 Image low brightness elimination on land with multi-temporal and multi-sensor data after land mask processing.

the map we expect due to a lot of low DN values appear on land part, in this tropical region it is corresponded to 80% cloud shadow, 15% hill shadow and 5% water body on land, but the favourite thing is shadow is moved, and also for hill shadow according to change of solar zenith angle and satellite zenith angle, temporal data overlay could remove 90% these low values on the land (Figure 3.29). The five images of multi-temporal and multi-sensor (TM and ASTER) data are overlain and choice maximum value on image will remove the most shadow on the image, but land border will be move closely to the coastline in low tide due to image acquired in different tidal stage. Then all the original images are overlain with this terminal mask file to mask land.

The TM band or spectrum is tested for sensibility to the SSC in water, so as to detect the SSC. The samples of SSC *in situ* is compared to each TM bands (Figure 3.30), the brightness indicates that

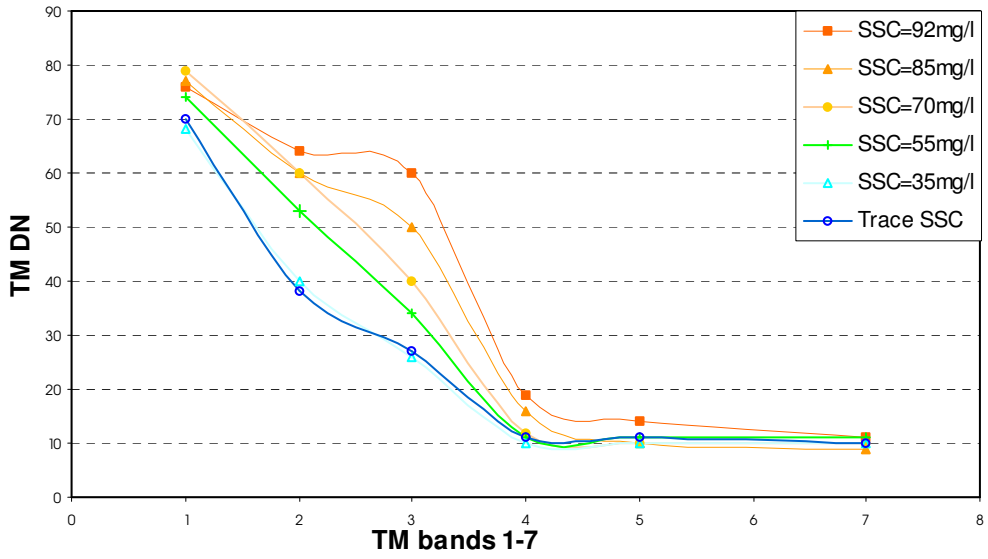

Figure 3.30 TM band brightness at varied SSC

brightness in TM band 1, 4, 5, 7 is changed a little when SSC increased, which are not suitable to apply to distinguish the SSC, TM band 2 and 3 both have large variety according to SSC change, TM band 3 is changed totally larger than band 2, but band 2 change larger in low SSC, so at last we select TM band 3 as detection band, so as to ASTER band 2. For water objective detection, the atmosphere

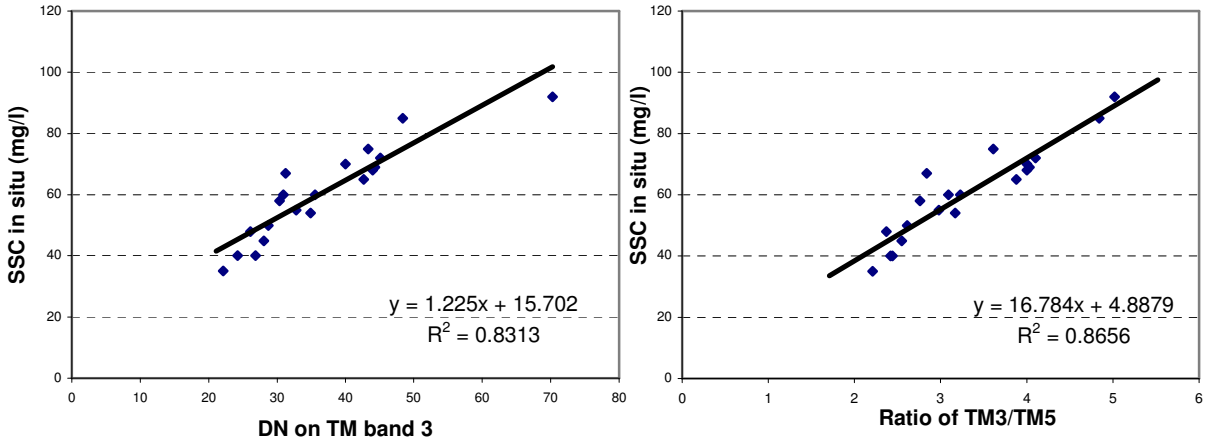

Figure 3.31 Correlation of SSC *in situ* with TM image

can't be neglected, there are a little change in TM band 5 of SSC, and band 5 has atmosphere absorption and scattering, so TM band 3/5 is alternative to TM band 3 for detection of SSC in water, which can remove most of atmosphere impact on the image (Figure 3.31), correlation of SSC in situ with DN in TM band 3 and ratio of TM band 3/5 are compared to check its quality, result shows that ratio of TM band 3/5 has higher correlation than TM band 3, it improves 3.43 % error accuracy, that means this alternative is suitable to detect SSC in this region, and we check the correlation between SSC in

situ and image DN in pervious algorithm mentioned above (Figure 3.32), log (SSC)correlation with ratio of TM band3/5 is not as good as linear correlation, it reduces the coefficient of determination, the reason only I can infer is that SSC in this region is range in low level, and it is not suitable to log

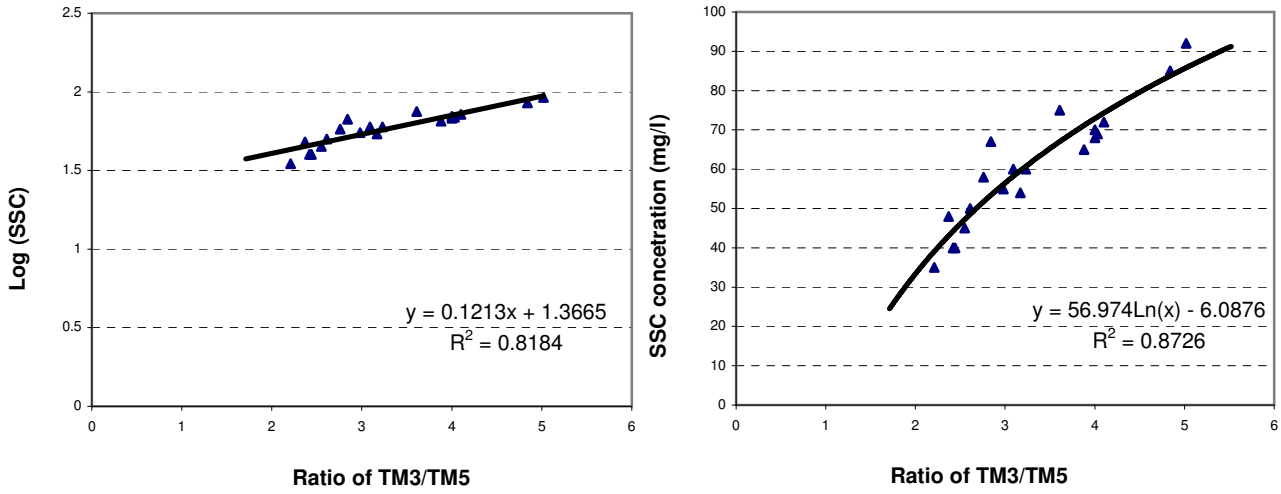

(SSC). But Ln (TM band 3/5) has good correlation with SSC *in situ* (Figure 3.32), coefficient of determination is highest. This equation is applied to this region SSC detection. The 4-time SSC distribution maps are produced according to this algorithm, another ASTER image only covers little test site.

Figure 3.32 Correlation of SSC *in situ* with TM image

3.6. Sea current speed and direction detection

Knowledge of wind velocity over the ocean is of critical importance for understanding and predicting many oceanographic, meteorological, and climate phenomena. Wind stress is the single largest source of momentum to the upper ocean, and winds drive oceanic motions on scales ranging from surface waves to basin-wind current systems. Wind momentum transferred from the air to the sea by the wind causes the surface of the ocean to become rough. Changes in wind velocity cause changes in surface roughness, which in turn modify the radar cross-section of the ocean and hence the magnitude of the backscattered power. Scatterometers measure this backscattered power, allowing estimation of the normalized radar cross-section (σ_0) of the sea surface. A scatterometer's ability to measure vector winds derives from the fact that σ_0 is a sensitive function both of wind speed *W* and relative direction *X*. In our case study, the two data sources are involved, Seawind scatterometer data with 25

km spatial resolution are applied to detect the wave speed and direction, these data and products of each day since August, 1999 are available on internet http://podaac.jpl.nasa.gov/quikscat/; and ERS AMI image data in January and February, 2001 will be merged to one image to analyse detail texture features of wave speed and direction.

ERS AMI data is processed in speckle suppression and Luminance enhancement, speckle suppression is operated in moving window with size 3 to remove noise points with high DN value on image; Luminance Modification option of the Image Enhancement functions is an adaptive enhancement filter, which separates the original image into two parts: the scene luminance and the scene contrast. The two parts are modified and recombined to create the enhanced output (Figure 3.33).

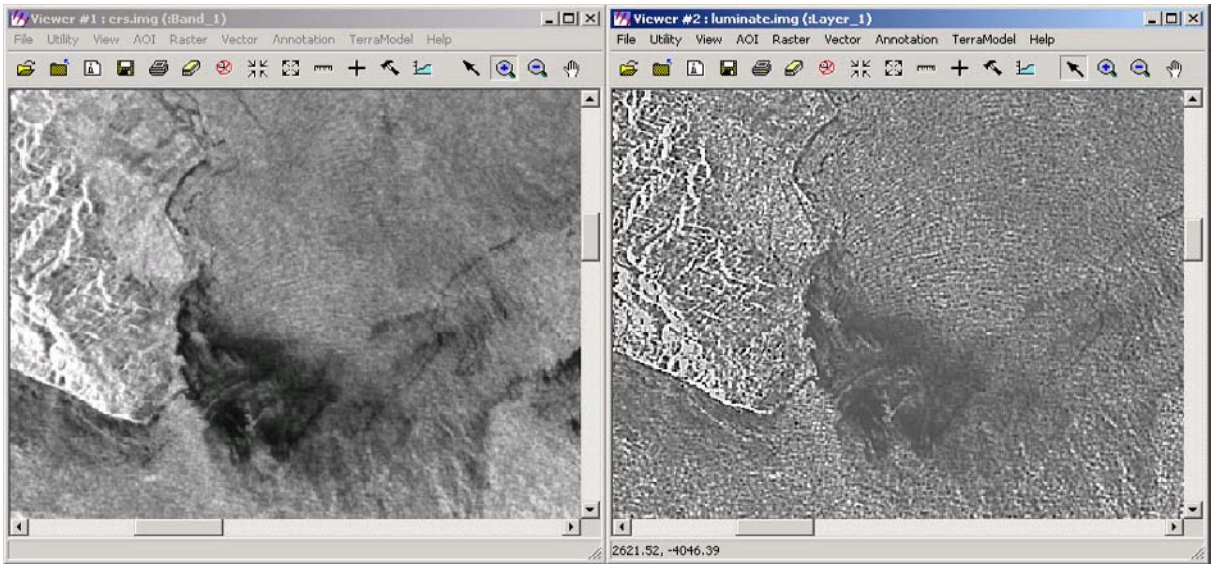

Figure 3.33 ERS AMI SAR (C-band) image enhancement with luminance modification (left: speckle process; right: luminance process)

3.7. Conclusion

The methodology for this case study focused on the processes and calculations of sea surface temperature, phytoplankton PPC, SSC and wave direction and speed. The raw data, calculation formula, and result quality have been compared and evaluated.

The sensor AVHRR has powerful 3 thermal bands for detection of SST; SeaWIFS has 20 nm narrow visible bands for measurement of PPC; TM has spatial resolution for measurement of SSC plumes; Seawind has ability of quick detection of wave height with SAR.

The calculation of non-linear SST is applied in this study, which have three advantages: (1) split window technique is used to remove atmosphere impact; (2) sun zenith angle correction; (3) real-time buoy *in situ* data correction. The match technique of date and time for mosaic of monthly SST is applied to remove temporal SST difference, and cloud top temperature technique is suitable for detection and removal of clouds. Total result quality of non-linear shows that the atmosphere impact reduces SST 7.88 °C in band 4 and 11.22 °C in band 5, satellite zenith angle reduces SST 0.21°C, date match affects SST ± 0.2°C, time match affects SST ± 0.15°C.

OC4.V4 algorithm is applied for calculation of phytoplankton PPC. This algorithm has an advantage over previous switching algorithms in that the maximum of band ratio is selected for calculation and there is no inherent discontinuity between chlorophyll values at the point where the switch occurs. The algorithm has consideration of the factor impacts of Rayleigh scattering, Ozone absorption, solar zenith angle, application of band ratio removes the most impacts of SSC and yellow organism and makes high quality of calculation.

Statistical algorithm of SSC calculation is applied in Golfo Dulce, Natural logarithm has R^2=0.87 high correlation with *in situ* samples. TM band 3 has sensitive to detect SSC in high SSC and TM band 2 has sensitive to SSC in low SSC, the ratio of band 3/5 can remove atmosphere impact, and improves accuracy 3.43 %.

Chapter 4: Spatio-temporal analyses of physical processes in Golfo Dulce

4.1. The Gulf geomorpholoy and closeness

The gulf landform, especially underwater morphology, extremely affected the local ocean physical process and gulf chemical features. The Golfo Dulce is a special gulf in the tropical ocean due to its tectonic formation in geological history; it has an underwater "sill" at gulf mouth, which makes the more close to the features of lakes.

The bathymetry map is produced to simulate the underwater gulf morphology. 231 points of depth are input in ILWIS and the "moving average" method is applied to interpolate bathymetry map (Figure 4.1), and the VirtualGIS function in ERDAS is applied to model 3-D of gulf bathymetry, vertical scale is enlarged 30 times (Figure 4.2). The gulf displayed in map shows a long narrow gulf, and it is very deep inside gulf base, the deepest of gulf is distributed in northwest base with –200 meter deep, and it gradually changes to shallow in the mouth of Gulf and forms a sill underwater with depth of –60 meter, gradient degree of slope inside base (in section C) is 0.042, gradient degree of slope at sill (section A) is 0.007; the slope inside base is 6 times higher than it at sill. Now we analyse its closeness of gulf. The principles of dividing the closeness of gulf are depended on the two parts: horizontal closeness and vertical closeness, horizontal closeness contributes more affection to water physical processes and vertical closeness contributes more affection to water chemical features, vertical closeness is more important than horizontal closeness, the quantitative formula is set up to evaluate gulf closeness (Equation 4.1), and we classify the ocean according to this closeness (Table 4.1).

$$GC = \frac{2GC_h + GC_a + GC_s}{4} \tag{4.1}$$

Where: GC = total gulf closeness, value between 0-100%;

GC_h = vertical depth closeness, the water maximum depth in gulf divided by maximum depth of water at gulf mouth

GC_a = vertical intercept area closeness, vertical water intercept area at inside base divided by difference between water intercept area at inside gulf and gulf mouth; if the difference is negative, $GC_a = 0$

GC_s = surface closeness, gulf perimeter divided by gulf coastline;

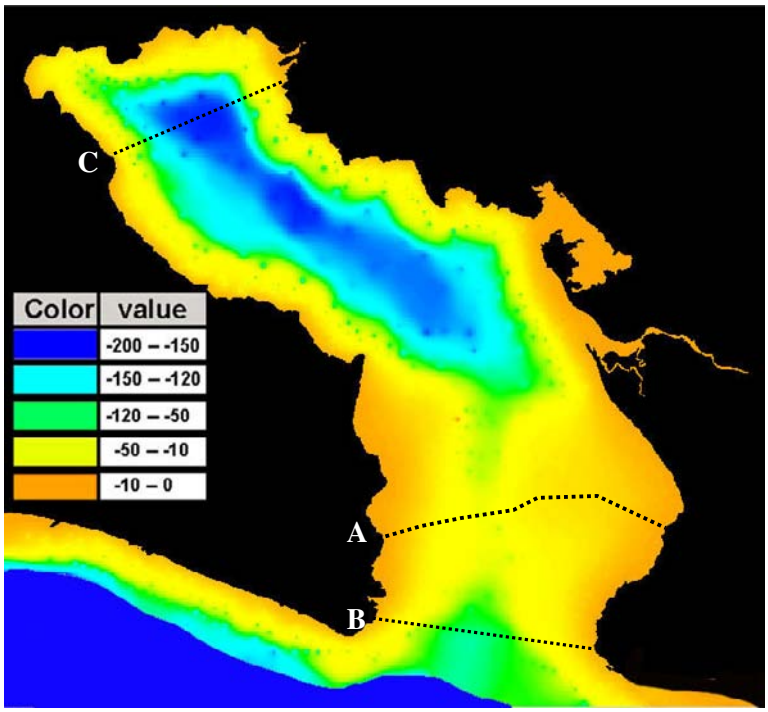

Figure 4.1 Bathymetry map in Golfo Dulce, Costa Rica

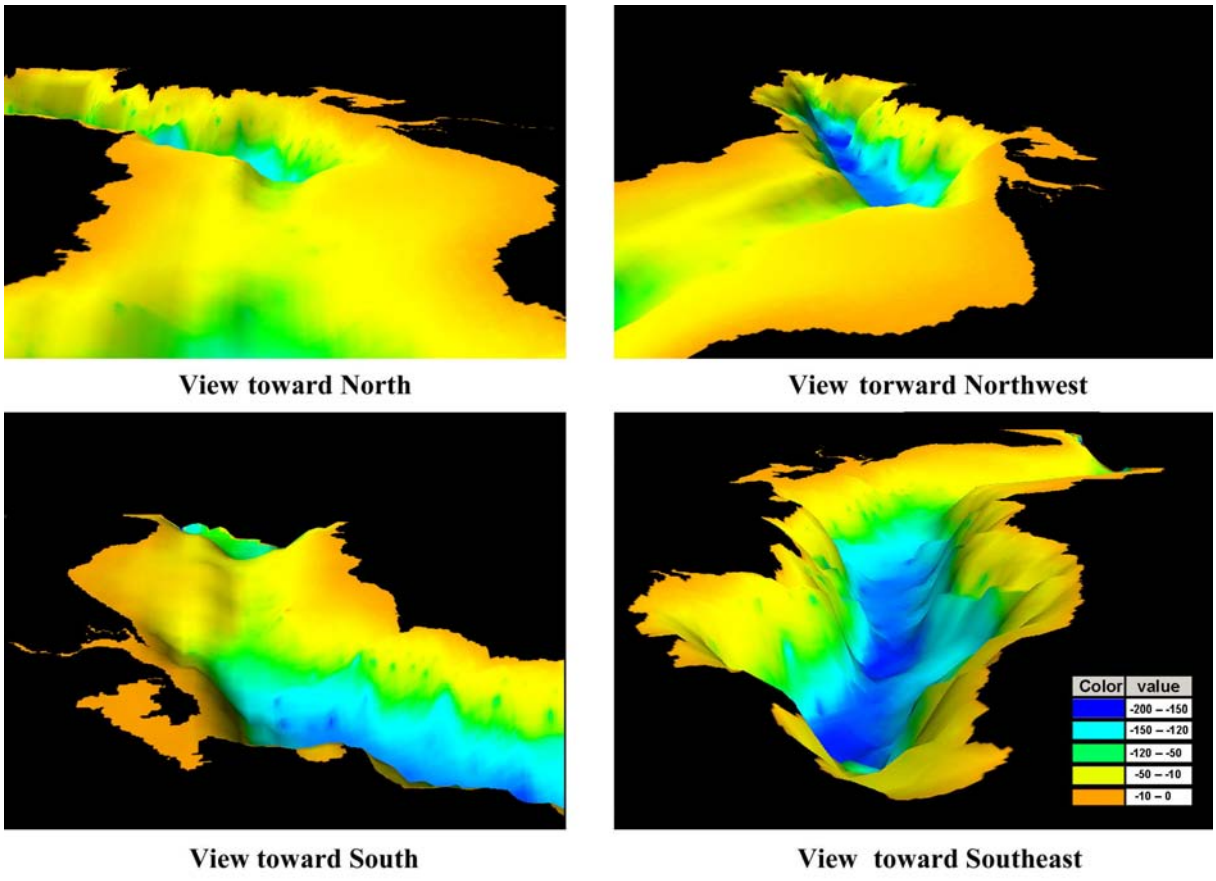

Figure 4.2 Gulf morphology display in a 3-D model of bathymetry from different directions

The total gulf closeness is calculated (Table 4.2), surface closeness is performed from gulf perimeter divided by gulf coastline, it belongs to high closeness of gulf with 92.86%. The vertical border of Golfo Dulce is located at sill, vertical depth closeness is about 70.3%, and we calculate the vertical water profile area at sill and inside base, which are corresponded to seawater exchange with the Gulf. The water profile inside base is higher than it at sill, the vertical closeness

Table 4.1 The gulf closeness classification total ocean closeness

Type	Open sea	Low closeness gulf	Moderate closeness gulf	High closeness gulf	Lake
Classes	0-30%	30-50%	50-70%	70-90%	90-100%

Table 4.2 The gulf horizontal and vertical closeness in Golfo Dulce, Costa Rica

Approaches (m)	Gulf coastline	Gulf perimeter	Closeness (%)
Surface closeness (GC_h)	191529.93	206245.82	92.86%
	At "sill"	Inner base	
Vertical depth closeness (GC_h)	- 60	- 202	70.30%
Vertical intercept area closeness (GC_s) (m^2)	1156163.55	1540985.08	75.03%
Total gulf closeness (GC)			77.12%

reaches 75.3%, the total gulf closeness of Golfo Dulce is 77.12%, which belongs to high closeness ocean gulf. Therefore, the seawater is limited to come into the gulf when tide and wave are active, it leads to anoxide features inside base in depth of 80 meter and reduced marine environment, this layer of reduced environment is more higher than outside of gulf mouth, which looks as features of lake, since it is located at equator, water temperature are always the same year round, and the depth of gulf is quite deep, vertical water convection is weaker than normal lake in high latitude.

4.2. Spatio-temporal SST analysis

Sea surface temperature is important factor affected on the global climate change and marine species distribution. Normally, sea surface temperature is controlled by solar irradiance, seawater in equator absorbed more energy transfer the heat from equator to poles, but varied atmosphere condition and seasonal change of irradiance cause complex SST distribution in the ocean, predominated wind and trade wind change heat propagation direction and cause anomalous SST.

4.2.1. Spatial SST distribution and anomaly analysis

The SST distributed in Golfo Dulce change smoothly at spatial scale, high temperature is around 29.88 °C according to 11 year's average at 21:00 January, which is located inside gulf, average temperature in the gulf is about 29.34 °C, SST range from 28.8 to 30.5 °C (Figure 4.5), and lowest

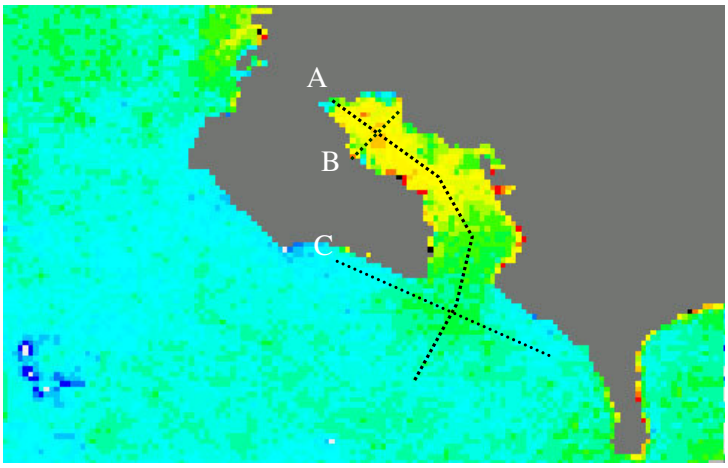

Figure 4.3 Annual average sea surface temperature distributions. A: profile along the Gulf; B: profile across the Gulf; C: profile across the Gulf mouth.

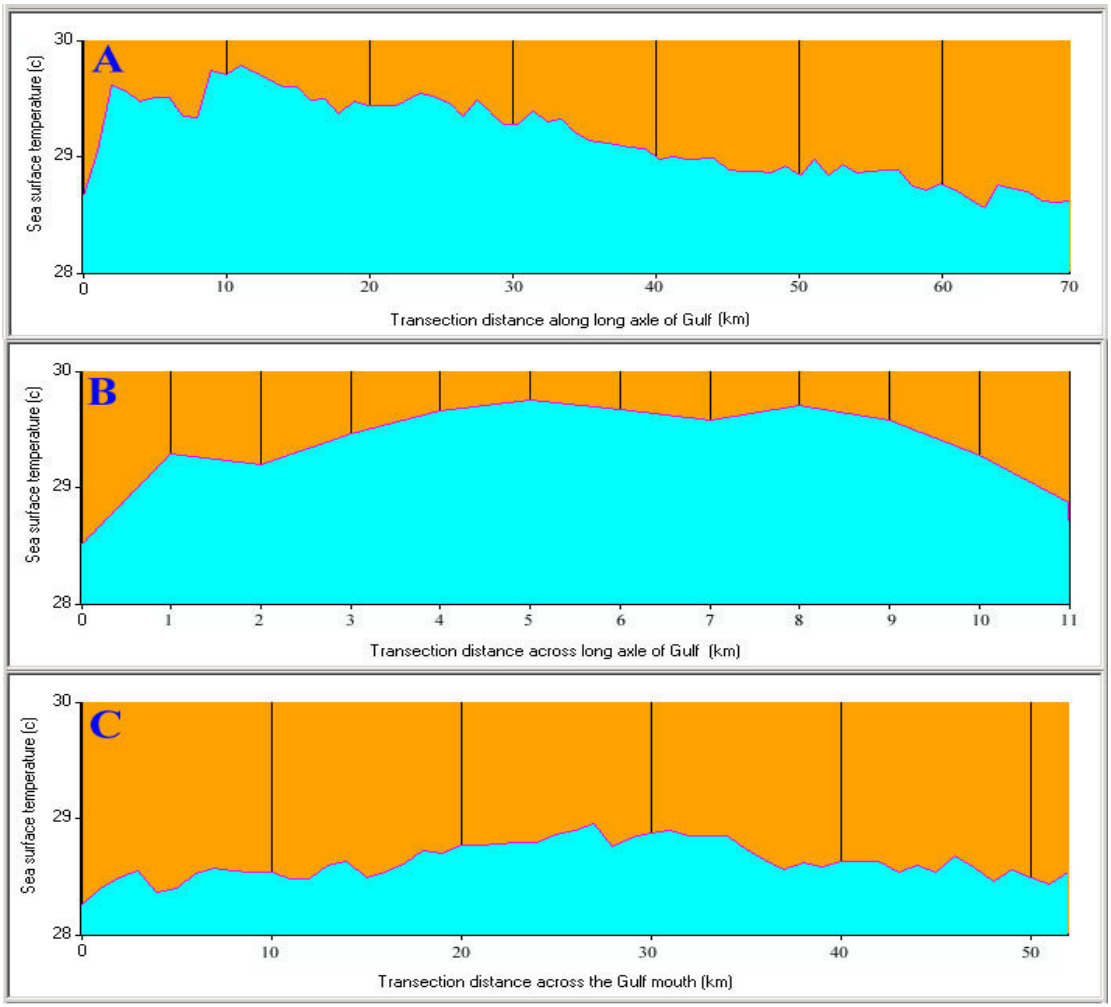

Figure 4.4 Transaction sea surface temperature analyses in the Gulf

temperature is around 28.22 °C, which is located in open sea, average SST in open sea is around 28.65 °C, SST ranges from 28.3 to 28.9 °C, the SST is higher than outside of gulf and SST range is also larger than open sea.

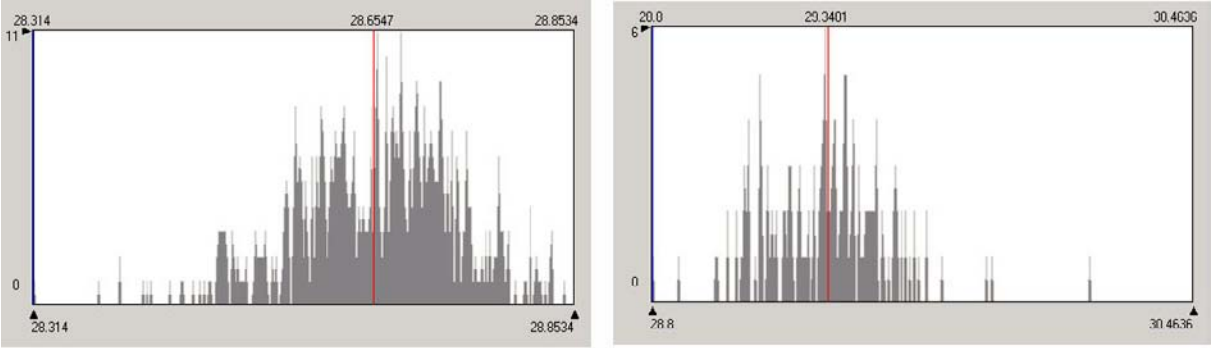

Figure 4.5 Sea surface temperature histogram inner gulf and outside of gulf

The spatial profiles of A, B, C are made to analyse the spatial SST change gradient (Figure 4.3; Figure 4.4), the SST is reduced from inner gulf to open sea according to profile A, the SST gradient is 0.02 °C/km, the profile B of inner gulf shows the middle of gulf has higher temperature than coastal water, the SST gradient is 0.25 °C/km, the profile C at gulf mouth indicates gentle change of SST, the SST gradient is 0.027 °C/km, there are three conclusions from above analyses: (1) The SST is higher inside gulf than outside gulf; (2) The SST in middle gulf is higher than in coast water; (3) heat in surface water is transferred from gulf to open sea. It is can be inferred that sea current is weaker and more stagnant than open sea due to the morphology of the Gulf, heat flux is difficult or slow to transfer to deep water, keep surface temperature high; other reason can be inferred that peninsula OSA and Puntarenas mountain surrounding the Gulf, which have elevation more than 600 meter high and 30-40 degree steep slope, result in the sea wind blocked and weakened, sensitive heat and evapotranspiration from sea surface to air in the Gulf is comparatively slow; land reflects more solar radiance to atmosphere comparing to water reflection, land keeps lower amount of energy than water, coastal land absorbs part of heat of water and balances the energy lost to the air, so water temperature along coastline is lower than it in the middle gulf.

4.2.2. Annual SST tendency and anomaly analysis

There are two product series of SST for analysis: annual SST 1991-2001 and monthly SST in 1998 in Golfo Dulce, annual SST analysis is focused on annual anomalous oscillation and relation to ENSO event, monthly SST analysis will be focused on season's change and its response to the solar radiance and local climate action.

Annual SST changes a little in this small study area, there is 1.5 °C oscillated annually in open sea from 1991 to 2001, 2 °C oscillated annually inside the gulf (Figure 4.6), but except for the year 1997-1998 when El-Niño happened. SST in the Gulf are oscillated larger than in open sea, we can infer that SST inner Gulf has more impact by coastal land temperature or local mountain-base climate, but now we have not more evidences show its affection. Considering the long term SST ten-

dency, no any sign for SST, no matter in open sea or inner gulf, indicates the increase or decrease trend, probably due to too short time series. Now the absolute SST and relative SST are analysed on annual SST results between 1991 and 2001.

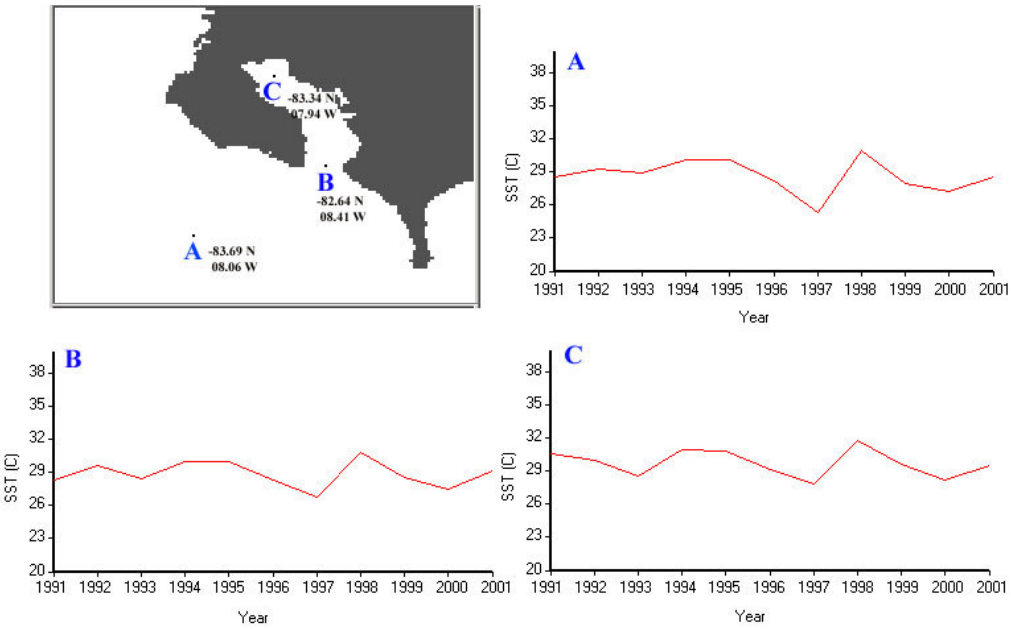

Figure 4.6 Annual sea surface temperature oscillation in 1991-2001 at open sea (section A), the Gulf mouth (section B), inner Gulf base (section C).

Absolute SST changed is characterized in Golfo Dulce, Costa Rica. The SST in last decade is ranged from 28.0 to 31.0 °C for most part water surface (Appendix 1); we define SST more than 31.0°C as "hot spot" or "warm pool" according to its size and temperature, and consider SST less than 28.0 °C as "cool poor" or "cold tongue" also according to its size and temperature. The maps of hot water and "cold tongue" are extracted from SST in 1991-2001 (Figure 4.7). We find "hot spot" of SST is located in inner base before El-Niño in 1998, when SST is increased, "hot spot" is stretched to northwest or southeast along the gulf long-axle, hot pool is moved to east of the Gulf since El-Niño event in 1998. "Hot spot" happen in 1991, 1994-1995, 1998, 2001, there is a 3-4 years cycles of "hot spot". The "cold tongue" happens around the gulf mouth, it normally shows a long shape like tongue inserting to the gulf from southwest to northeast, "cold tongue" starts at west border of the gulf mouth, then stretch to east of the gulf like meander, the furthest can reach end of the gulf, it happens in 1991, 1993, 1997, 1999, 2000, there is two year cycles, but not clear. Normally, "hot spot" event and "cold tongue" are occurred alternatively, the reason of "hot spot" occurred is mentioned in section 4.2.1, but why the "hot spot" move to east since El-Niño keeps unknown; "cold tongue" is moved from open sea and move along counter-clock direction, so "hot spot" is caused by the gulf morphology, and "cold tongue" is caused by open sea SST oscillation.

Anomalous SST is concerned about relative change compared to normal SST. The classification is divided to produce anomalous SST maps (Table 4.3), SST difference more than 0 represent the SST increased at the same place, and SST difference less than 0 represent the SST decreased, the 11 anomalous Maps are generated (Figure 4.8; Figure 4.9). Analysed on the anomalous maps, it is clear that there are no more anomaly of SST in 1991, 1992, 1993, 1996, 1999, 2001, the anomalous high SST happened in 1994, 1995, 1998, the anomalous low SST happened in 1997, 2001, the largest posi-

tive anomalous SST occurred in 1998, and the largest negative anomalous SST occurred in 1997, there is no rule or cycle of change at time scale, the interested phenomena is that water in the west

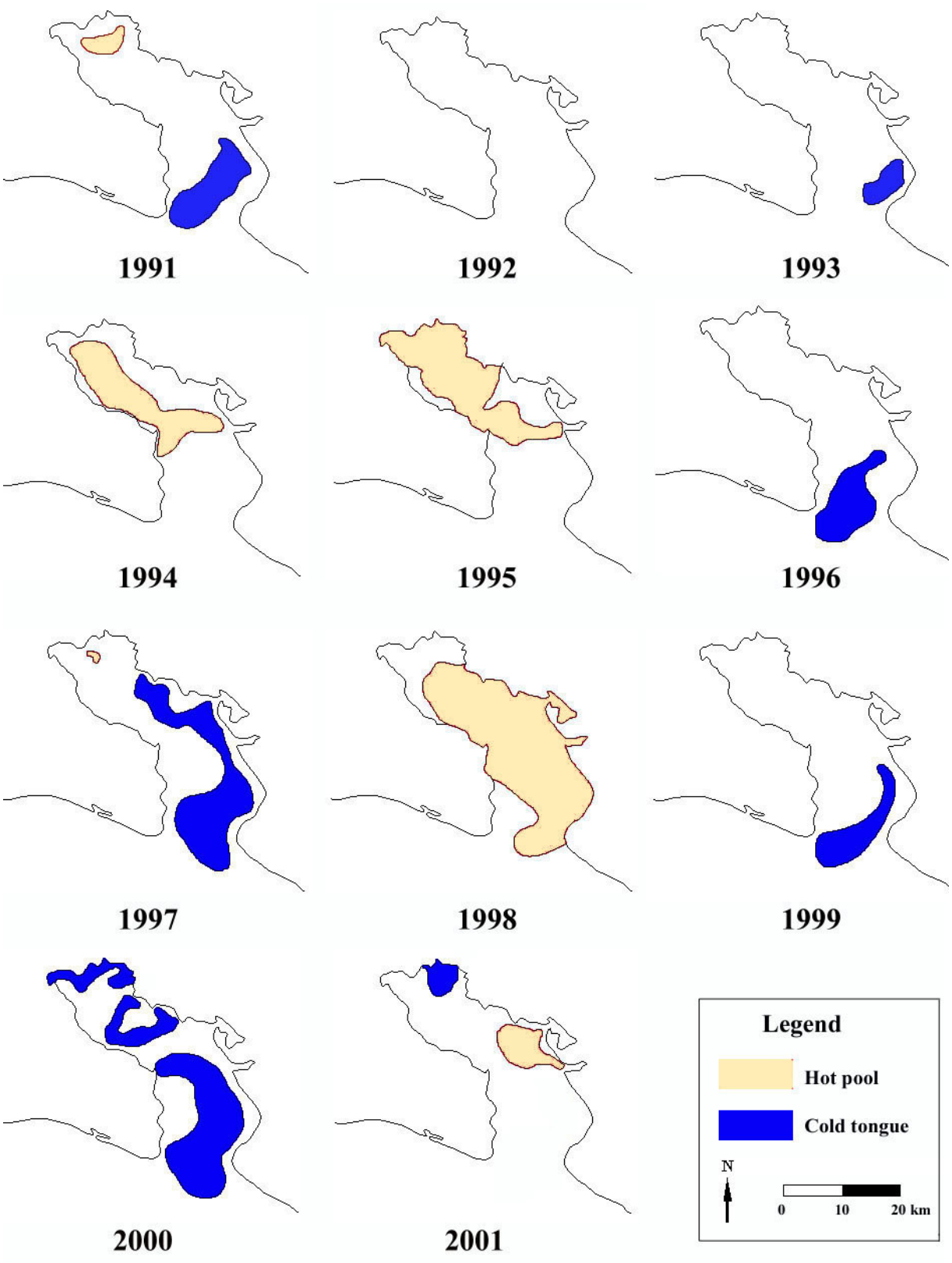

Figure 4.7 "Hot pools" and "cold tongues" of sea surface temperature in Golfo Dulce, Costa Rica

Table 4.3 Annual anomalous sea surface temperature classifications

Anomalous SST range (℃)	Classification
< -1.5	Very low SST
-1.5 — -0.5	Moderate low SST
-0.5 — 0.5	Normal SST
0.5 — 1.5	Moderate high SST
> 1.5	Very high SST

of inner gulf is insensitive to SST change in extremely SST occurred, such as in 1997 and 1998, the SST in this place is higher than most other place with anomalous low temperature in 1997, and the SST in this place is lower than most other place with anomalous high temperature in 1998, it is can be infer that anomalous temperature is caused by out of gulf, and inner base SST is impacted weaker than open sea due to its unique geomorphology.

4.2.3. Monthly SST tendency and anomaly analysis

Monthly SSTs in 1998 are produced for analysis. Monthly SST change much larger than annual mean SST changes. SST in first 6 months is different to the rest months in 1998 in Golfo Dulce (Appendix 2), SST in the most part of ocean are 31-32 °C in 1998, 2 °C higher than normal year in the same month, SST increase from January to April (Figure 4.10), and is peaked in April, then drop quickly from April to July, SST drop 5 °C from 32 °C to 27 °C, SST oscillate from August to the end of 1998, the mean lowest SST occur in October, SST of inner gulf is 1-1.5 °C higher than out of the gulf. The open sea has a little different curve, SST peak occurred in March, when it has 1-month earlier than inner gulf, it is inferred that water heat is conducted from open sea to the gulf.

The SST is controlled by solar irradiance, but it is extremely affected by atmosphere condition and other factors. Now the extraterrestrial solar radiance is calculated according to solar azimuth angle and zenith angle, sun-earth distance (Figure 4.11), the highest two solar radiance occur in March 26 and September 6 at top of atmosphere, when the distance is comparatively close and sun zenith angle is low. The extraterrestrial solar radiance is almost constant year round due to its tropical location, the standard deviation is 0.52 (MJ/m^2) (Figure 4.12), but the ground solar radiance is modified by air condition during the wet season from May to November, which there are a lot of cloud and rain during this time, the peak number of radiance is reduced to one, highest ground solar radiance appears in March and lowest radiance in October, that is why there are high SST in dry season from December to April, and low SST in rainy season from May to November.

The solar irradiance on sea surface is divided to the radiance reflection, radiance absorption and transmitted energy, the radiance absorption then emit its energy in three approaches: subsurface heat flux to deep water, sensible heat and latent evaporation to the air. The SST should have good correlation with ground solar radiance if the following factors are neglected:

(1) Wind condition keeps the same which affects the water surface evaporation;
(2) Water clarity keeps unchanged which affects water leaving radiance and transmittance;
(3) No sea current occurred which affects horizontal heat flux change.

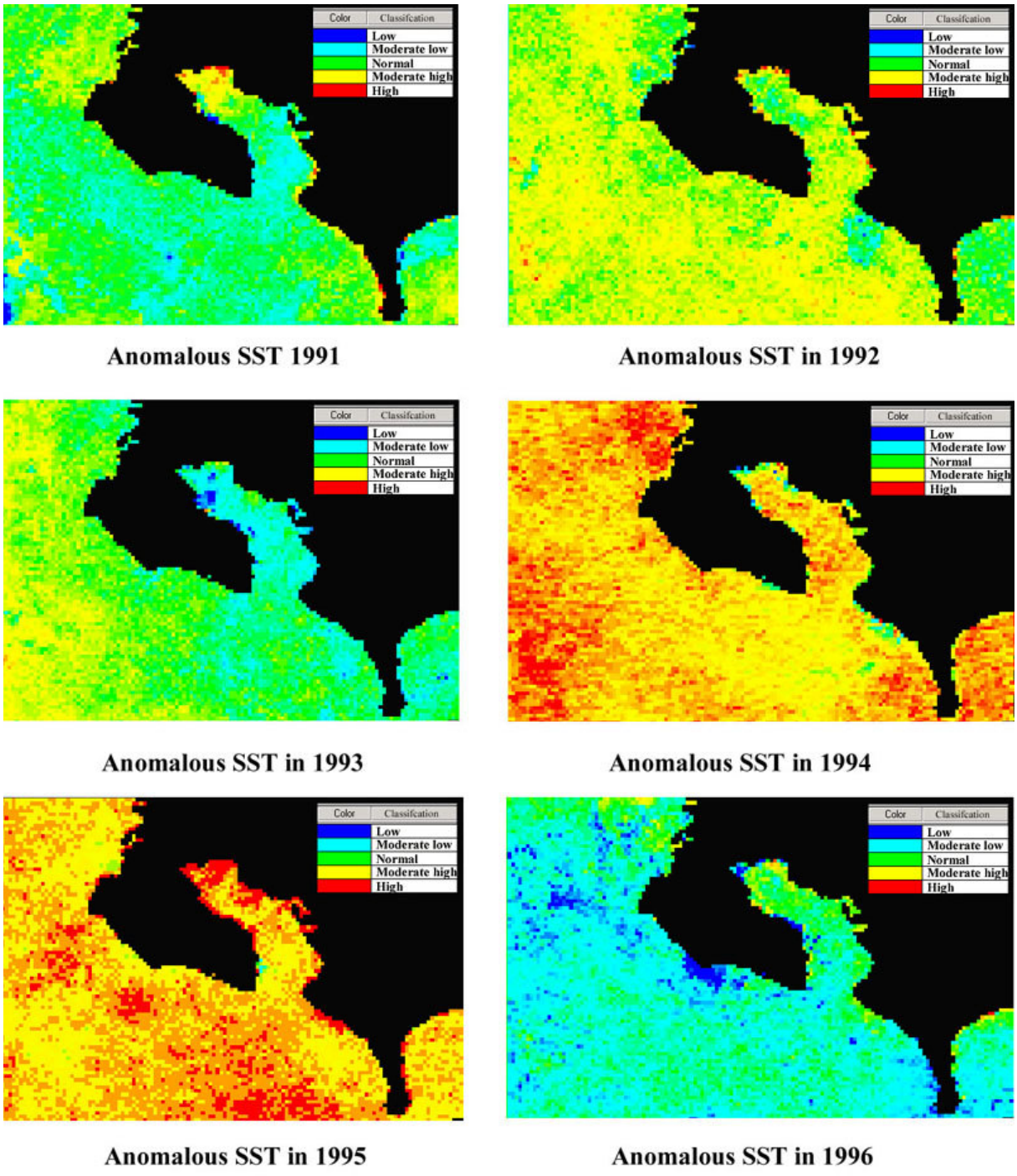

Figure 4.8 Annual anomalous sea surface temperature maps in Golfo Dulce, Costa Rica (Series 1)

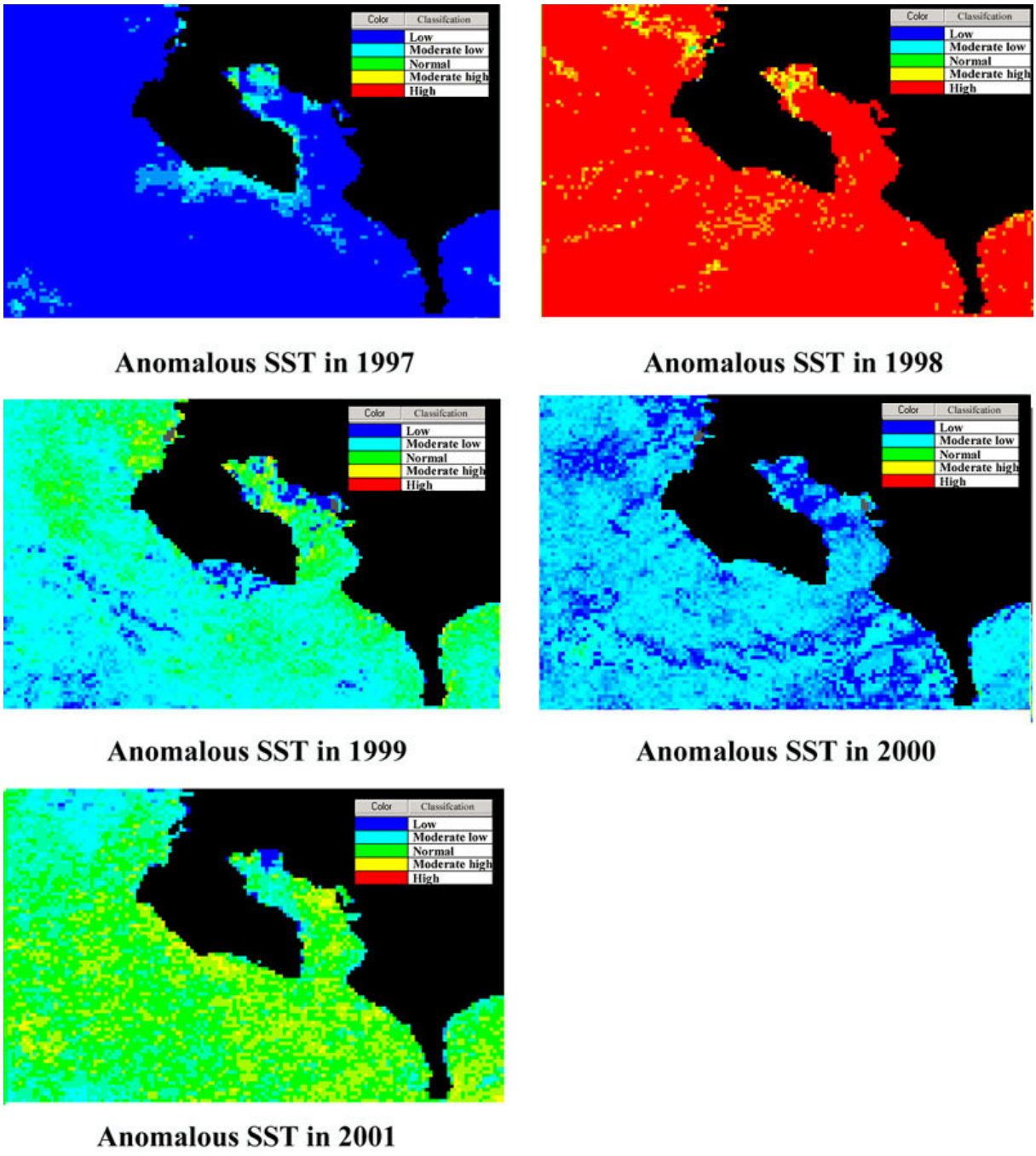

Figure 4.9 Annual anomalous sea surface temperature maps in Golfo Dulce, Costa Rica (Series 2)

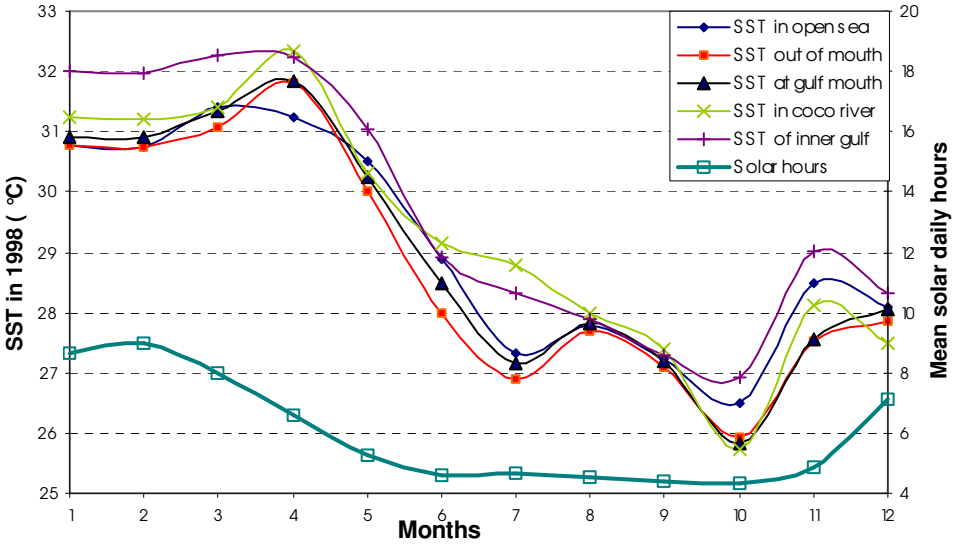

Figure 4.10 Monthly sea surface temperature from open sea to the inner gulf and daily solar hours in 1998

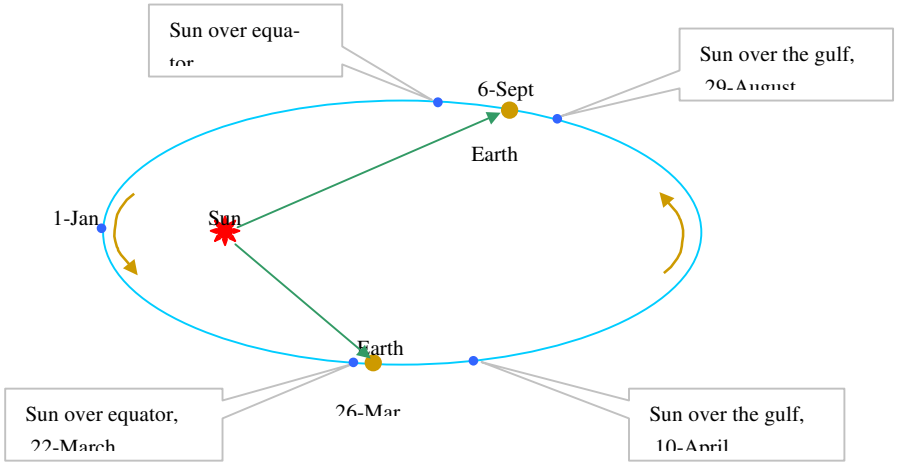

Figure 4.11 Relationship between peak solar radiance and earth rotation in Golfo Dulce

The monthly mean solar hours in 1998 replacing the ground radiance are compared to SST in open sea and inner Gulf (Figure 4.13), the SST both in open sea and inner gulf have bad correlation with ground solar hours, the inner gulf is better than in open sea, but it is noted that there is a phase change between the solar hour curve and SST curve (Figure 4.10), the correlation will be different if the curve of solar hours shift 2 month forward (all positions of solar hours on X-axle plus 1 unit), the results of correlation improve 60% and 50% in open sea and inner gulf respectively, the coefficient is changed from 0.24 to 0.84 in open sea, and from 0.49 to 0.99 in the inner gulf. The conclusion is that solar hours directly control the SST in the gulf, there are excellent correlation between SST and solar hours, but there is 2-month delay for seawater “warming up” by solar radiance, SST out of the gulf has bad correlation due to horizontal heat flux influence.

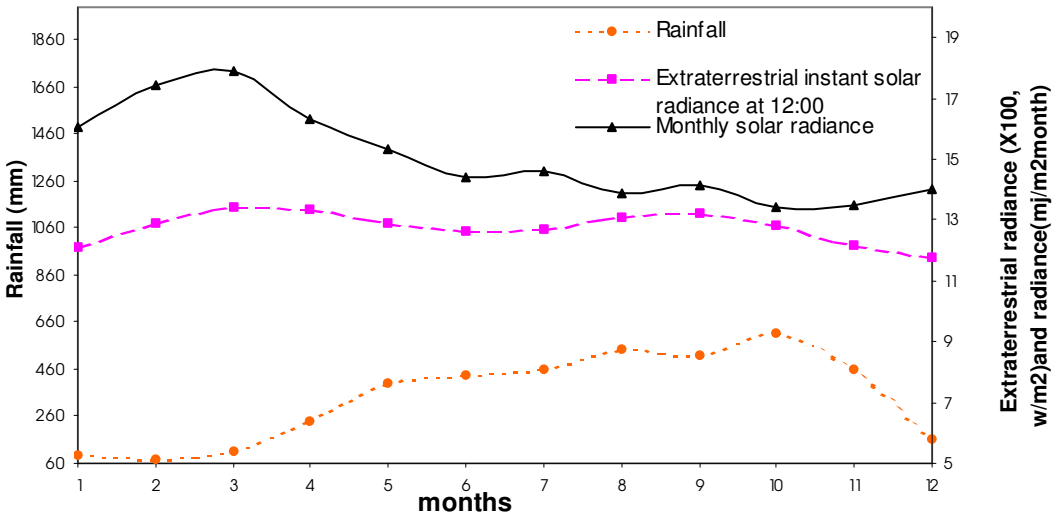

Figure 4.12 Ground solar radiance, extraterrestrial radiance and rainfall each month in 1998

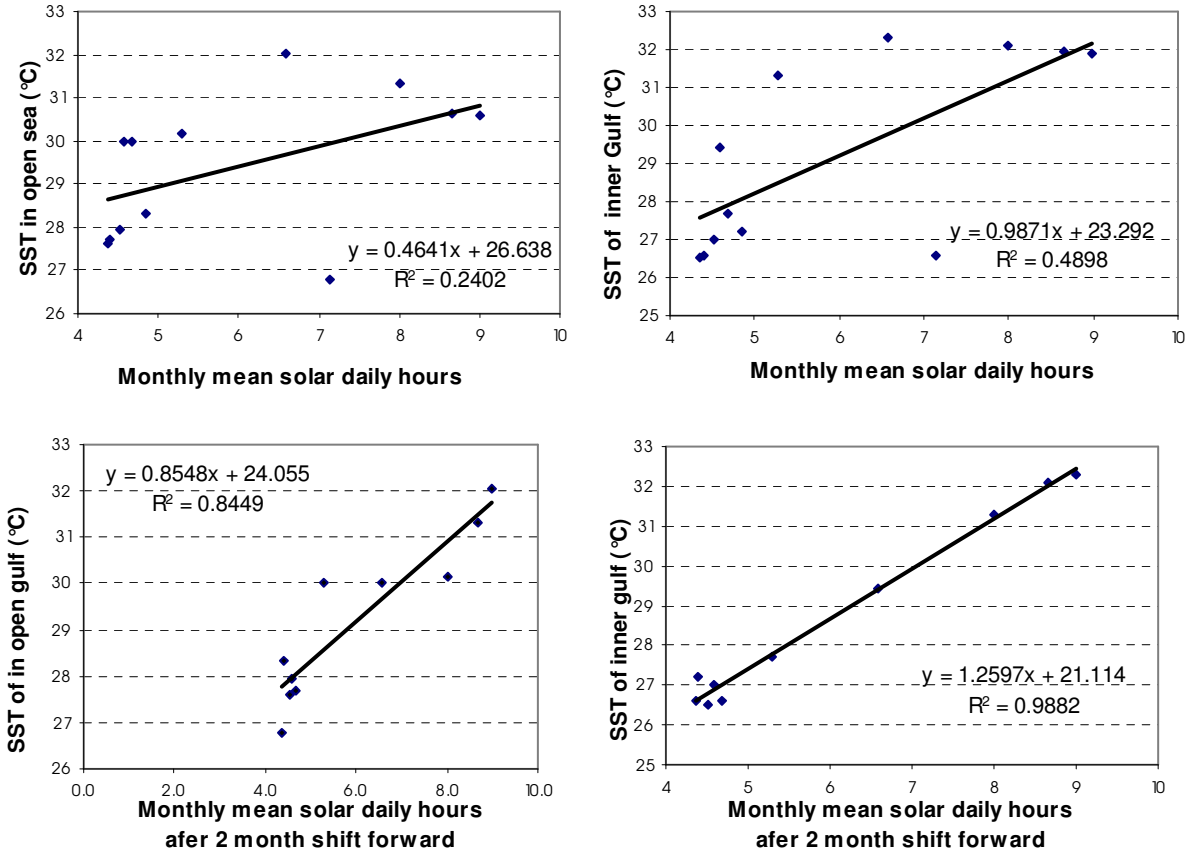

Figure 4.13 Correlation between solar daily hours and sea surface temperature

The gulf energy transfer model is built in Golfo Dulce (Figure 4.14), the seawater get solar highest energy or radiance in March and September without other factor impact, but warming up of seawater makes highest SST in May and November, which there is two months delay, El Niño event occurs before May, "uplift" the SST average 2-3 ºC in 1998, cloud coverage after May stresses SST

increase, reduces SST average 3-5 ºC, for normal year, there is no El Niño impact, high SST should occur between January and May, highest SST appears in April and lowest SST appears in October.

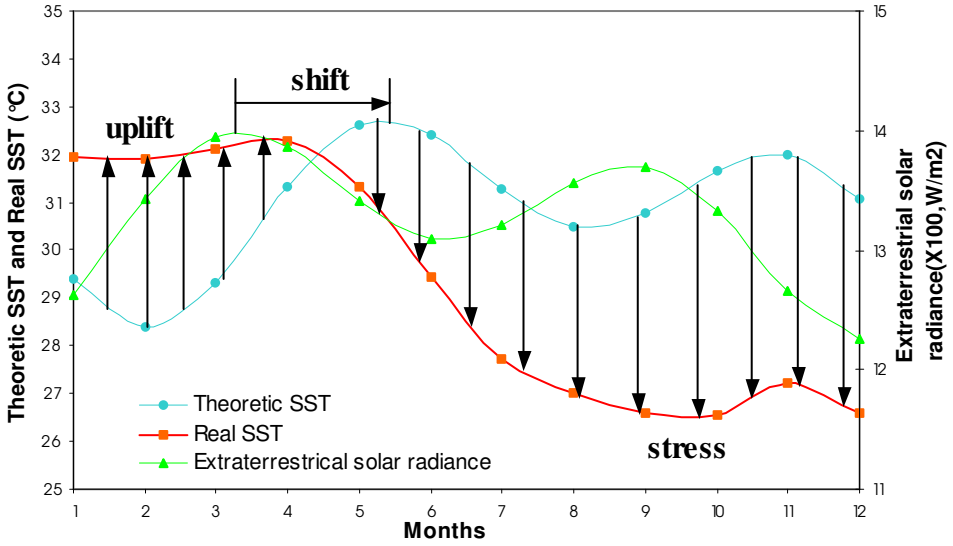

Figure 4.14 Monthly SST and energy transfer model in 1998

4.2.4. SST variability comparison to El-Niño Southern Oscillation

"El-Niño" is named after a Peruvian Christmas festival where the warming of the waters off Peru is said to occur near the birthday of "The Boy" (El Niño), or the Christ child. The El-Niño Southern Oscillation is the result of a cyclic warming and cooling of the surface ocean of the central and eastern Pacific in 100°-120° W, 0° N, which is 3000 km away to Golfo Dulce, Costa Rica. In this moment, we analyse the event impact on SST oscillation in Golfo Dulce directly or indirectly or no influence.

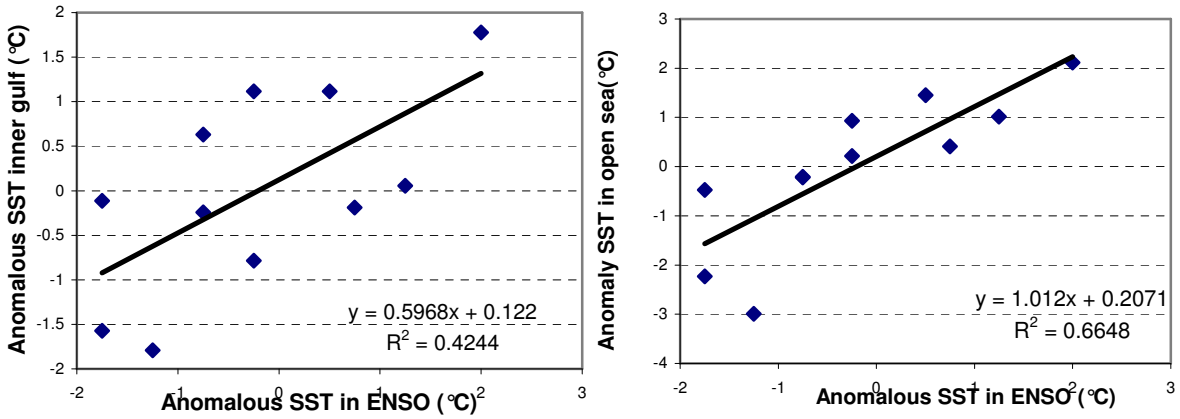

Figure 4.15 Comparison SST in the gulf and SST in ENSO in 1991-2001

The series anomalous SST in January 1991-2001 in ENSO are compared to the anomalous SST in same time in Golfo Dulce, the two observation spots are analysed in Golfo Dulce: out of the gulf and inner gulf, the SST out of gulf has relatively higher correlation to ENSO than in inner gulf (Figure 4.15), so the conclusion is obtained that ENSO has impact on SST in the gulf; the impact of

ENSO is conducted through sea surface heat flux rather than indirect impact through climate change; inner gulf indicates weaker being affection by ENSO.

4.3. Tide and wave actions

4.3.1. Tide-driven current

It has been known that the tidal rises and falls of the seas are related to the phases of the moon, it causes the coastal erosion and changes marine physical features. The sea currents in Golfo Dulce are very weaker than other the gulfs in tropical region, even though, tide action in this area plays relatively more important role than river current and wave current.

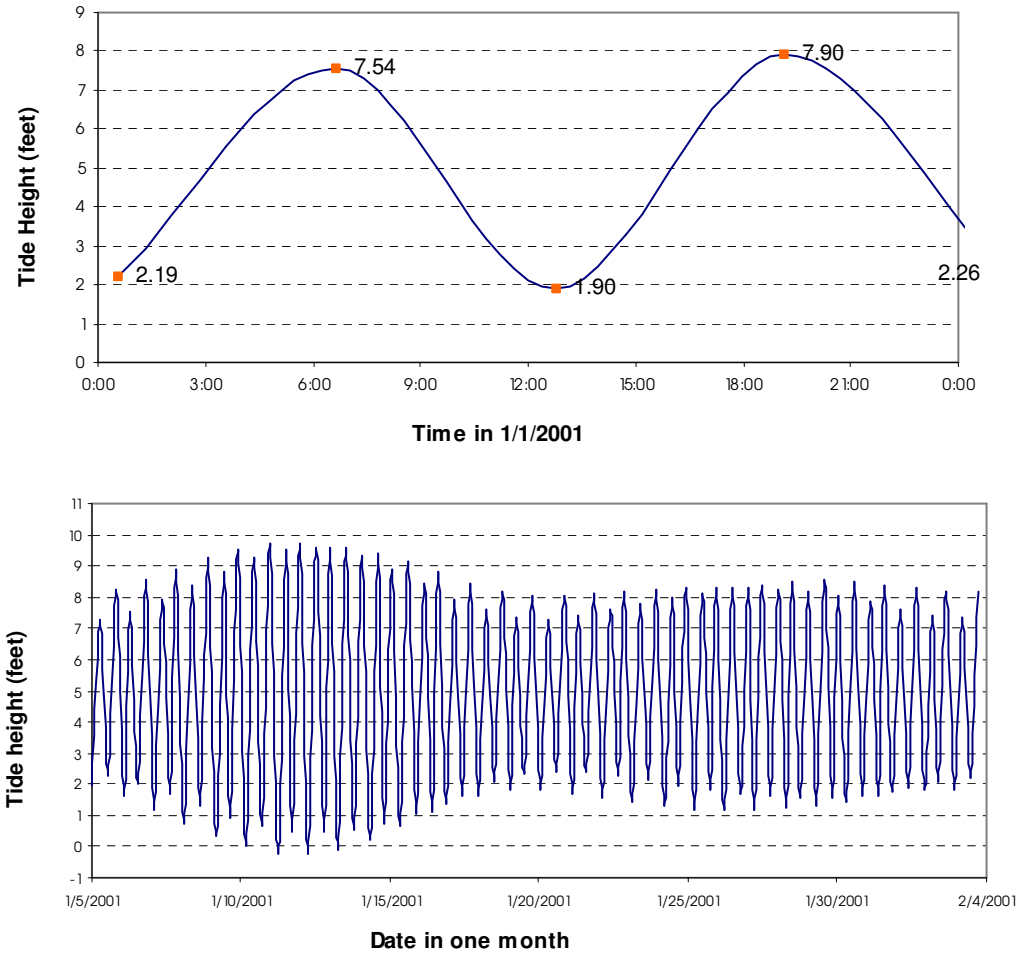

Figure 4.16 Tidal cycles at Rincon tide station in the west of Gulf. upper: lunar semidiurnal cycle; low: lunar fortnightly cycle

The tides in Golfo Dulce, are classified as irregular lunar semidiurnal tide, with two high and low tides (Figure 4.16), the high tide and high high tide occur respectively, V.S. low tide and low low tide, the statistics of tide in Rincon station, the west of the gulf, shows that the tide cycle has 12.37 hours period according to the data in January, 2001, the dominant cycle in one month is 14.75 days

according to the data in January, 2001, which belongs to lunar fortnightly tide. The average tidal amplitude is 7.02 feet, the maximum tide range is 9.97 feet, and lowest tide range is 4.79 feet, high tide changes between 7.12 and 9.74 feet, low tide changes between –0.23 and 2.42 feet, average minimum tide is 2.42 feet low.

Since the gulf shape and gulf location, the tide speed is very low except at the sill or gulf mouth, The flooding tide and ebbing tide have the same period according to the tide cycle, it is inferred that flooding tide and ebbing tide have same action in the gulf. The tidal currents movement are not direct forward and backward. The tide current dominant direction could be analysed according to the SSC plume direction, texture, and sediment spit, because it is difficult to directly detect the tide action using remote sensing, the two features are applied to analyse the tide current movement direction: the SSC plume direction and plume shape. The plume direction normally represents the dominant sea current direction or high sea current speed, the plume shape shows different sea current or river current action on the SSC, the sea current of anti-direction will form shear action and produce the series of eddy, make the SSC distribution looks like concave or convex shapes, we analyse the SSC in 1998, 2000, 2001, and produce the tide current model (Figure 4.17), the arrow direction shows

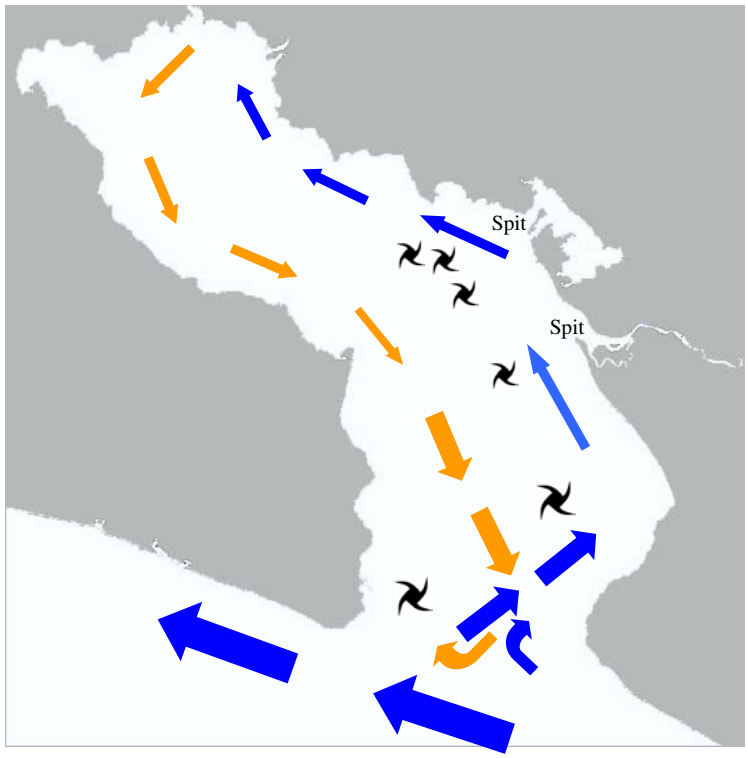

Figure 4.17 Tide current dominant direction in Golfo Dulce, Costa Rica

the dominant tide current directions, the sea current outside of gulf mainly head to northwest direction, main tide current enters the gulf along the west bank of the gulf mouth due to outside sea current and northeast tide current interaction during tide flooding period, then across the sill turn to the east bank of gulf, and enter the gulf along the east coast; during the ebbing period, SSC shows the eastward dominant current flows along the west or south coastline, passes the sill or mouth, then turns to westward, the tide cycling makes the main tide current counter-clockwise, there are a lot eddies occur between flooding period and ebbing period, when tide speed slow down and tide currents of entering

the gulf and going out the gulf exist in the same time, the eddies occur in the middle of gulf to mouth of gulf , and a little bit to the east coast, and eddies occurred in mouth are larger than in inner base.

The reason of counter-clockwise current formation is inferred that the sea current on north equator always flows turn right due to the earth self rotation action, and result in tide current flow along right coast, other reason is that largest river, named Colorado, and also the river Esquinas discharges the fresh water toward the right, which make kinetic energy to push to form the counter--clockwise current.

4.3.2. Wave-driven current

Wave current in this area is weak due to the small gulf month and High Mountain in peninsula, which hinder the most of winds coming to the gulf. The wind products now are available on website to monitor the global ocean wind directions and speeds (http://manati.wwb.noaa.gov/cgi-bin/qscat_arch .pl?year=1999&day=215), the sensor SeaWind on Quikscan satellite acquire each day SAR data, and

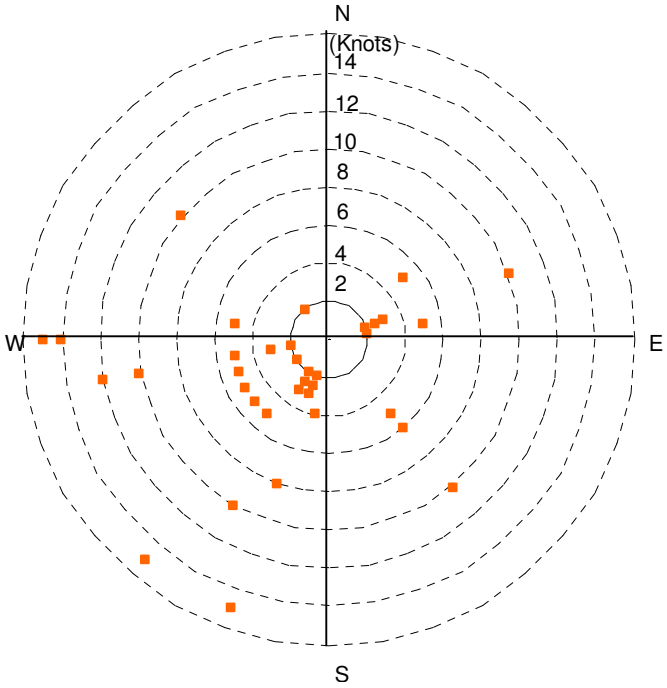

Figure 4.18 Wind directions and speeds each 10 days in 2001, out of Golfo Dulce, Costa Rica

process to calculate the direction and speed of the winds. The products of each 10 days monthly data in 2001 are analysed in this case studies (Appendix 5). There are two wind systems controlling the gulf climate: Costa Rica Coastal Current and Caribbean Trade Wind, prevailing wind is pacific Costa Rica Coastal Current, which bring the strong southwest wind to the gulf during the long rainy season, Caribbean Trade Wind only affects the region in dry season with weaker northeast wind (Figure 4.18). There is no clear dominant direction in January and February, wind changes arbitrarily, because these two wind systems keep the balance of action on the study area during the this time, the wind speed around 3-5 knots (it should be mentioned that the data analysed is located out of Golfo Dulce, the winds in Golfo Dulce could be relatively weaker), during March and April, Caribbean Trade Wind

controls the study area, but this wind system go over the high mountain in Costa Rica, and brings the weak wind to the Golfo Dulce, speed is about 2-5 knots, but this wind is brown backward the gulf, which is favourite to the upwelling of nutrients, the winds are dominated by Costa Rica Coastal Current from May to December, wind directions are concentrated between 180° and 270°, winds gradually change directions from south to west, these months have larger wind speeds than in the dry season, the speeds of wind in September and October are largest in a year, significant wind force caused wave current is in September and October with 260° direction and 10-15 knots speeds.

The ERS AMI images in Jan. 02, 1999 and Feb. 26, 1999 are merged to analyse wave roughness in Golfo Dulce, SAR image has sensitive to sea surface roughness and wave directions, the texture, shape and brightness of sea surface patches indicate the wave direction and speed. The open sea has higher signal than the inner gulf interpreted on SAR image, the wave has parallel to the gulf, the wind has decreased when it closes to coastal zone, it is obvious that the OSA peninsula plays an important role to change the shape of the wave of inner gulf, which has height more than 600 meter reduce and change wind speed and direction, sea waves in the mouth show wave direction likes "fan" due to the narrow mouth of gulf, the wind is blown through this channel to the inner gulf, the wave has high reflectance with parallel linear textures indicating the large wind and regular waves (Figure 4.19 A), the waves in the middle gulf shows the irregular features on image (Figure 4.19 B), but

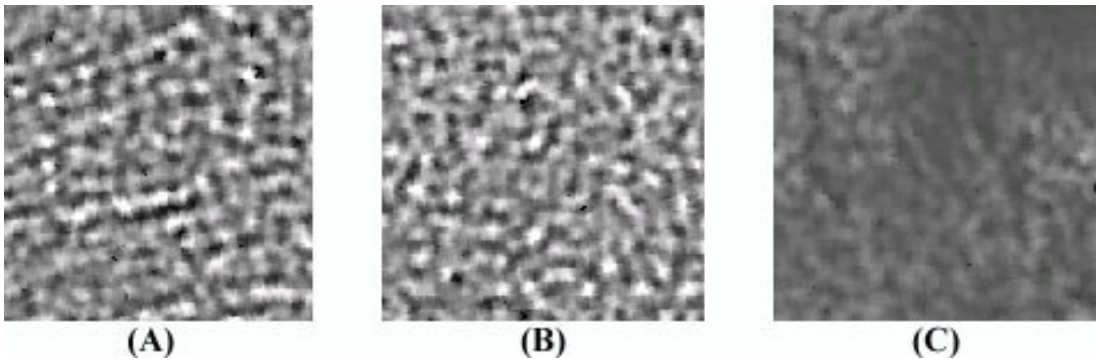

Figure 4.19 Roughness analyses on ERS SAR image data. (A) Parallel wave patch on the mouth; (B) multiple direction wave patch in middle gulf; (C) Dark wave patch in the estuary of Colorado River.

brightness of reflectance is not reduced too much, it is inferred that valley-mountain breezes and land-sea breezes in the northeast direction intersect the wind direction of northwest coming from the gulf mouth. The darkness of feature is displayed in inner gulf, representing the smooth water surface. There is big weaken darkness patch occurred out of Coloralo river stretching westward (Figure 4.19 C), it can't match with bathymetry, but it can match part of SSC, the patch could be the fresh water of the river with high SSC, which has different the physical features from the open seawater, and result in the different Rader backscatter cross-section (σ_0).

The conclusions are obtained that strong and regular wave occur in the gulf mouth, the narrow gulf mouth forms the wave shape like "fan" and wind driven current directly move to the middle gulf, the waves in middle gulf are disturbed and irregular due to different direction wind action; there is weak wave occurred in inner gulf.

4.4. SSC and marine environment

4.4.1. SSC spatial distribution and change detections

High sediment loads in normally clean coastal waters can be a problem to sea-bottom communities not adapted to such conditions, such as impact on coral reefs, and its accumulation of sand bars to create navigational hazards and coastal buildings.

The SSC in Golfo Dulce are most distributed at the estuaries, there are four main rivers discharge to the gulf, namely R. Coto-Colorado, Rio Esquinas, Rincon and P. Jimenez, R. Coto-Colorado is largest river in the gulf, Rio Esquinas ranks second, therefore, there are four major plumes of SSC distributed in the gulf (Figure 4.20), one is out of R. Coto-Colorado river, the second is on the west of gulf month, the third is out of Rio Esquinas, the fourth is on the east of gulf month. The big patch of SSC is distributed out of R. Coto-Colorado, the patch stretch along north coast, then flow to the small gulf of Golfito, the gradient of SSC coming out of the river is more higher toward the gulf than toward Golfito, it indicates main freshwater flow counter-clockwise around the coast, and forms a big sand spit inside of Golfito due to the sea current reduced. The plume of SSC in Tamales is smaller, but it has high SSC, it flows directly to the gulf, and a little bit skew to the gulf mouth, the another plume of SSC forms a spit of SSC in the east of gulf mouth which indicates the SSC movement to inner gulf, the SSC in Rio Esquinas shows a long plume from river mouth to the gulf, the SSC is changed according to sea current action. The above SSC distribution is in 2000, the SSC in 2001 and 2000 are compared to SSC in 1998, the change detections processing are delivered to analyze the SSC movement direction, the difference of SSC in 2001 and 2000 minus SSC in 1998 are calculated to check their increase or decrease of SSC, the classification of change detection is as following (Table 4.4):

Table 4.4 SSC change detection classification between 2000 and 2001

No.	Classification (mg/l)	SSC change
1	< -8	More decrease
2	-8 — -3	Decrease
3	-3 — 3	Normal
4	3 — 8	Increase
5	> 8	More increase

The SSC in gulf changes fast due to tidal current and river discharge actions (Figure 4.21; 4.22), the SSC in the estuaries of Rio Esquines and Colorado rivers have decreased more than 8 mg/l in 2000 against in 1998, but it is increased in 2001 in mouth of Colarado river, the SSC in Tamales is always increased, the SSC around the coastline out of gulf and the gulf mouth shows some increased, but it declined in 2001, the most of gulf during the 2000-2001 show the trend of clarified water.

The SSC areas are calculated between 1998-2001 in the gulf, the gulf border of mouth is according to the sill to calculate, the total area of the gulf is 609.38 km^2 (Table 4.5), 82% area of the gulf is composed of SSC less than 50 mg/l, which distributed in middle gulf, 14.5% area of gulf has

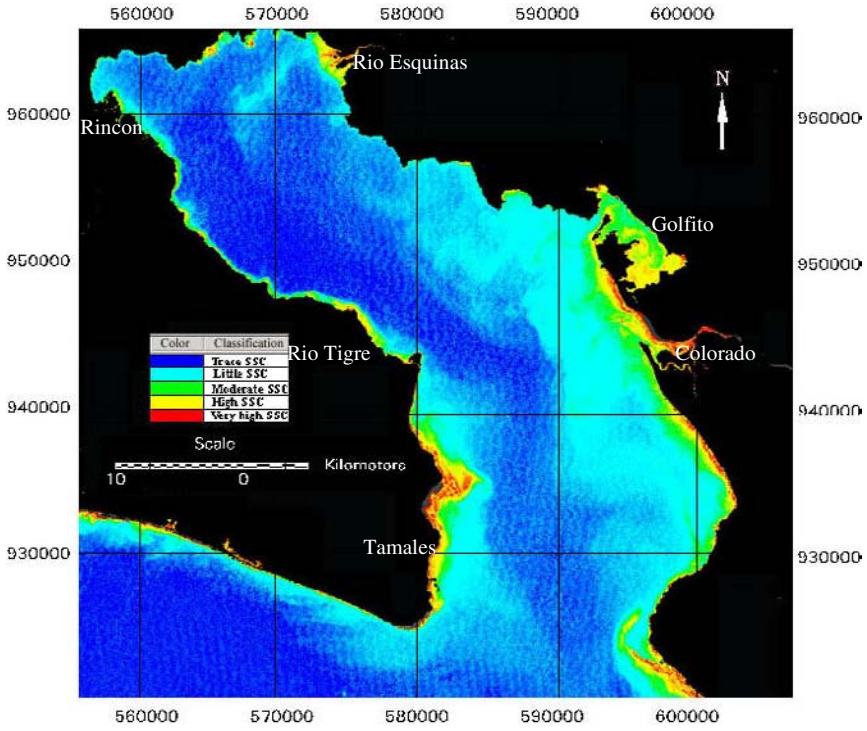

Figure 4.20 Suspended sediment in January 2000 using radiometric enhancement on TM band 3

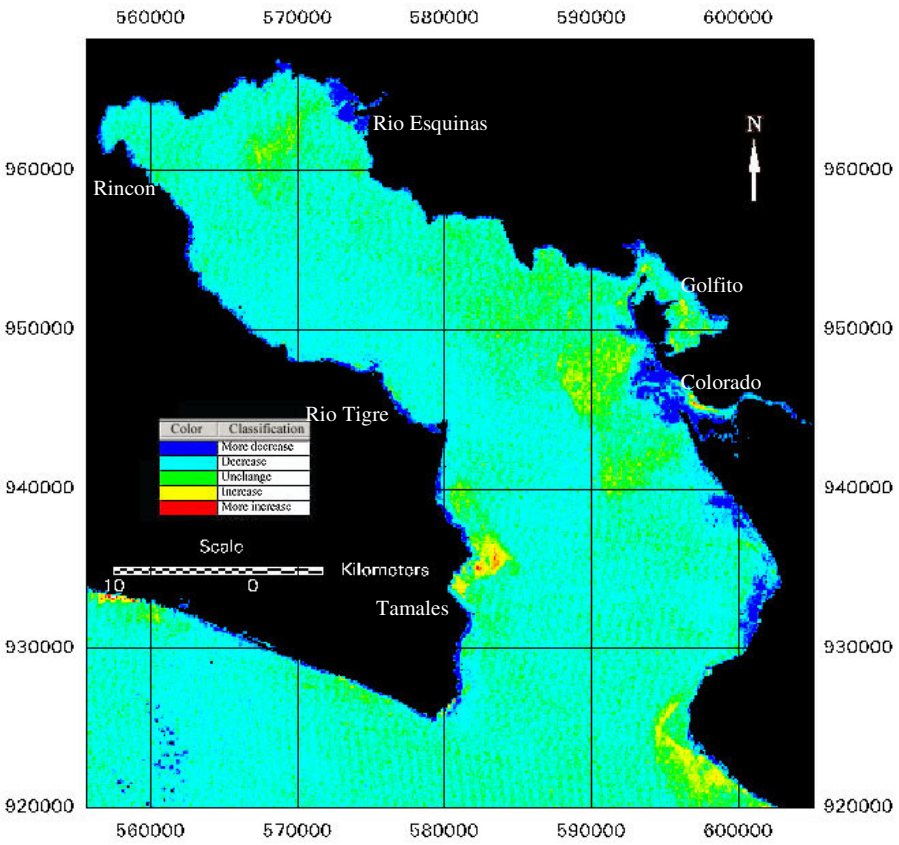

Figure 4.21 Change detection of SSC between 1998 and 2000

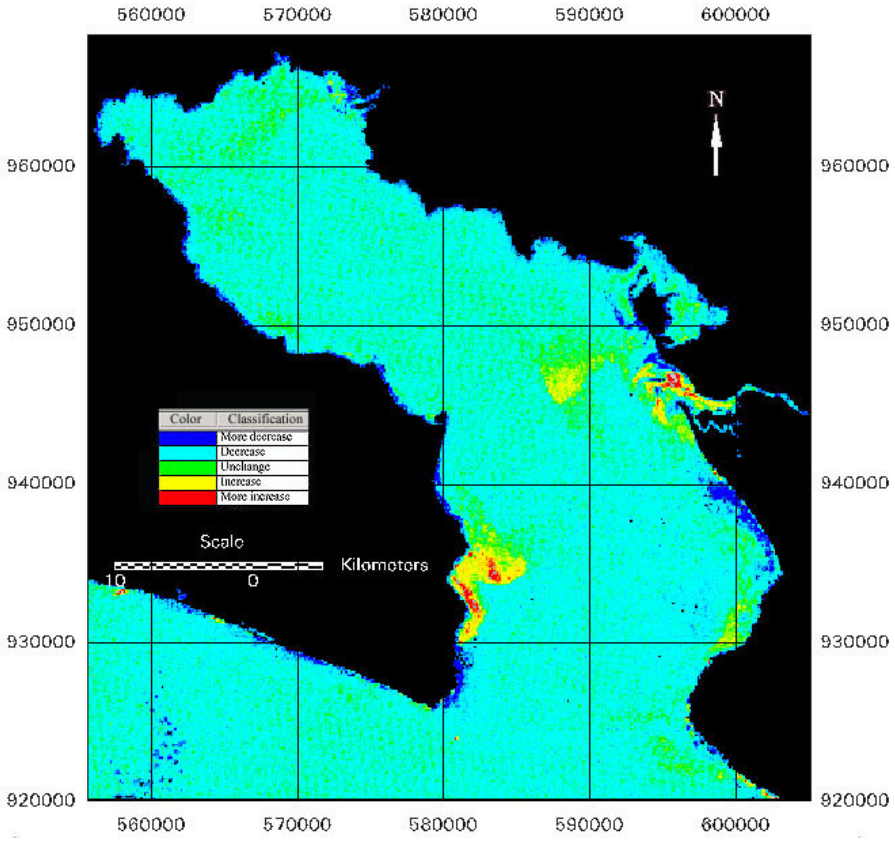

Figure 4.22 Change detection of SSC between 1998 and 2001

SSC 50-60 mg/l which distributed in far reach of estuary, only 3.1% area of the gulf has SSC more than 60 mg/l, which distributed on the estuary, Golfo Dulce is regarded as the water gulf according to the SSC. The area changes in the different SSC ranges are analysed in the gulf (Figure 4.23), the

Table 4.5 SSC area calculation in Golfo Dulce, in 2000 and 2001

No.	Classification (mg/l)	SSC degrees	SSC area in 1998 (km^2)	SSC area in 2000 (km^2)	SSC area in 2001 (km^2)	SSC percentage in 2001 (%)
1	<40	No SSC	0.00	32.14	106.47	17.5%
2	40-50	Low SSC	520.13	516.46	396.18	65.0%
3	50-60	Moderate SSC	58.46	54.3	88.07	14.5%
4	60-70	Moderate high SSC	20.63	5.31	14.46	2.4%
5	70-80	High SSC	5.53	0.91	3.42	0.6%
6	80-90	Very high SSC	2.24	0.26	0.79	0.1%
7	>90	Extremely high SSC	2.39	0.00	0.00	0.0%
Total			609.38	609.38	609.38	100.0%

SSC in 1998 is considered as basic year of the comparison, the results show that SSC in 2000 has little changes, some SSC between 60-70 mg/l has changed to less than 40 mg/l, water becomes clear in this year, SSC in 2001 shows irregular change, that means there are many factors affect SSC.

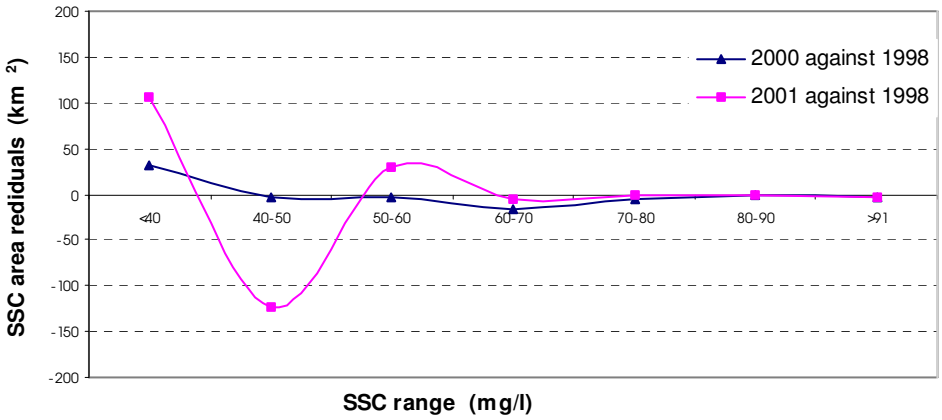

Figure 4.23 SSC changes in 2000 and in 2001 comparing to SSC in 1998 in Golfo Dulce

4.4.2. Water kinetic energy impact on SSC

The distribution and change of SSC are mainly dependent on two variables, the water kinetic energy and sand source supply. Sea currents disturb the water and make suspended sediment keeping a long time in the water; sand source supply is main reason determining water SSC.

Tide current's circulation within the gulf appears to be counter-clockwise, so it makes large speed water flow occurred on right side of moving direction, which is close to the shore and makes big contribution to disturbance of suspended sediment, the speeds of tide current at gulf mouth and the sill are larger than inner gulf, so it makes large plume distributed between the gulf mouth and Golfito. Comparing to Figure 4.19 and Figure 4.20, the spit of SSC in east gulf mouth has moved northward 5 km along the east shore from 2000 to 2001, meanwhile, the SSC in Tamales estuary on west gulf mouth has moved southward 1 km along the west shore from 2000 to 2001.

The wave action only affects sea current from the gulf mouth to Golfito due to the gulf morphology barrage, the southwest direction of prevailing wind go through the gulf mouth, the large wind appears in middle of gulf mouth, the wind of inside gulf is weakened by land-sea breeze and mountain breeze of different directions, so the strong action of wave in the gulf is on middle part of the gulf mouth, but in this area, there is a little SSC supply and has a little impact on SSC except for the area in Colorado river mouth.

4.4.3. Sand supply impact on SSC

There are two sand sources coming to the gulf: river discharge and beach sand supply from out of gulf. The river discharge contribute 70-80% SSC to the gulf, which is controlled by upward catchment's soil erosion. The soil erosion is corresponded to vegetation coverage, soil composition, rainfall and mountain slope, but the factors of mountain slope and soil composition are unchanged at temporal scale, so the vegetation coverage and rainfall are important factors on monitoring and prevention of soil erosion. Deforestation is major problem in Golfo Dulce in history, OSA peninsula is once the place of gold mining, deforestation, road and building construction are appeared around OSA peninsula in that time, meanwhile agriculture for banana planting in the upward of Colorado river makes heavy soil erosion, high sediment load through the river discharge to the gulf. But re-

cently the industry has declined and the situation has changed, the soil erosion of the gulf catchments between 1998-2001 are analysed, the vegetation intensity and coverage are very high due to tropical region, but because of human activities, the bare land or rare grass occur in northeast slope of OSA peninsula and the east of Colorado river in 1998 (Figure 4.25), it result in more SSC in the estuaries of Colorado and

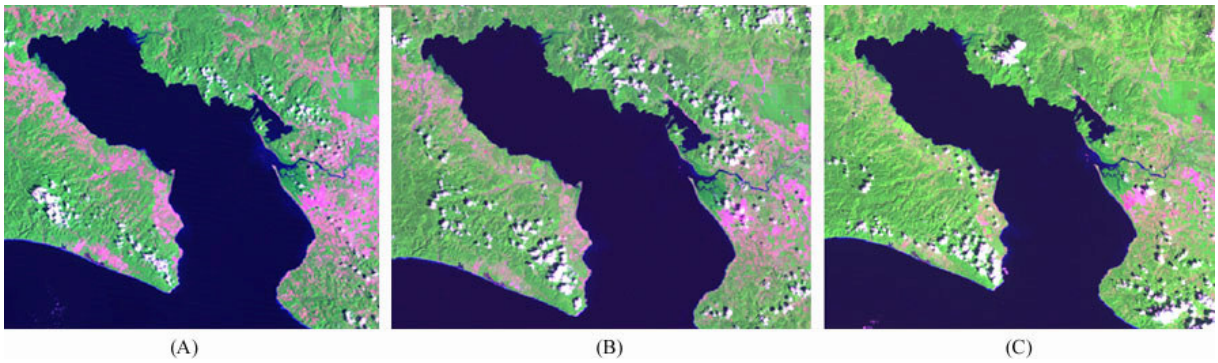

Figure 4.25 Soil erosion in upward rivers using TM band 643 composite, the green colour represents vegetation; purple colour represents bare land. A: 1998; B: 2000; C: 2001

Tamales, there is also low -density vegetation in Rincon, the west of gulf, but it has gentle slope and low elevation, which discharge low SSC in the outlet, the vegetation coverage has increased since 1998, the vegetation in the west of gulf had recovered in 2000, and the vegetation in Colorado river catchments shrank to the south of river bank in 2001, so the most area of SSC in the gulf in 2000 and 2001 are decreased in Figure 4.19 and 4.20, but the area in the mouth of Colorado river and Tamales river still keep increase of SSC in 2001, this is reason there is higher rainfall in dry season in 2001 than in 1998, the more soil erosion supplied SSC in the gulf.

4.5. Conclusion

The concept of gulf closeness has been defined; it concerns factors of gulf perimeter, depth and intercept area. The total gulf closeness is 77.12 %, which includes surface closeness 92.86 %, vertical depth closeness 70 %, vertical intercept area closeness 75.03 %, it belongs to high closeness gulf.

The SST is controlled by the factors of extra-terrestrial solar radiance, rainfall, gulf morphology, horizontal water heat flux in Golfo Dulce. The SST is higher inside gulf than outside gulf with the temperature gradient 0.02 °C/km, the SST in middle gulf is higher than in coast water with gradient 0.25 °C/km. This is reasons of (1) sea current is more weak and more stagnant than open sea due to the morphology of the Gulf, heat vertical and horizontal flux is difficult or slow; (2) peninsula OSA and Puntarenas mountain surrounding the Gulf result in the sea wind blocked and weakened in the Gulf, sensible heat and evapotranspiration to air is comparatively low; (3) the gulf coast emits more solar heat to atmosphere than sea surface, coastal land absorbs part of heat of water and balances the energy lost to the air.

There is 1.5 °C and 2 °C oscillated annually in open sea and inner gulf in 1991-2001 respectively. Anomalous “hot spot” of SST is located in the west inner gulf. “Hot spot” is stretched to northwest or southeast as SST is increased, it occurs in 3-4 years; anomalous “cold tongue” happens around the gulf mouth, it normally shows a long shape like tongue inserting to the gulf from south-

west to northeast, it starts at west border of the gulf mouth, then stretches to east of the gulf like meander, it has 2 year cycles. “Hot spot” is caused by the gulf morphology, and “cold tongue” is the reason of open sea SST oscillation. SST in dry season is 31-32 °C 1998, 2 °C higher than normal year, SST decrease to 27 °C in rainy season, SST summit occurred in March, the lowest SST occur in October, The SST in open sea has 1-month earlier reach peak temperature than inner gulf, it is can be infer that water heat is conducted from open sea to the gulf in early 1998 due to El Niño event. The gulf SST in 1991-2001 are compared to El Niño temperature shows that: (1) the SST out of gulf has relatively higher correlation to El Niño than in inner gulf, (2) inner gulf demonstrates weaker being affection by El Niño; (3) the impact of El Niño is confirmed again its advection through sea surface heat flux rather than indirect impact through climate change.

Solar hours directly control the SST in the gulf, there are excellent correlation between SST and solar hours if solar hours are shifted 2-month forward, that mean 2-month delay for seawater “warm up” by solar energy, SST out of the gulf has bad correlation due to horizontal heat flux influence. The gulf energy transfer model is built for analysis of SST change in 1998, the seawater get solar highest energy or radiance in March and September without other factor impact, but warming up of seawater makes highest SST in May and November, which there is two months delay, El Niño event occurred before May “lift” the SST average 2-3 ºC, cloud coverage after May stresses SST 3-5 ºC.

Tide current plays a main role in all currents in Golfo Dulce. The dominant tide current displays counter-clockwise horizontal cycling, some eddies occur in the middle of gulf between flooding period and ebbing period, high speed current occurs at “sill”. There are two reason inferred for the formation of counter-clockwise current: (1) sea current on north equator always flows turn right due to the earth self rotation; (2) main river currents head to the gulf in right angle of 30-80° and assist kinetic energy of cycling. Two wind systems (Caribbean Trade Wind, pacific Costa Rica Coastal Current) control wave current in study area, the southwest wave current in dry season is favourite to the upwelling of nutrients but it is weaker than in rainy season, so there is rare upwelling occurrence except for west gulf mouth. The southwest wave current in rainy season is comparative strong and strengthens the flooding tide current and reduces the ebbing tide current. Strong and regular parallels of sea waves likes “fan” occur in the gulf mouth, the waves in middle gulf are disturbed and irregular due to valley-mountain breezes and land-sea breezes in the northeast direction intersect the wind direction of northwest coming from the gulf mouth; there is weak wave occurs in inner gulf.

The distribution and concentration of SSC are mainly depended on the water kinetic energy and sand source supply. The SSC are most distributed at the estuary. The biggest patch of SSC is distributed out of R. Coto-Colorado due to sand supply and tide current disturbing, the plume of SSC in Tamales is smaller, but it has high SSC. The total area of the gulf is 609.38 km^2, 82% area of the gulf is composed of SSC less than 50 mg/l, which distributed in middle gulf, 14.5% area of gulf has SSC 50-60 mg/l which distributed in far reach of estuary, only 3.1% area of the gulf has SSC more than 60 mg/l, which distributed at the estuary. Counter-clockwise tide current generates the spit of SSC in east gulf mouth and pushes it northward 5 km along the east shore from 2000 to 2001, meanwhile, the SSC in Tamales estuary on west gulf mouth has moved southward 1 km along the west shore. The most parts of gulf during the 2000-2001 show the trend of clarified water due to vegetation coverage recover, except for the mouth of Colorado river and Tamales river where still keep increase of SSC in 2001, this is reason there is higher rainfall in dry season this year which results in the more soil erosion in the gulf.

Chapter 5: Phytoplankton pigment analysis and ocean primary production estimate modelling in Golfo Dulce

5.1. Phytoplankton pigment concentration analysis

5.1.1. Phytoplankton pigment concentration distribution

It is now obvious that the satellite sensors have the ability to detect phytoplankton pigment on sea surface, Through analysis of satellite data over long time of periods, The information of distribution and changes of water phytoplankton chlorophyll-a can be obtained. This kind pigment has well relation to the phytoplankton abundance, the concentration of chlorophyll-a representing the phytoplankton is analysed to evaluate the gulf marine biomass and biological environment.

The products of PPC each month in 1998 and annual mean have made for analysis (Figure 5.1). The PPC in Golfo Dulce is higher than it out of the gulf, the PPC in the gulf range from 0.08 to

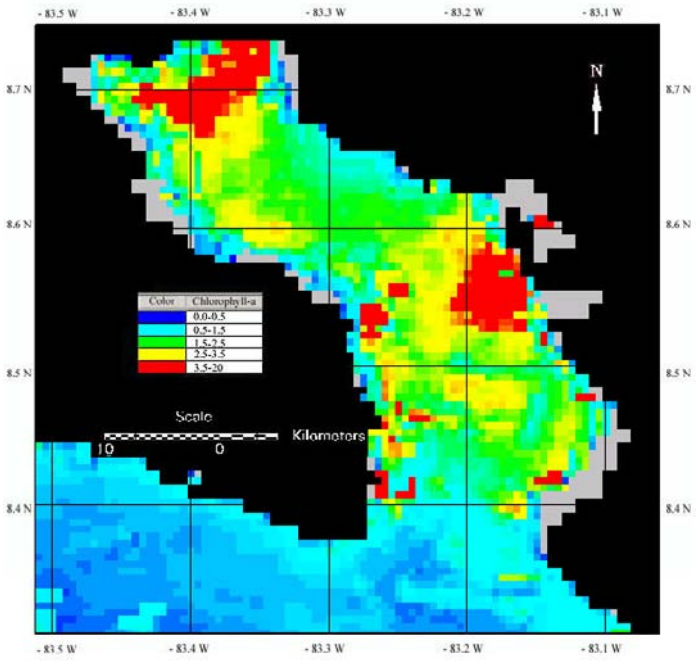

Figure 5.1 Mean daily PPCs in 1998 in Golfo Dulce, Costa Rica (black colour represents land mask, grey colour represents cloud mask)

18.25 mg/m^3 (Table 5.1), the mean of chlorophyll-a is 2.68 mg/m^3, there are some features on chlorophyll-a spatial distribution: (1) high PPC is distributed out of the mouths of Colorado river and Rio

Esquians river, and these two plumes of chlorophyll have a little shift away from the river mouth at counter-clockwise due to sea current action; (2) the PPC is higher in the middle gulf than in the coast; (3) the PPC in the north coast of inner gulf is lower than in south coast of inner gulf; (4) the PPC is

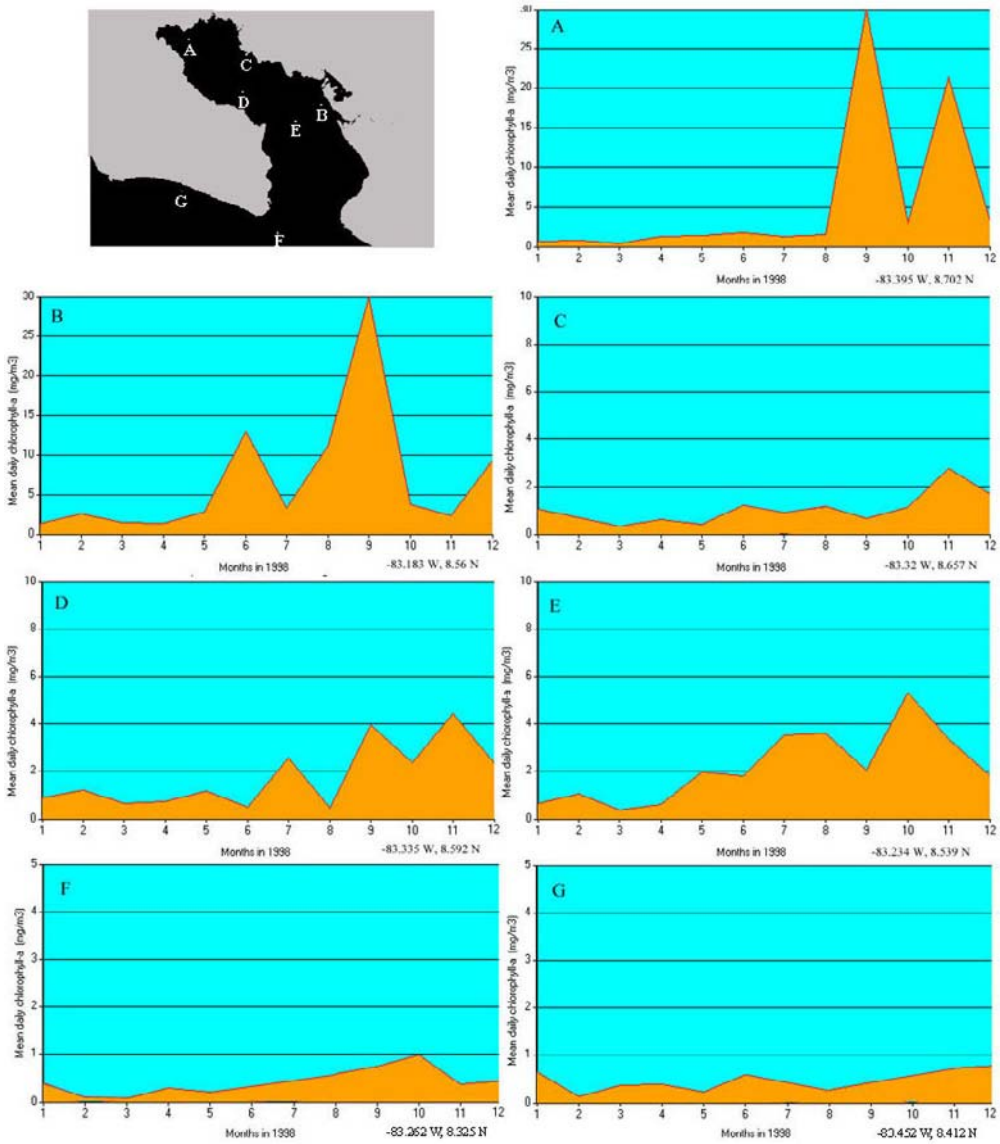

Figure 5.2 Temporal profiles of PPC in 1998 in Golfo Dulce, Costa Rica. (A: out of Rio Esquinas river; B: out of Coloralo river; C: north coast of inner gulf; D south coast of inner gulf; E: middle of gulf; F: mouth of gulf; G: coast of out of gulf)

Table 5.1 The statistics of daily mean PPC in 1998 in Golfo Dulce

Statistics	Chlorophyll-a (mg/m^3)
Minimum	0.08
Maximum	18.25
Mean	2.68
Median	2.21
Mode	1.98
Standard deviation	1.99

higher along shore than off shore out of gulf; (5) the west mouth of gulf has higher PPC than in the east mouth of gulf. Considering monthly changes of PPC, the 7 temporal profile of PPC are selected in Golfo Dulce, the principle of the profile choice is according to following factors: profile E represents the PPC without impacts of coastal factors, profile A and B represent the PPC impacts of river, profile C and D represent the coastal impacts with shadow slope and sunny slope, profile F represents the mouth tidal current interactions, profile G represents the coastal environment with sunny slope and global sea current action. The chlorophyll temporal changes have three characteristics: (1) the PPC in profile demonstrates that high value of 4-5 mg/m^3 occurs in October-November, the second peak occurs in July-August, the low value less than 1 mg/m^3 occurs between January and April, which is during the dry season; (2) The seasonal variety of PPC is higher in the river mouth than other place, the seasonal standard deviation is 8.36 mg/m^3 out of river and 1.32 mg/m^3 in the middle gulf; the seasonal variety is also higher in the gulf than out of the gulf, the seasonal standard deviation is 0.30 mg/m^3 in the mouth of gulf; (3) there is lower concentration and lower variety of concentration in the north of coast in the gulf than in the south coast.

5.1.2. Reason analysis on phytoplankton formation and distribution

The chlorophyll-a is a kind of popular pigment contained in chloroplast, and chloroplast is a part of phytoplankton body, PPC is correlated to the phytoplankton health and population, the formation of phytoplankton is depended on the light intensity, illumination duration, nutrient supply, seawater temperature, sea current action, etc. sometimes these factors affect the phytoplankton at the same, which make the frequencies of phytoplankton changed quickly, on the other hand, it is quite difficult to keep the sampling time and image acquired time at the same time, especially on rainy season, which makes analysis quite difficult.

The phytoplankton population in Golfo Dulce is determined by the river nutrients supply rather than upwelling supply of the deep water nutrients, because there are 2-3 times higher of phytoplankton population occurs in rainy season, and high concentration is located on the estuary, and there are the gradients of concentration from estuary to the middle gulf and from the gulf to open sea, heavy

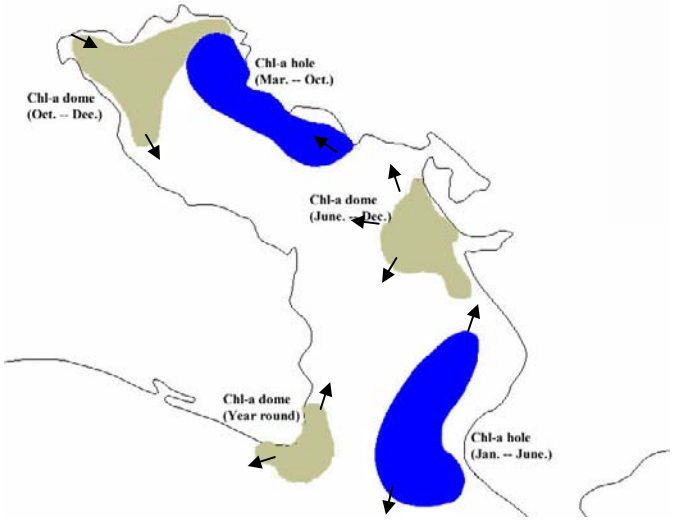

Figure 5.3 Simulation of chlorophyll-a "domes" and "holes" in Golfo Dulce

rain occurs in October and August, the rainfall is 5 times higher than in dry season, and phytoplankton peak population is also occurs in October and August. The PPC simulation is made to demonstrate distribution and formation (Figure5.3), Chlorophyll-a “dome" represents high concentration of chlorophyll-a, chlorophyll-a “hole” represents rare distribution of chlorophyll-a, there is different distribution of chlorophyll-a with SSC distribution, though there are the formation reason of river discharge, SSC is most depended on soil erosion, and chlorophyll-a is most depended on the catchments, so SSC is focused on the river mouths of Colorado and Tamales due to deforest, and PPC is focused on the river mouths of Colorado and Rio Esquinas due to the largest the catchments, because the big catchments will bring more nutrients which is not easy sinked. These two “domes” of chlorophyll is not clear in dry season. Another “dome” which is not as high as former two “domes” is distributed in the west mouth of gulf, but it is significant that it is formation of wind current action, the “dome” will move to west coast in dry season, in which northeast wind bring the current leaving the south corner coast and make water upwelling, bring the nutrient to euphotic zone, in other situation, the dome shift to a little inside of gulf mouth due to southwest sea current during the rainy season. The chlorophyll-a “hole” is located in the north coast of inner gulf, which is cliff coast without river nutrient supply, and valley climate bring more clouds in the afternoon than in south coast of inner gulf, that makes a few daily solar hour for phytoplankton growth. East “hole” of chlorophyll-a is the tide current action; it brings open seawater to the gulf and dilutes the water PPC.

5.2. Phytoplankton primary production estimate modelling

The ratio of PPC to carbon appears to vary predictably with light intensity (incident solar radiation), temperature, and nutrient concentration (Laws & Bannister 1980, Dubinsky et al.1986, Sakshauget al. 1988). The simplest empirical equations use only chlorophyll-a to predict phytoplankton productivity integrated over daily, seasonal or annual scales (Smith etal. 1982, Eppley et al.1985, Campbell & O'Reilly 1988). Eppley et al. (1985) used standard 14C-based estimates of daily productivity (DPPP: gmC $m^{-2}d^{-1}$), along with average chlorophyll a concentrations, collected from a range of marine environments during various seasons to calculate using linear regression analysis the empirical relationship (Equation 5.1).

$$\text{Log (DPPP)} = 3.0 + 0.5 * \log (\text{PPC}) \quad (5.1)$$

Which was revised using data of Berger (1989) to (Equation 5.2).

$$\text{Log (DPPP)} = 2.793 + 0.559 * \log (\text{PPC}) \quad (5.2)$$

The annual primary production algorithm was parameterized using measurements of daily phytoplankton particulate organic carbon production averaged monthly, then annually (PPP: gC $m^{-2} yr^{-1}$) and annual mean PPC within the top optical depth, all data being treated using methods of Platt and Harrison (1985). Annual phytoplankton primary production (APPP) was calculated using the trapezoidal rule, while PPC was integrated using arithmetic averages of daily chlorophyll-a for each environment. In this manner, the annual primary production algorithm was calculated using linear regression analysis methods (Equation 5.3).

$$APPP = 135.3 + 47.8 * PPC \quad (5.3)$$

Cloud-free scenes of 3-4 composite of PPC each month are averaged to generate mean daily chlorophyll-a each month, then to calculate the annual average APPP (Figure 5.4). Mean DPPP in 1998 in Golfo Dulce is 263.344 g C m^{-2} yr^{-1}, APPP is 160476.56 Ton in 1998 according to the "sill" border with gulf area 609.38 km^2. The distribution of PPP is familiar with PPC; it ranges from 138.1

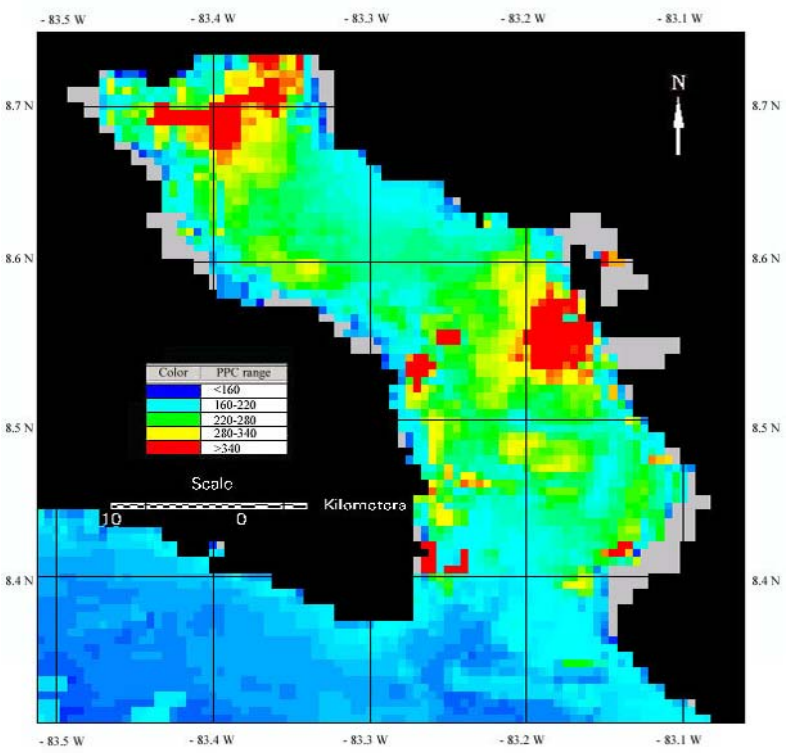

Figure 5.4 Phytoplankton primary production of carbon in 1998 in Golfo Dulce

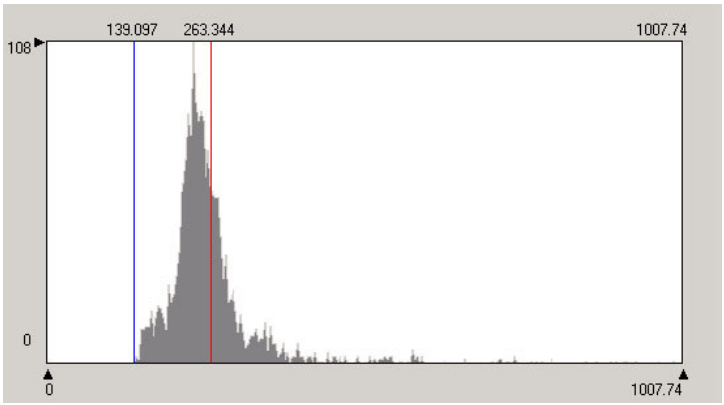

Figure 5.5 The histogram distribution of primary production of carbon in 1998 in Golfo Dulce

to 1007.7 g C m^{-2} yr^{-1} (Figure 5.5), it is skew distribution of phytoplankton, most phytoplankton has values between 200-300 g C m^{-2} yr^{-1}, 15 levels of PPC is classified, then the area of each level of PPC is calculated (Table 5.2), it shows that the gulf has low concentration of chlorophyll-a. The primary production in Golfo Dulce is lower than other tropical gulfs, but it is different in each month, the

Table 5.2 The area range of annual PPP in 1998 in Golfo Dulce

No.	PPC range ($gCm^{-2}yr^{-1}$)	Area (km^2)
1	0—150	5.06
2	150—200	73.27
3	200—250	280.56
4	250—300	160.24
5	300—350	38.42
6	350—400	18.76
7	400—450	7.45
8	450—500	4.77
9	500—550	6.85
10	550—600	5.06
11	600—650	0.30
12	650—700	0.60
13	700—750	3.57
14	750—800	1.49
15	800—1010	2.98
Total		609.38

PPC each month data is applied to calculate monthly primary production with the equation 5.3 (in this equation PPP is divided by 12 for monthly calculation in this moment), the high PPP occurs in the rainy season from June to December (Table 5.3), then annual PPP is pulsed from the 12 month PPP, the total PPP in 1998 is 140559.59 g C m^{-2} yr^{-1}, monthly PPP in rainy

Table 5.3 Monthly primary productions in 1998 in Golfo Dulce

Months	Mean PPP ($g C m^{-2}mon^{-1}$)	Gulf area (km^2)	PPP (ton)
1	14.836	609.38	9040.76
2	15.729	609.38	9584.94
3	14.015	609.38	8540.46
4	14.951	609.38	9110.84
5	16.652	609.38	10147.40
6	21.800	609.38	13284.48
7	21.190	609.38	12912.76
8	21.599	609.38	13162.00
9	21.241	609.38	12943.84
10	20.640	609.38	12577.60

11	25.491	609.38	15533.71
12	22.516	609.38	13720.80
Total			140559.59

season has 39.76 % higher than dry season. There is 14% error of calculation between annual and monthly calculation approaches, the problems is that products of chlorophyll-a each month have a lot of cloud mask area, where is replaced by the mean concentration of each month, but the monthly method is more reasonable than annual calculation.

5.3. Potential phytoplankton primary production estimate modelling

The idea of annual potential primary production estimate is that main impact factors are considered to calculate the largest contribution to the maximum primary production. The primary production is changed each day in the seawater; it is depended on the marine environment factor impacts. For the gulf in Golfo Dulce, the upwelling of nutrient caused by the sea current is limited within the west mouth coast, the tide action causes the phytoplankton moved around “sill” of the gulf, but total PPP is

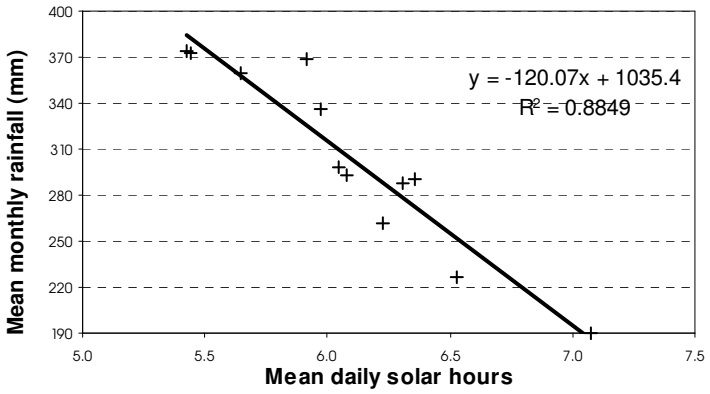

Figure 5.6 Relation between annual mean daily solar hours and mean monthly rainfall 1974-1985 at Palmar Sur station

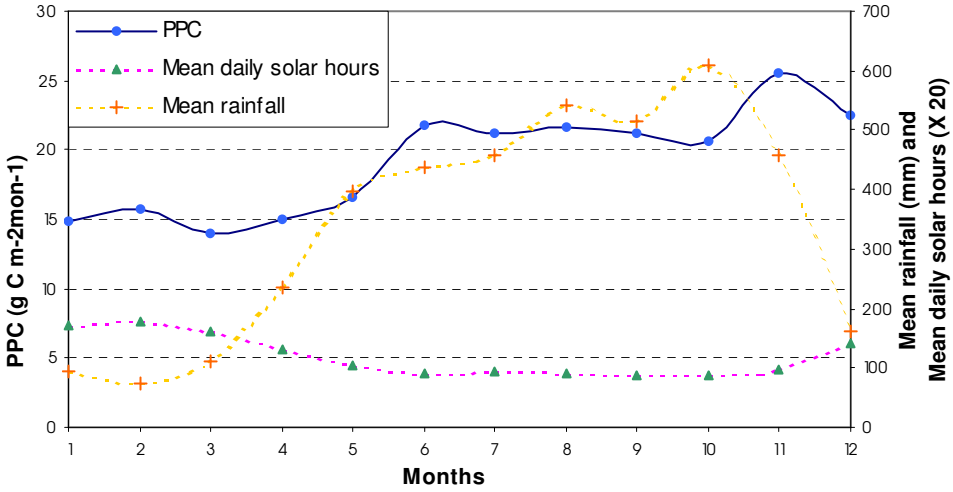

Figure 5.7 Relation between PPP in 1998 and mean solar hours and rainfall in Golfo Dulce

constant, it keeps unchanged and no impact on annual PPP, only river nutrients and ground solar radiance is changed year round, so the research is focused on these two factor impacts on the PPP, the ground solar radiance has considerable correlative to the daily solar hours, and river nutrient is also correlative to rainfall if the vegetation coverage change is neglected. The higher rainfall it has, the more PPP can be produced; the more daily solar hours it has, also the more PPP is produced, but the unfortunate thing is that these two factors are correlated themselves (Figure 5.6), normally, the higher rainfall drops, the lower solar hours it has, they have some relations to monthly PPP (Figure 5.7), these two factors must be considered together, because these correlation between two factors and PPP is very bad if considering factors respectively, coefficient of determination around 0.45, you will got some information that the PPP has well correlative with solar hours in dry season and well correlative with rainfall in rainy season (Figure 5.7), it is presumed that both factors are the variables of PPP, the concept of climate integrate factor (CIF) is introduced, the equation is following:

$$CIF = a \cdot P + b \cdot H \tag{5.4}$$

Where P and H represent monthly precipitation (mm) and monthly mean daily solar hours separately, a, b are constants

Then climate integrate factor CIF each month is compared to monthly PPP to calculate the constants a and b, the best match formula is following equation:

$$CIF = 0.04 \cdot P + 0.5 \cdot H \tag{5.5}$$

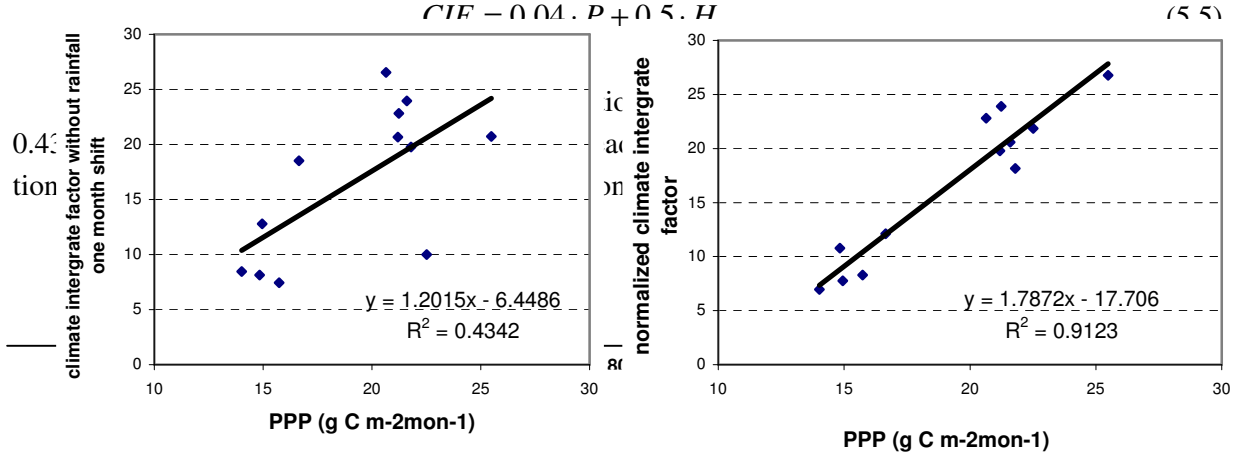

Figure 5.8 Correlation between monthly PPP and climate integrate factor

factor, then compare to PPP, the result is really different (Figure 5.8, right), coefficient increases to 0.9123, it is well correlative between PPP and CIF, so the data of rainfall and daily solar hours from 1976 to 1986 at Palmar Sur station are analysed to calculate the CIF (Table 5.4), the maximum of CIF occurred in 1984, that means the factor combination of solar hours and rainfall each month in this year make the largest contribution and produce the highest annual PPP, so the CIF both in 1984 and 1998 are calculated from solar hours and rainfall in both years, the climate data in 1998 is lack, rainfall each month in 1998 downloaded from internet at low resolution, solar hour each month in 1998 is calculated based on formula in Figure 5.6, then the CIF each month and mean CIF of each

Table 5.4 Climate Integrate Factor calculation during 1976-1986

Year	Mean monthly rainfall (mm)	Mean monthly daily solar hours	CIF
1976	226.07	6.82	12.45
1977	190.20	6.75	10.98
1978	290.77	6.36	14.81
1979	336.66	5.98	16.45
1980	293.38	6.08	14.77
1981	359.72	5.64	17.21
1982	261.16	6.23	13.56
1983	288.03	6.45	14.75
1984	372.03	5.44	17.60
1985	298.78	6.04	14.97
1986	236.61	6.08	12.51
Maximum			17.60
Minimum			10.98

month are calculated, the mean CIF of each month in 1998 is 13.3, which lower than the potential PPP in 1984, therefore, the change of Δ CIF between in 1984 and in 1998 are calculated, and at last the potential PPP is produced from percentage of Δ CIF and PPP in 1988, which is 186020 ton.

Table 5.5 Climate Integrate Factor and annual potential PPP calculations

Year	Types	Jan.	Feb.	Mar.	Apr.	May	Jun.	Jul.	Aug.	Sep.	Oct.	Nov.	Dec.	Year
1998	Rainfall	10.0	25.0	25.0	50.0	300.0	400.0	400.0	300.0	400.0	400.0	400.0	300.0	3010.0
1984	Rainfall	63.2	177.3	189.7	204.6	613.7	382.3	333.4	382.2	723.8	764.0	611.8	18.4	4464.4
1998	Solar hours	8.5	8.4	8.4	8.2	6.1	5.3	5.3	6.1	5.3	5.3	5.3	6.1	6.5
1984	Solar hours	7.7	7.4	7.8	6.7	5.2	3.1	4.5	4.1	3.9	3.6	3.6	7.7	5.4
1998	CIF	4.7	5.2	5.2	6.1	15.1	18.6	18.6	15.1	18.6	18.6	18.6	15.1	13.3
1984	CIF	6.4	10.8	11.5	11.5	27.1	16.8	15.6	17.3	30.9	32.4	26.3	4.6	17.6
	Δ CIF	37%	107%	121%	89%	80%	-10%	-16%	15%	66%	74%	41%	-70%	32%
1998	PPP	9041	9585	8540	9111	10147	13284	12913	13162	12944	12578	15534	13721	140560
1984	PPP	12347	19864	18841	17217	18289	11999	10794	15151	21452	21828	21887	4178	186020

5.4. Conclusion

The chlorophyll-a in Golfo Dulce is determined by the river nutrients rather than upwelling of the deep-water nutrient supply, which previous scientist estimated. The river nutrients are most depended on the area catchments rather than only soil erosion, since the large catchments bring more nutrients.

The PPC is higher in Golfo Dulce than out of the gulf, which in the gulf range from 0.08 to 18.25 mg/m^3, the mean of chlorophyll-a is 2.68 mg/m^3, there are some features on chlorophyll-a spatial distribution: (1) high chlorophyll-a "dome" is distributed at estuaries of Colorado river and Rio Esquians river and low chlorophyll-a "hole" is distributed in gulf mouth and the north gulf coast; (2) the PPC is higher in the middle gulf than in the coast; (3) the PPC in the north coast of inner gulf is lower than in south coast of inner gulf; (4) the PPC is higher along shore than off shore out of gulf; (5) higher PPC is in the west mouth of gulf than in the east. Temporal changes have following characteristics: (1) high value of 4-5 mg/m^3 occurs in October-November, the second peak occurs in July-August, the low value less than 1 mg/m^3 occurs in January-April, which is during the dry season; (2) the seasonal variety of PPC is higher in the river mouth than other place, the seasonal standard deviation is 8.36 mg/m^3 out of river and 1.32 mg/m^3 in the middle gulf; (3) there is lower concentration and lower variety of concentration in the north of coast of the gulf than in the south coast.

There is low phytoplankton population in Golfo Dulce, Mean PPP in 1998 in Golfo Dulce is 263.344 g C m^{-2} yr^{-1}, it ranges from 138.1 to 1007.7 g C m^{-2} yr^{-1}, total PPP is 140559.59 ton, and monthly PPP in rainy season has 39.76 % higher than dry season. The concept of climate integrate factor (CIF) is presented to evaluate potential PPP in 1991-2001, which is variables of monthly precipitation and monthly mean daily solar hours, CIF has best correlation with PPP with R^2=0.91 if monthly precipitation shifts one month forward, and PPP in 1984 has highest CIF 17.6, which indicates the potential PPP with 186020 ton.

Chapter 6: Impacts of physical processes on phytoplankton primary production in Golfo Dulce

Oceans regulate carbon in 3 different ways: by physical processes, chemical processes, and biological processes. Physical processes include the movement of carbon by ocean circulation from one location to another, and changing nutrient supply. Differences in temperature and salt content (salinity), in addition to the driving force of the wind and rotation of the earth, lead to bulk transport of carbon within and between major ocean basins. Another physical process is the diffusive mixing of water from one vertical level to another. Carbon dioxide dissolved in surface water is in equilibrium with CO_2 in the atmosphere because of efficient mixing in the ocean surface water. The river current is more important factor in the coastal zone due to the nutrients supply to the sea euphotic layer, SSC in estuary is also not neglect factor of impact due to its attenuation of seawater, it makes thin euphotic layer, there are five major factors concerned in the gulf (Figure 6.1), there are river current, tide current, upwelling current, SSC, radiance and SST.

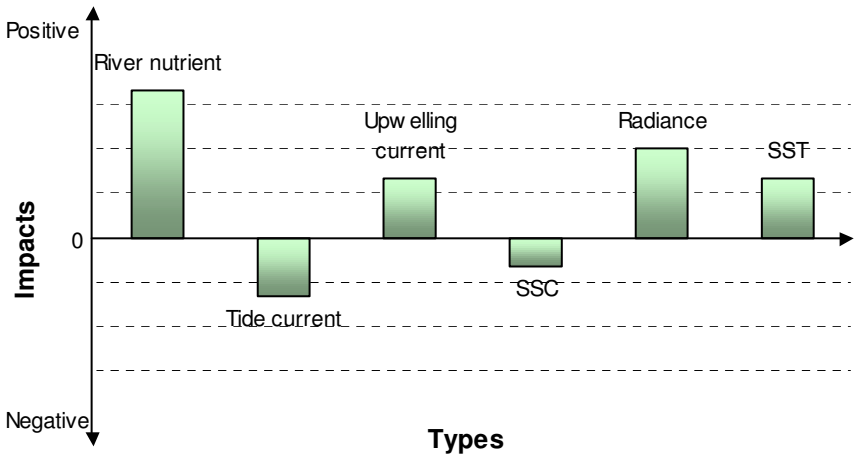

Figure 6.1 The ocean physical impacts on phytoplankton abundance

6.1. SST influence on phytoplankton abundance

According to the Eppley experiment in lab shows that water temperature affects the phytoplankton growth speed, but this impact is not a linear relationship (Figure 6.2), different phytoplankton species have different curve but in the same shape between 0-30 ºC. The Organisms of phytoplankton grow

faster as temperature increase, but reach some critical temperature, the organism has stress action on the body growth; the growth rate and population will be decreased.

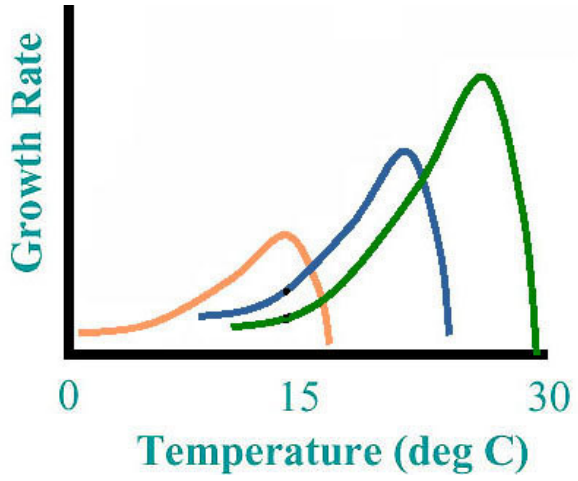

Figure 6.2 Relationship between SST and phytoplankton species growth rate (Eppley, 1972)

Considering many factors affect the phytoplankton abundance in the gulf, the test site in open sea at the same latitude is selected for analysis, which can remove the impacts of river current, tide current and radiance difference, the products of SST and PPC in the same day in March 1998 is tested for relationship between SST and PPC (Figure 6.3),

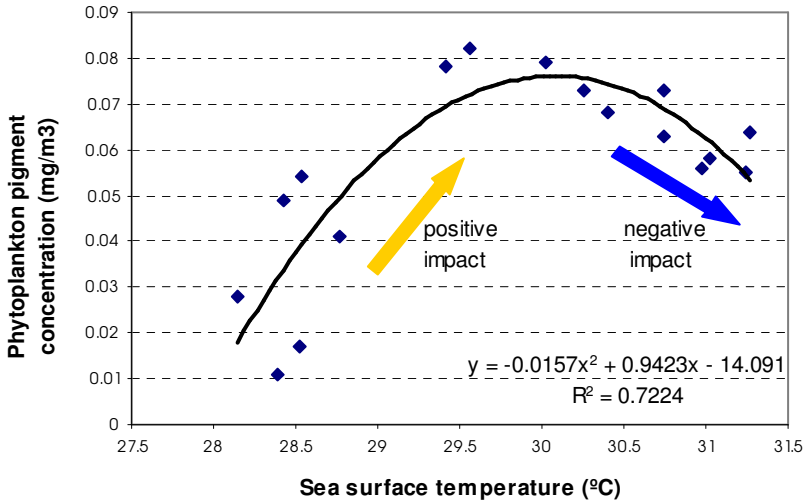

Figure 6.3 SST impacts on phytoplankton PPC (SST from AVHRR and chlorophyll-a from SeaWIFS in March 16, 1998)

the relationship curve in Golfo Dulce is consistent to the lab analysis in figure 6.2 right curve, water temperature has positive impact on phytoplankton growth less than 30.01ºC according to trend-line equation, the increase gradient is between 0.03-0.05 mg/m^3*ºC, but it has negative impact more than that degree, the decrease gradient is about 0.02 mg/m^3*ºC, this phenomena is not clear in the gulf due to other factor affections, SST in 1998 is very high in dry season due to the El-Niño appearance, the

SST before May 1998 has stress action on the phytoplankton growth, but SST after May 1998 has the stimulated action to the phytoplankton growth, but calculation of the growth population of phytoplankton by SST impact is quite difficult in the gulf due to many factors affections.

Season's vertical water temperature is possible to lead to the upwelling of nutrient and cause the bloom of phytoplankton theoretically. The vertical water temperature in the gulf has two layers: mixed layer and thermocline layer, mixed layer above 40 m depth in the gulf is the most easily influenced with solar energy, wind and rain, temperature changes between 26 and 33 ºC. The thermocline layer below 40 m depth has the water temperature dropped slowly as the depth increases (Figure 6.4). The season's change of SST is less than 8 ºC and normally minimum SST year round is more than 25 ºC, it is

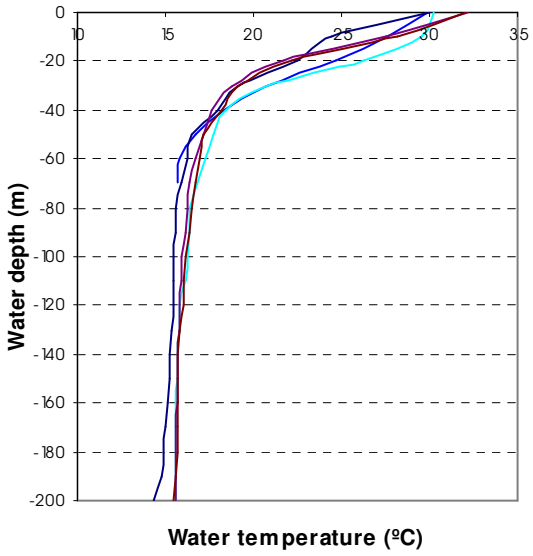

Figure 6.4 Vertical water temperature profiles of inner gulf in March 1969 (data source from Francis A.R. 1971)

impossible for SST less than the temperature in deep water. The temperature gradient-caused upwelling is quite difficult in this gulf.

6.2. Light attenuation impact of SSC on PPC abundance

It appears that the impacts of suspended sediments are related to turbidity, which result in light attenuation in water and make the euphotic layer shallow. Phytoplankton is light-limited species; its lifetime is as same as daily cycle, the surface seawater less than 15 m depth includes 90% of total phytoplankton population.

The impacts of SSC on phytoplankton abundance have two factors: grain size and depth of suspended sediment. Different grain size has different type scattering of light, and different depth of suspended sediment will affect light attenuation degrees. The suspended sediment around estuary is almost distributed at water surface due to the saline difference; the suspended sediment in the middle gulf is mixed with seawater and distributed in a little bit low subsurface, which has weak impact on phytoplankton. The sample points on SSC map and PPC map in the same place are selected to analyse

the relationship of impact, in this moment, the points had to be selected on open sea and middle gulf, because high SSC are always combined with abundant nutrients, especially in the estuary, so the selection should be far away the estuary to remove the other factor of nutrient impact, the two maps have one day difference, there is reason of some errors happens, 15 points are combined SSC with PPC (Figure 6.5), they have a polynomial relation with coefficient of determination 0.82 (Equation 6.1), it can be concluded that SSC less than 45 mg/l has little impact on PPC, which keep oscillated

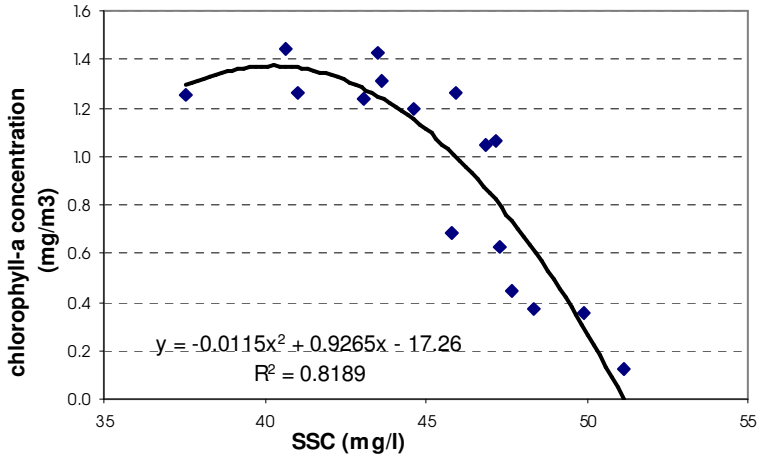

Figure 6.5 SSC impact on PPC in open sea (SSC derived from TM in Jan 31, 2001; chlorophyll-a derived from SeaWIFS in Jan 30, 2001)

between 1.2 and 1.5 mg/m^3, the first order derivative is calculated to analyse chlorophyll-a decrease rate as SSC increase (Equation 6.2), it shows a linear decrease trend of PPC (Figure 6.6), high SSC

$$Y = -0.0115X^2 + 0.9265X - 17.26 \tag{6.1}$$

$$\frac{dY}{dX} = -0.023X + 0.9265 \tag{6.2}$$

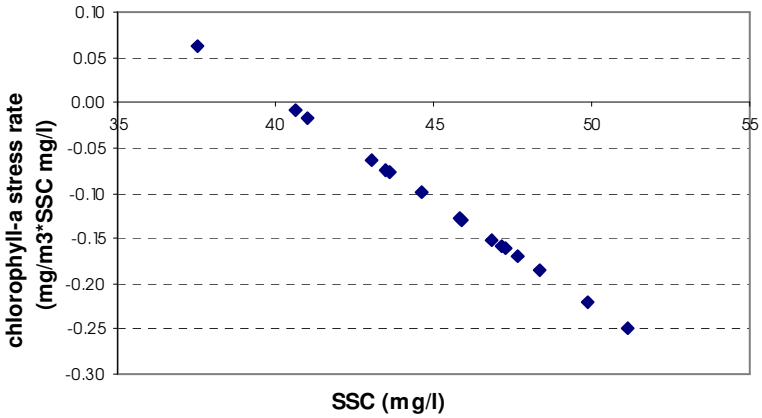

Figure 6.6 First order derivative form on PPC

With impact of -0.25 mg/m^3*SSC mg/l affects the PPC larger than low SSC with impact of -0.02 mg/m^3*SSC mg/l, this correlative formula of Equation 6.1 has not universal use, the SSC more 52 mg/l and less than 41 mg/l have different conclusion, because there are no more samples out of this range in open sea, and we can't make samples in coast zone, so this formula need improvement in future study.

6.3. Tide and wave current action devoted to phytoplankton distribution

Tide or wave current can't directly change phytoplankton biomass, but they can change the phytoplankton distribution horizontally and vertically, and their action can lead to upwelling of nutrients to euphotic layer, then increase the phytoplankton abundance.

Tide current in Golfo Dulce is weak, and comparative larger current occurred at the gulf "sill", the big patches of phytoplankton re-distributed by tide current around this region, the models of phytoplankton movement at "sill" are made for analysis according to PPP maps each months in 1998 (Figure 6.7). Normally, PPP distribution has a gentle gradient from the gulf to open sea because coastal nutrient supply, other any distribution of phytoplankotn is considered as tide current action or wave action in Golfo Dulce. Phytoplankton plume direction and abundance are analysed for tide movement, flooding current is stronger than ebbing current in the gulf, there are three horizontal tide and wave flow types in Golfo Dulce: flooding dominant current, counter-clockwise current and

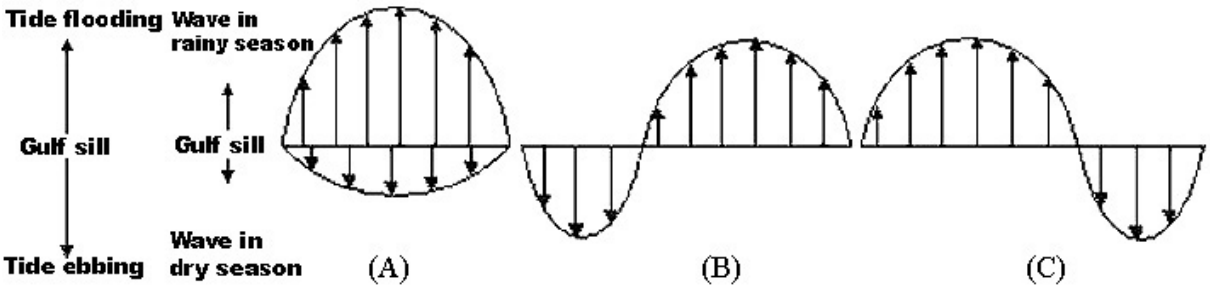

Figure 6.7 Tide and wave current horizontal flow model on phytoplankton patch movement at "sill" (A) flooding dominant type; (B) counter clockwise type; (C) clockwise type

clockwise current. Flooding current is stronger than ebbing current due to prevailing the northward wind action, the counter-clockwise type is more popular than others, the big patches of phytoplankton movement occur at sill, the flooding tide pushes the patch northward, and ebbing tide pushed the patch southward, the distances of the patches are measured based on the sill line (Table 6.1), pushing force to the gulf is bigger than out of the gulf, the distance to inner gulf is longer than to the open sea, mean total distance is 10.92 km, that means there are 11 km diameter wide range for exchange of large phytoplankton patch around gulf mouth, the residual of movement (the distance of push-in minus push-out) is positive, the patches are pushed in more than push out, it demonstrates that sea current in the gulf plays an role of barrier to hinder phytoplankton flowing out of the gulf due to the concentration gradient. The tide current has horizontal circulation in the gulf, counter-clockwise account for 60%, it is depended on the rotation position of sun, earth and moon, which cause different tide

currents. The tide current of gulf mouth has dilution function of phytoplankton abundance with tide rise and fall, and make the big patch and low gradient of phytoplankton spatial change.

Table 6.1 Phytoplankton movement measurement in and out at "sill"

Month	Push-out distance from sill (km)	Push-in distance from sill (km)	Total distance of movement (km)	Residual of movement (km)	Tide circulation direction
1	3.21	10.94	14.15	7.73	Clockwise
2	0.00	8.03	8.03	8.03	Counter Clockwise
3	0.00	9.54	9.54	9.54	Flooding dominant
4	4.93	9.42	14.35	4.49	Clockwise
5	1.51	8.65	10.16	7.14	Counter Clockwise
6	0.00	2.11	2.11	2.11	Counter Clockwise
7	3.84	5.83	9.67	1.99	Clockwise
8	0.00	2.23	2.23	2.23	Counter Clockwise
9	8.88	7.75	16.63	-1.13	Counter Clockwise
10	12.53	5.01	17.54	-7.52	Counter Clockwise
11	5.79	10.11	15.90	4.32	Counter Clockwise
12	4.05	6.73	10.78	2.68	Clockwise
Mean	3.73	7.20	10.92	3.47	

6.4. Upwelling current action devoted to phytoplankton biomass

Seawater upwelling is a phenomenon of nutrients going up to euphotic layer caused by wave current or tide current. Upwelling is a rare phenomenon in most of the gulf due to stagnant geomorphology, but in the fjord mouth, convex coastline causes high-speed sea current and pulls seawater off the

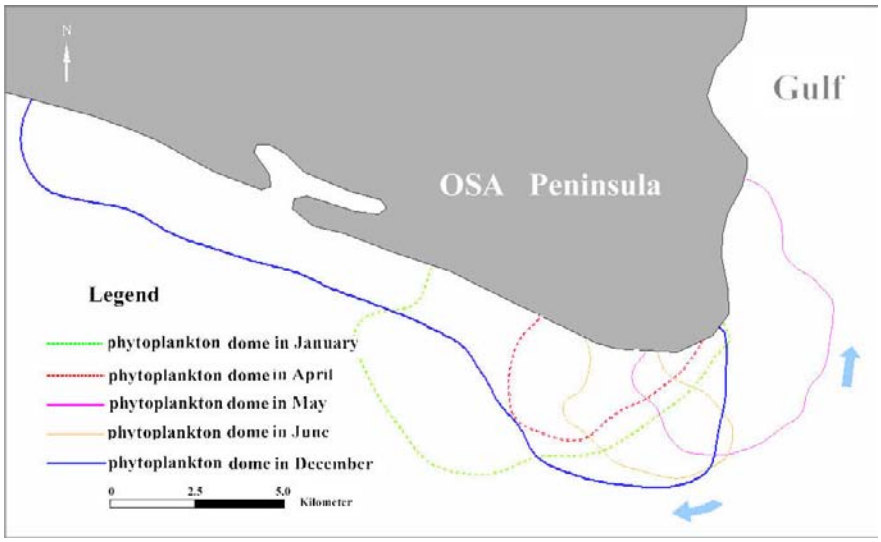

Figure 6.8 Upwelling-driven chlorophyll-a abundance in 1998

shore (Figure 6.8). The sea current moving northward will cause the effect of pulling water away east coast, the sea current moving southward will lead to the effect of pulling water away form south coast, and cause phytoplankton "dome" in this area. Phytoplankton abundance is applied to analyse upwelling intensity and range in this moment, and phytoplankton "dome" in this area occurs only in January, April, May, June and December in 1998, it shows that most upwelling areas occur along the south coast and in the dry season, only in May the patch moves into the gulf due to northward action of tide or sea wave, the largest upwelling occurs in December, which caused by northeast Caribbean trade wind, other patches show plume direction to the west, it is concluded that leaving currents from the gulf are stronger than sea current moving into gulf in the west coast and cause more upwelling in this south fjord corner. The ebbing tides most time along the west coast are dominant contribution to nutrient upwelling, and wave-driven current in dry season has the same direction coming out of the gulf, therefore, we can't conclude which reason is contributed to the upwelling in dry season in this moment except in May and June.

6.5. River current action devoted to phytoplankton biomass

River currents affect the phytoplankton in two ways: kinetic energy and nutrient load, which result in the phytoplankton changes of distribution and biomass. Different direction of river discharges to the gulf cause the patch distribution of phytoplankton, the measurement of angle between discharge direction and perpendicular of coastline are carried out (Table 6.2), R.Coto-Colorado and Rio Esquinas are large river in the gulf, the discharge of two river account for 90% of total river discharge to the gulf,

Table 6.2 Slant angles of river flowing direction to the gulf at outlet

River names	River discharge rank	River outlet incident angle (Skew to right)
R.Coto-Colorado	1	80º
Rio Esquinas	2	30º
Rincon	3	-45º
Rio Tigre	4	0º
Tamales	5	0º

These two rivers have right skew angles to the gulf, which make the contribution to the tide counter clockwise circulation, the patches of phytoplankton around estuary have shifted to the right (counter clockwise), the distance is depended on the river discharge, normally, the distance is larger in rainy season than in dry season (Figure 6.9), there are 3.5 times bigger of patch in rainy season than in dry season in 1998 at R.Coto-Colorado estuary, the patch is shifted 6 km to the northwest in dry season, and shifted 14 km to the northwest in rainy season at the same estuary.

Another impact is nutrient load. The phytoplankton primary production is 1.45 times higher in rainy season than in dry season according to precious calculation (Table 5.3), and it is concluded these are both contributions of solar hours and rainfall-driven discharge in precious research, this radio of 1.45 will increase if the factor of solar hours is neglected and only river discharge is considered, the river discharge-loaded nutrients are main factor affect the phytoplankton biomass.

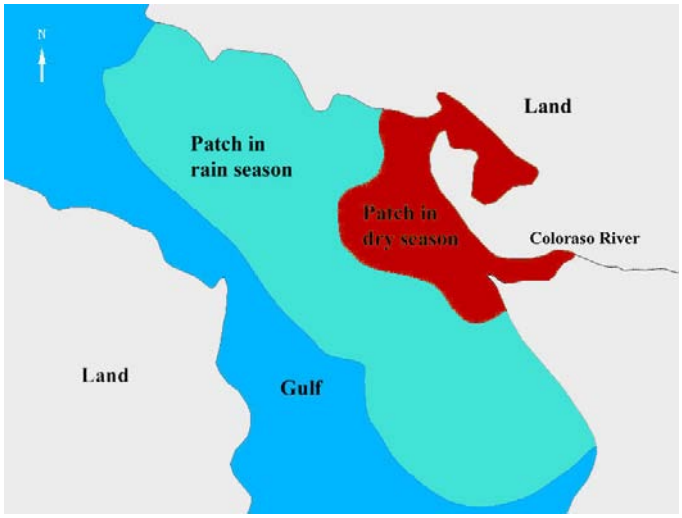

Figure 6.9 Colorado River current impacts on phytoplankton in dry and rainy season

6.6. Conclusion

Physical process plays an important role in phytoplankton abundance and distribution, there are five factors affect phytoplankton in Golfo Dulce: river current, tide current, SSC, solar radiance and SST. River current has main impact on the nutrient supply of phytoplankton; tide current has main contribution to the phytoplankton distribution.

Tide current dilutes the phytoplankton concentration and changes the distribution. There are three horizontal flow types of tide and wave in Golfo Dulce: flooding dominant current, counter-clockwise current and clockwise current. The counter-clockwise type is more popular than others, the impact of large patch phytoplankton movement occur at sill, flooding current is stronger than ebbing current due to prevailing the northward wind action, it demonstrates that sea current in the gulf plays an role of barrier to hinder phytoplankton flowing out of the gulf due to the concentration gradient. There is 10.92 km diameter wide area for exchange of large phytoplankton patch around gulf mouth, which has 3.47 km shifted to inner gulf from sill. Upwelling is a rare phenomenon in most of the gulf due to stagnant geomorphology except in the west gulf mouth, where convex coastline causes high-speed sea current and pulls seawater off the shore, sea currents moving out of the gulf are stronger than sea current moving into gulf in the west coast and cause more upwelling in the south corner in dry season.

River currents affect the phytoplankton in two approaches: kinetic energy and nutrient load, The main large rivers have right skew angles to the gulf, which makes the contribution to the tide counter-clockwise cycle, the patches of phytoplankton around estuary have shifted to the right, the shifted distance is 8 km longer in rainy season than in dry season in Colorado estuary. The phytoplankton primary production is 1.45 times higher in rainy season than in dry season due to river nutrient load.

Water temperature has polynomial relation impact on the phytoplankton growth speed, it has positive impact on phytoplankton growth less than 30.01ºC in open sea, the increase gradient is between 0.03-0.05 mg/m^3*ºC, but it has negative impact larger than that degree, the decrease gradient is about 0.02 mg/m^3*ºC, this phenomena is not clear in the gulf due to other factor affections. The SST

before May 1998 has stress action on the phytoplankton growth due to the El-Niño appearance, but SST after May 1998 has the stimulated action to the phytoplankton growth. The season's change of SST is less than 8 ºC and minimum SST year round is more than 25 ºC, it is impossible for SST less than the temperature in deep water. The gradient-caused upwelling of vertical temperature is quite difficult in the gulf.

SSC has light attenuation action on the phytoplankton growth, and has negative impact on the phytoplankton abundance, SSC less than 45 mg/m^3 has little impact on PPC, which keep chlorophyll-a oscillated between 1.2 and 1.5 mg/m^3, the first order derivative is calculated to analyse chlorophyll-a decrease rate as SSC increase, it shows a linear decrease trend of PPC, high SSC With impact of -0.25 mg/m^3*SSC mg/l affects the PPC larger than low SSC with impact of -0.02 mg/m^3*SSC mg/l, this correlative formula has not universal use, the SSC more 52 mg/m^3 and less than 41 mg/m^3 have different conclusion.

Chapter 7: Conclusions and recommendations

7.1. Conclusions

Remote sensing technique is available to apply on researches of SST, SSC, PPC, PPP and wave current, especially on daily monitoring of SST, PPC, wave current at mesoscale. The calculation accuracies of SST and SSC are higher than PPC. The physical processes have more complicate variability in the gulf than in open sea, and extremely affect the phytoplankton growth, biomass and distribution.

7.1.1. Methodology and data

The methodologies for case study are focused on the processes and calculations of sea surface temperature, phytoplankton PPC, SSC and wave direction and speed. The raw data, calculation formula, and result quality are compared and evaluated.

The sensor AVHRR has powerful 3 thermal bands for detection of SST; SeaWIFS has 20 nm narrow visible bands for measurement of PPC; TM has spatial resolution for measurement of SSC plumes; Seawind has ability of quick detection of wave height with SAR.

The calculation of non-linear SST is applied in this study, which have three advantages: (1) split window technique is used to remove atmosphere impact; (2) sun zenith angle correction; (3) real-time buoy *in situ* data correction. The match technique of date and time for mosaic of monthly SST is applied to remove temporal SST difference, and cloud top temperature technique is suitable for detection and removal of clouds. Total result quality of non-linear shows that the atmosphere impact reduces SST 7.88 °C in band 4 and 11.22 °C in band 5, satellite zenith angle reduces SST 0.21°C, date match affects SST ± 0.2°C, time match affects SST ± 0.15°C.

OC4.V4 algorithm is applied for calculation of phytoplankton PPC. This algorithm has an advantage over previous switching algorithms in that the maximum of band ratio is selected for calculation and there is no inherent discontinuity between chlorophyll values at the point where the switch occurs. The algorithm has consideration of the factor impacts of Rayleigh scattering, Ozone absorption, solar zenith angle, application of band ratio removes the most impacts of SSC and yellow organism and makes high quality of calculation.

Statistical algorithm of SSC calculation is applied in Golfo Dulce, Natural logarithm has R^2=0.87 high correlation with *in situ* samples. TM band 3 has sensitive to detect SSC in high SSC and TM band 2 has sensitive to SSC in low SSC, the ratio of band 3/5 can remove atmosphere impact, and improves accuracy 3.43 %.

7.1.2. Ocean physical processes

The concept of gulf closeness is defined; it concerns factors of gulf perimeter, depth and intercept area. The total gulf closeness is 77.12 %, which includes surface closeness 92.86 %, vertical depth closeness 70 %, vertical intercept area closeness 75.03 %, it belongs to high closeness gulf.

The SST is controlled by the factors of extra-terrestrial solar radiance, rainfall, gulf morphology, horizontal water heat flux in Golfo Dulce. The SST is higher inside gulf than outside gulf with the temperature gradient 0.02 °C/km, the SST in middle gulf is higher than in coast water with gradient 0.25 °C/km. This is reasons of (1) sea current is weaker and more stagnant than open sea due to the morphology of the Gulf, heat vertical and horizontal flux is difficult or slow; (2) peninsula OSA and Puntarenas mountain surrounding the Gulf result in the sea wind blocked and weakened in the Gulf, sensible heat and evapotranspiration to air is comparatively low; (3) the gulf coast emits more solar radiance to atmosphere than sea surface, coastal land absorbs part of heat of water and balances the energy lost to the air.

There is 1.5 °C and 2 °C oscillated annually in open sea and inner gulf in 1991-2001 respectively. Anomalous “hot spot” of SST is located in the west inner gulf. “Hot spot” is stretched to northwest or southeast as SST is increased, it occurs in 3-4 years; anomalous “cold tongue” happens around the gulf mouth, it normally shows a long shape like tongue inserting to the gulf from southwest to northeast, it starts at west border of the gulf mouth, then stretches to east of the gulf like meander, it has 2 year cycles. “Hot spot” is caused by the gulf morphology, and “cold tongue” is the reason of open sea SST oscillation. SST in dry season is 31-32 °C 1998, 2 °C higher than normal year, SST decrease to 27 °C in rainy season, SST peak occurred in March, the lowest SST occur in October, The SST in open sea has 1-month earlier reach peak temperature than inner gulf, it is can be infer that water heat is conducted from open sea to the gulf in early 1998 due to El Niño event. The gulf SST in 1991-2001 are compared to El Niño temperature shows that: (1) the SST out of gulf has relatively higher correlation to El Niño than in inner gulf, (2) inner gulf indicates weaker being affection by El Niño; (3) the impact of El Niño is confirmed again its advection through sea surface heat flux rather than indirect impact through climate change.

Solar hours directly control the SST in the gulf, there are excellent correlation between SST and solar hours if solar hours are shifted 2-month forward, that mean 2-month delay for seawater “warm up” by solar energy, SST out of the gulf has bad correlation due to horizontal heat flux influence. The gulf energy transfer model is built for analysis of SST change in 1998, the seawater get solar highest energy or radiance in March and September without other factor impact, but warming up of seawater makes highest SST in May and November, which there is two months delay, El Niño event occurred before May “lift” the SST average 2-3 ºC, cloud coverage after May stresses SST 3-5 ºC.

Tide current plays a main role in all currents in Golfo Dulce. The dominant tide current displays counter-clockwise horizontal cycling, some eddies occur in the middle of gulf between flooding period and ebbing period, high speed current occurs at “sill”. There are two reason inferred for the formation of counter-clockwise current: (1) sea current on north equator always flows turn right due to the earth self rotation; (2) main river currents head to the gulf in right angle of 30-80° and assist kinetic energy of cycling. Two wind systems (Caribbean Trade Wind, pacific Costa Rica Coastal Current) control wave current in study area, the southwest wave current in dry season is favourite to the upwelling of nutrients but it is weaker than in rainy season, so there is rare upwelling occurrence except for west gulf mouth. The southwest wave current in rainy season is comparative strong and

strengthens the flooding tide current and reduces the ebbing tide current. Strong and regular parallels of sea waves likes “fan” occur in the gulf mouth, the waves in middle gulf are disturbed and irregular due to valley-mountain breezes and land-sea breezes in the northeast direction intersect the wind direction of northwest coming from the gulf mouth; there is weak wave occurs in inner gulf.

The distribution and concentration of SSC are mainly depended on the water kinetic energy and sand source supply. The SSC are most distributed at the estuary. The biggest patch of SSC is distributed out of R. Coto-Colorado due to sand supply and tide current disturbing, the plume of SSC in Tamales is smaller, but it has high SSC. The total area of the gulf is 609.38 km^2, 82% area of the gulf is composed of SSC less than 50 mg/l, which distributed in middle gulf, 14.5% area of gulf has SSC 50-60 mg/l which distributed in far reach of estuary, only 3.1% area of the gulf has SSC more than 60 mg/l, which distributed at the estuary. Counter-clockwise tide current generates the spit of SSC in east gulf mouth and pushes it northward 5 km along the east shore from 2000 to 2001, meanwhile, the SSC in Tamales estuary on west gulf mouth has moved southward 1 km along the west shore. The most parts of gulf during the 2000-2001 show the trend of clarified water due to vegetation coverage recover, except for the mouth of Colorado river and Tamales river where still keep increase of SSC in 2001, this is reason there is higher rainfall in dry season this year which results in the more soil erosion in the gulf.

7.1.3. Phytoplankton pigment and primary production

The chlorophyll-a in Golfo Dulce is determined by the river nutrients rather than upwelling of the deep-water nutrient supply, which previous scientist estimated. The river nutrients are most depended on the area catchments rather than only soil erosion, since the large catchments bring more nutrients.

The PPC is higher in Golfo Dulce than out of the gulf, which in the gulf range from 0.08 to 18.25 mg/m^3, the mean of chlorophyll-a is 2.68 mg/m^3, there are some features on chlorophyll-a spatial distribution: (1) high chlorophyll-a “dome” is distributed at estuaries of Colorado river and Rio Esquians river and low chlorophyll-a “hole” is distributed in gulf mouth and the north gulf coast; (2) the PPC is higher in the middle gulf than in the coast; (3) the PPC in the north coast of inner gulf is lower than in south coast of inner gulf; (4) the PPC is higher along shore than off shore out of gulf; (5) higher PPC is in the west mouth of gulf than in the east. Temporal changes have following characteristics: (1) high value of 4-5 mg/m^3 occurs in October-November, the second peak occurs in July-August, the low value less than 1 mg/m^3 occurs in January-April, which is during the dry season; (2) the seasonal variety of PPC is higher in the river mouth than other place, the seasonal standard deviation is 8.36 mg/m^3 out of river and 1.32 mg/m^3 in the middle gulf; (3) there is lower concentration and lower variety of concentration in the north of coast of the gulf than in the south coast.

There is low phytoplankton population in Golfo Dulce, Mean PPP in 1998 in Golfo Dulce is 263.344 g C m^{-2} yr^{-1}, it ranges from 138.1 to 1007.7 g C m^{-2} yr^{-1}, total PPP is 140559.59 ton, and monthly PPP in rainy season has 39.76 % higher than dry season. The concept of climate integrate factor (CIF) is presented to evaluate potential PPP in 1991-2001, which is variables of monthly precipitation and monthly mean daily solar hours, CIF has best correlation with PPP with R^2=0.91 if monthly precipitation shifts one month forward, and PPP in 1984 has highest CIF 17.6, which indicates the potential PPP with 186020 ton.

7.1.4. Ocean process impacts on phytoplankton primary production

Physical process plays an important role in phytoplankton abundance and distribution, there are five factors affect phytoplankton in Golfo Dulce: river current, tide current, SSC, solar radiance and SST. River current has main impact on the nutrient supply of phytoplankton; tide current has main contribution to the phytoplankton distribution.

Tide current dilutes the phytoplankton concentration and changes the distribution. There are three horizontal flow types of tide and wave: flooding dominant current, counter-clockwise current and clockwise current. The counter-clockwise type is more popular than others, the impact of large patch phytoplankton movement occur at sill, flooding current is stronger than ebbing current due to prevailing the northward wind action, it demonstrates that tide current in the gulf plays an role of barrier to hinder phytoplankton flowing out of the gulf due to the concentration gradient. There is 10.92 km diameter wide area for exchange of large phytoplankton patch around gulf mouth, which has 3.47 km shifted to inner gulf from sill. Upwelling is a rare phenomenon in most of the gulf due to stagnant geomorphology except in the west gulf mouth, where convex coastline causes high-speed sea current and pulls seawater off the shore, sea currents moving out of the gulf are stronger than sea current moving into gulf in the west coast and cause more upwelling in the south corner in dry season.

River currents affect the phytoplankton in two approaches: kinetic energy and nutrient load, The main large rivers have right skew angles to the gulf, which makes the contribution to the tide counter-clockwise cycle, the patches of phytoplankton around estuary have shifted to the right, the shifted distance is 8 km longer in rainy season than in dry season in Colorado estuary. The phytoplankton primary production is 1.45 times higher in rainy season than in dry season due to river nutrient load.

Water temperature has polynomial relation impact on the phytoplankton growth speed, it has positive impact on phytoplankton growth less than 30.01ºC in open sea, the increase gradient is between 0.03-0.05 mg/m^3*ºC, but it has negative impact larger than that degree, the decrease gradient is about 0.02 mg/m^3*ºC, this phenomena is not clear in the gulf due to other factor affections. The SST before May 1998 has stress action on the phytoplankton growth due to the El-Niño appearance, but SST after May 1998 has the stimulated action to the phytoplankton growth. The season's change of SST is less than 8 ºC and minimum SST year round is more than 25 ºC, it is impossible for SST less than the temperature in deep water. The gradient-caused upwelling of vertical temperature is quite difficult in the gulf.

SSC has light attenuation on the phytoplankton growth, and has negative impact on the phytoplankton abundance, SSC less than 45 mg/m^3 has little impact on PPC, which keep chlorophyll-a oscillated between 1.2 and 1.5 mg/m^3, the first order derivative is calculated to analyse its decrease rate as SSC increase, it shows a linear decrease trend of PPC, high SSC With impact of -0.25 mg/m^3*SSC mg/l affects the PPC larger than low SSC with impact of -0.02 mg/m^3*SSC mg/l, this correlative formula has not universal use, the SSC more 52 mg/m^3 and less than 41 mg/m^3 have different conclusion.

7.2. Recommendation

The accuracy of parameter calculation are required to be improved, the factors of sea bottom reflectance remove from SSC, PPC, SST will be concerned in future study, so as thin cloud detection and

spectrum remove. SeaWIFS data has some noise and affect the image quality; coming launched satellite is expected to solve this problem.

The multi sensor approaches followed in this study was a variety of image data, field data, algorithms and spatial data handling software. Beside the field data, almost all other image data and tools can be obtained through the Internet. This fact enables the researchers, and other users, to apply the approach to similar marine coastal environment in other part of the world. It is, therefore, envisaged to continue this type of coastal remote sensing work in China's marine coastal area. This thesis may serve a practical guide in how to obtain the image data and how to implement these in the algorithms used to describe and model the marine coastal dynamics.

Literature reference

1. Abudaya M.I., 2001. Analysis of multitemporal satellite imagery for total suspended sediments in coastal waters of Golfito and Golfo Dulce, Costa Rica. ITC-Coastal Zone Studies report.
2. Alfoldi, T. T., 1980. Remote sensing for water quality monitoring. In remote sensing for resource management, pp. 317-328.
3. Allen, P.H.1956. The rain forest of Golfo Dulce. Univ. of Florida Press, Gainesvill, Fl. 390 p.
4. Anderson, J.J. and Devol, A.H. 1987. Extent and intensity of the anoxic zone in basins and fjords. Deep-sea research 34: 927-944.
5. Barton, I.J. and R.P. Cechet. 1989. Comparison and optimization of AVHRR sea surface temperature algorithms. Journal of Atmospheric and Oceanic Technology 6: 1083–1089.
6. Berrange, J.P. & R.S. Thorpe. 1988. The geology, geochemistry and emplacement of the Cretaceous-Tertiary ophiolithic Nicoya complex of the Osa peninsula, southern Costa Rica. Tectonophysics. 147: 193-220.
7. Berrange, J.P. & R.S. Thorpe. 1989. The Osa Group: An auriferous Pliocene sedimentary unit from the Osa peninsula, southern Costa Rica. Rev. Geol. Amer. Centr. 10: 67-93
8. BOZA, M. 1996. Refugio Nacional de Fauna Silvestre Golfito. In: Boza, M (ed.): Costa Rica Parques Nacionales, San José, Costa Rica. Edit. INCAFO. 180-187.
9. Campbell, J.W. & J.E. O'Reilly. 1988. Role of satellites in estimating primary productivity on the Northwest Atlantic continental shelf. Cont. Shelf Res. 8:179-204.
10. Cornillon, P., C. Gilman, C., L. Stramma, O. Brown, R. Evans and J. Brown. 1987. Processing and analysis of large volumes of satellite-derived thermal infrared data. Journal of Geophysical Research 92: 12,993–13,002.
11. Cortes, J. 1993. A reef under siltation stress: a decade of degradation. In: Global aspects of corals: health, hazards and history. University of Miami, Miami.
12. Dubinsky, Z., P.G. Falkowski, & K. Wyman. 1986. Light harvesting and utilization by phytoplankton. Plant Cell Physiol. 27:1335-1349.

13. Eileen Hofmann, 1999. 1999 EOS reference handbook.

14. Eppley, R.W., E. Stewart, M.R. Abbot & V. Heyman. 1985. Estimating ocean primary production from satellite chlorophyll; Introduction to regional differences and statistics for the Southern California Bight. J. Plankton Res. 7:57-70.

15. Fiancis A. Richards, James J.A. and Joel D.G, 1971, chemical and physical observations in Golfo Dulce, an anoxic basin on the pacific coast of Costa Rica. Limnology and oceanography, January 1971, V. 16(1)

16. Fischer, R. 1980. Recent tectonic movements of the Costa Rica Pacific Coast. Tectonophysics 70: T25-T33.

17. Glynn P.w., Druffel, E.M., and Dunbar, R.B. 1983. A dead central American coral reef tract: possible link with the little ice age. J. Marine research 41:605-637.

18. Gordon, H., R., and Brown, O.B., 1973.Irradiance reflectivity of a flat ocean as a function of its optical properties. Applied Optics, 12, 1549-15551.

19. Gordon and Monrel 1983, remote assessment of ocean color for interpetation of satellite visible imagery: a review. In Lecture notes on coastal and estuarine studies. Pp 1-114.

20. Gordon, H.R., 1996. MODIS Normalized Water-leaving Radiance Algorithm Theoretical Basis Document (Version 3).

21. Herrera, W.1985. Clima de Costa Rica. Editorial universidad estatial a distancia, San Jose, Costa Rica.

22. Hartman, H.J, 1996. The Golfo Dulce marine enviroment: review and assessment.

23. Hobma T.W. *et al.,* 2002. Geoinformation for Coastal Zone Management in Golfito Costa Rica. Report on an integrated assessment of the coastal environment using RS & GIS, 14 May – 12 July 2001. ITC-Coastal Zone Studies report.

24. Jagdish krishnaswanmy, Danniel D. Patriick N., & Michael S. 2001. sptial patterns of suspended sediment yields in a humid tropical watershed in Costa Rica. Hydrological processe. 15: 2237-2257 .

25. Jamdes L. Mueller, 2000. SeaWIFS postlaunch technical report series, NASA technical memorandum 2000-206892, Vol. 11.

26. JIMENEZ, Q. y L. POVEDA. 1996. Lista actualizada de los árboles maderables de Costa Rica. Aportes al desarrollo sostenible 2. Facultad de Ciencias de la Tierra y del Mar, Universidad Nacional. 36p.

27. Jorge cortes,1990. The coral reefs of Golfo Dulce, Costa Rica: distribution and community structure.

28. Laws, E. A. & T. T. Bannister. 1980. Nutrient- and light-limited growth of Thalassiosira fluviatilis in continuous culture with implications for phytoplankton growth in the ocean. Limnol. Oceanogr. 25:457-473.

29. Lews, L.R. 1983. The geology of the Osa Peninsula, Costa Rica: observations and speculations about the evolution of par of the outer are of the southern central American Orogen. Master Thesis, Pennsylvania State Univ., Pennsylvania. 91 p.

30. L.HAN, 1994. The spectral responses of algal chlorophyll in water with varying levels of suspended sediment. INT. J. remote sensing, Vol. No. 18, 3707-3718.

31. Li Jing, 1986. A study on determination of concentration of suspended sediment in water by remote sensing, Acta Scientiae Circumstantiae, 6, 166-173.

32. Li Xia, 1993. A united model for quantitative remote sensing of suspended sediment concentration, INT. J. remote sensing, Vol. 14, 2665-2676.

33. Martin, J.H. 1992. Iron as a limiting factor in oceanic productivity. In: Primary Productivity and Biogeochemical Cycles in the Sea. [eds.] P.G. Falkowski and A.D. Woodhead, Plenum Press, New York, pp.123-137.

34. McClain, E.P., W.G. Pichel and C.C. Walton. 1985. Comparative performance of AVHRR-based multichannel sea surface temperatures. Journal of Geophysical Research 90: 11,587–11,601.

35. Minnett, P.J. 1990. The regional optimisation of infrared measurements of sea surface temperature from space. Journal of Geophysical Research 95: 13,497–13,510.

36. Munday, J. C., and Alfoldi, T. T., 1979. Landsat test of diffuse reflectance models for aquatic suspended solids measurement. Remote sensing of environment, 8, 169-189.

37. NUBN, H. 1978. Atlas preliminar de Costa Rica. Información Geográfico Regional. San José, Costa Rica. 47p.

38. P.Cracknell, 1997. The advanced very high resolution radiometer, Taylor &Francis, 193p.

39. Philot, W., 1981. A radiative transfer model for remote sensing of inhomogeneous water. Ph.D. dissertation, university of Delaware.

40. Platt, T. and W.G. Harrison. 1985. Biogenic fluxes of carbon and oxygen in the ocean. Nature. 318:550-558.

41. Quesada, F.; Q. Jimenez; N. Zamora; R. Aguilary J. Gonzalez. 1997. Árboles de la Península de Osa. InBio. Heredia, Costa Rica. 411p.

42. Quiros, G.E.1991. Establecimiento de una finca productora de camarones en el alto Golfo Dulce: informacion tecnica fundamental, climatologia, oceanogrfia, ecologia. Manuscrip. Seccion de oceanogfia, departamento de fisica, universidad nacional, Heredia, Costa Rica. 17p.

43. Richards, F.A., Anderson, J.J., and Cline, J.D. 1971. Chemical changes, including nitrate reduction, in Darwin bay, Galapagos Archipelago, over a 2-month period, 1968. Limnol. Oceanogr. 16: 758-765.

44. Sakshaug, E., D.A. Kiefer, & K. Andresen. 1988. A steady-state description of growth and light absorption in the marine diatom Skeletonema costatum. Limnol. Oceanogr. 43:198-205.

45. Schwalb, A. 1978. The TIROS-N/NOAA A-G satellite series. NOAA Technical Memorandum NESS 95. U.S. Government Printing Office. Washington, DC. 75 p.

46. Smith, R.C., R.W. Eppley, & K.S.Baker. 1982. Correlation of primary production as measured aboard ship in southern California coastal waters and as estimated from satellite chlorophyll images. Mar. Biol. 66:281-288.

47. SOTO, R. and J. JIMÉNEZ, 1992. Evaluación ecológica rápida de la península de Osa. Costa Rica. Fundación Neotrópica. Fondo Nacional para la Conservación de la Naturaleza. 252p.

48. S.Tassan 1993. An improved in-water algorithm for the determination of chlorophyll and suspended sediment concentration from Thematic Mapper data in coastal waters. International journal of remote sensing. Vol. 14: No. 6, 1221-1229.

49. Vermote E.F. and Vermeulen A. 1999. atmosphereic correction algorithm: spectral reflectances (MOD09), MODIS algorithm technical background document.

50. Volk and Hoffert, 1985 Ocean carbon pumps: Analysis of relative strengths and efficiencies in ocean-driven atmospheric CO_2 exchanges. *In:* E. T. Sunquist and W. S. Broeker.(ed) The Carbon Cycle and Atmospheric CO_2: Natural Variations Archean to Present, American Geophysical Union, Washington, D C 99-110 pp .

51. Walton, C.C. 1988. Nonlinear multichannel algorithm for estimating sea surface temperature with AVHRR satellite data. Journal of Applied Meteorology 27: 115–124.

52. Walton, C.C., E.P. McClain and J.F. Sapper. 1990. Recent changes in satellite based multichannel sea surface temperature algorithms. Marine Technology Society Meeting, MTS' 90, Washington D.C, September 1990.

53. Weyl, R. 1980.Geology of Central America. Borntrager, Berlim. 371 p.

54. Wim H.B. 2001. Principles of Remote Sensing, ISSN 1567-5777

Appendix

A1: Annual sea surface temperatures between 1991-2001

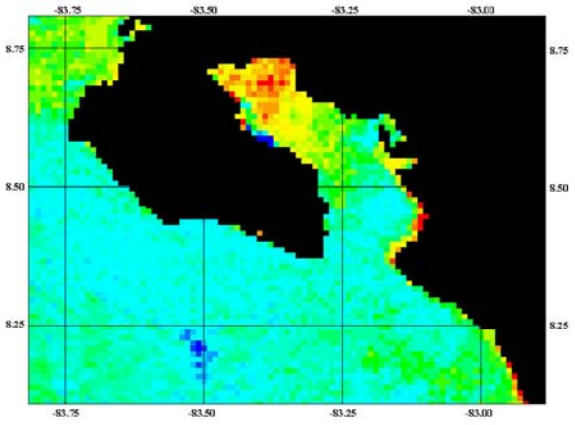

SST in 1991

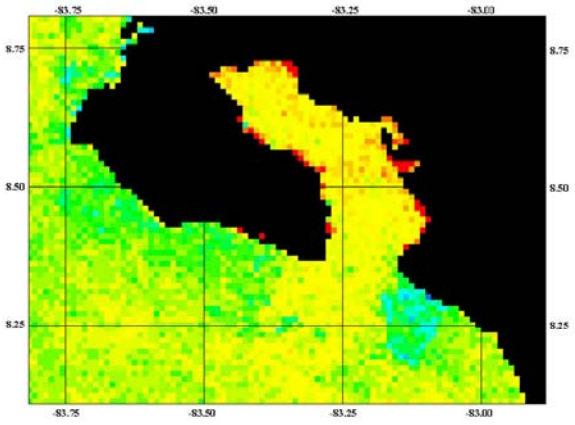

SST in 1992

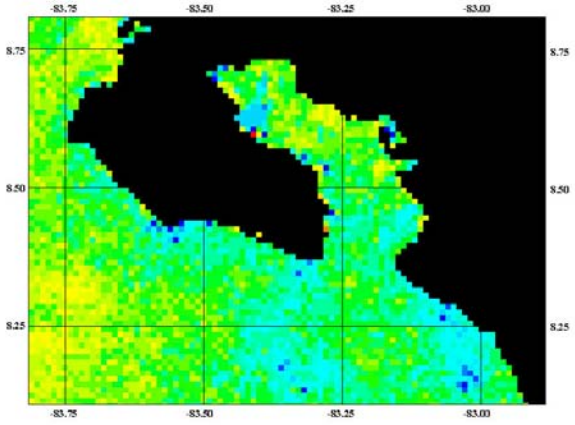

SST in 1993

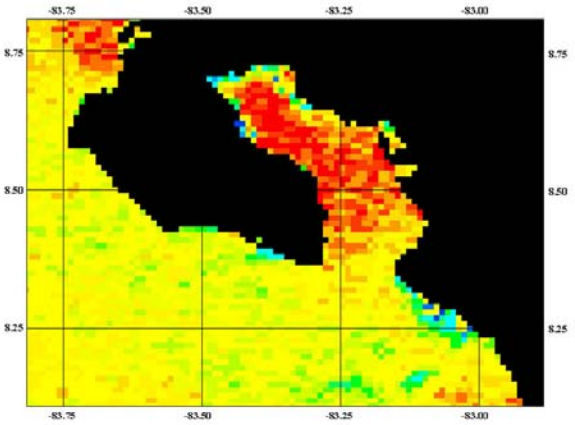

SST in 1994

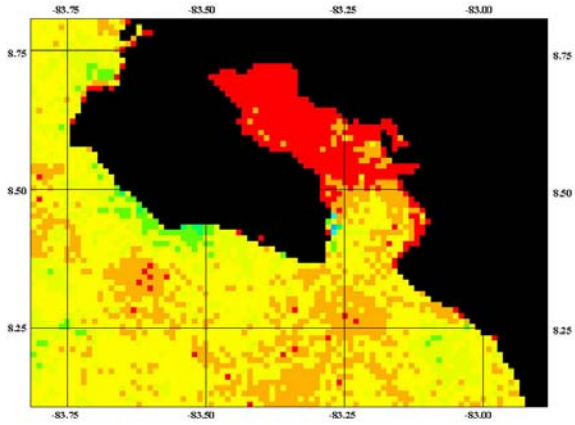

SST in 1995

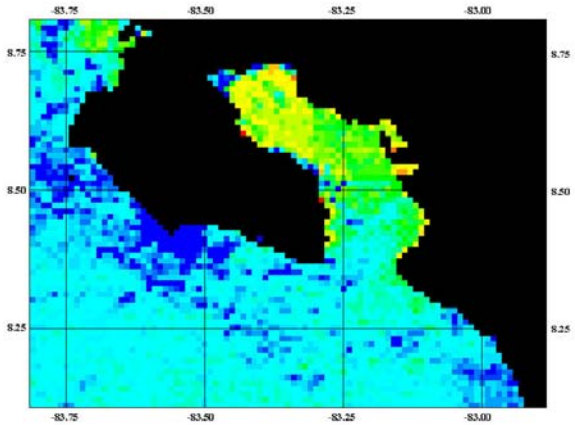

SST in 1996

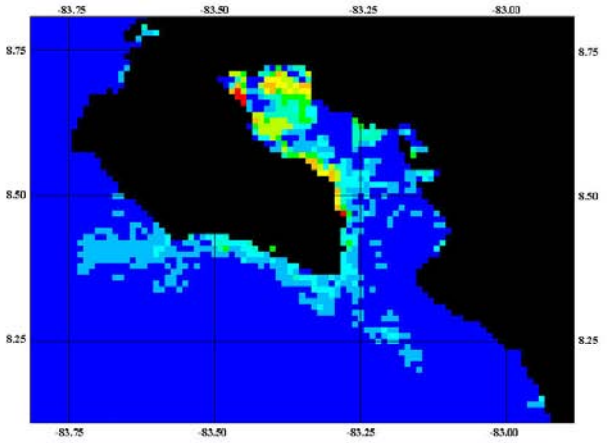

SST in 1997

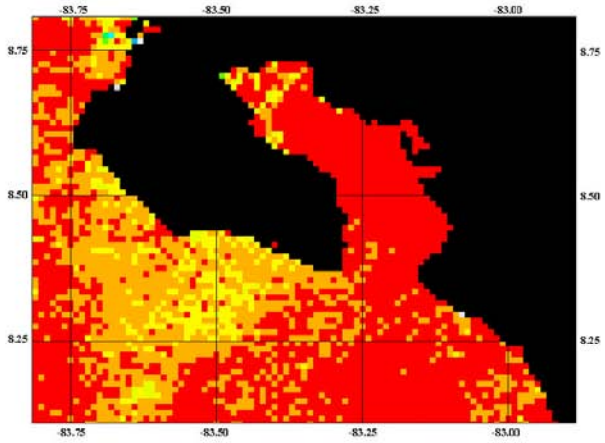

SST in 1998

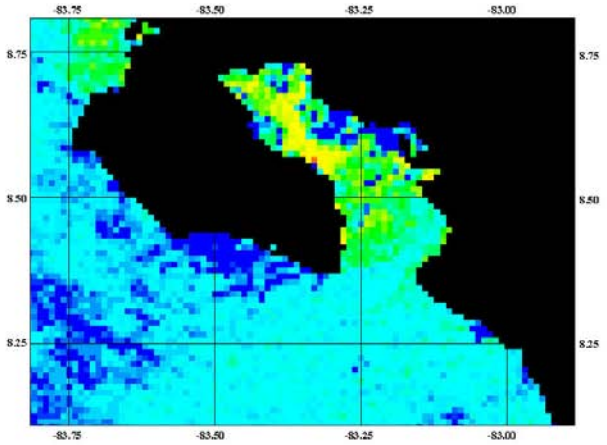

SST in 1999

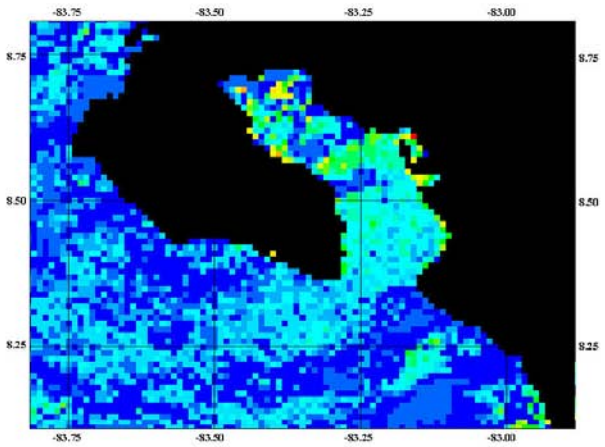

SST in 2000

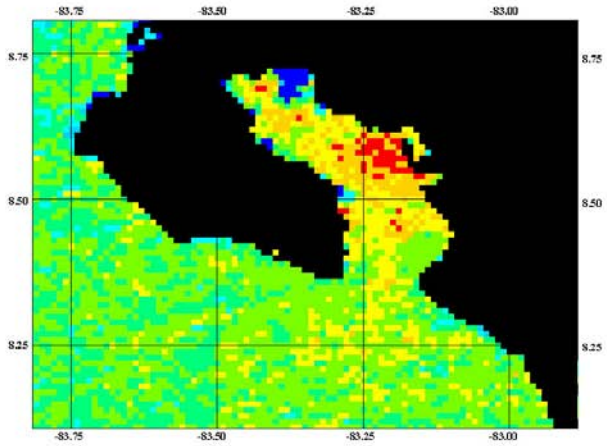

SST in 2001

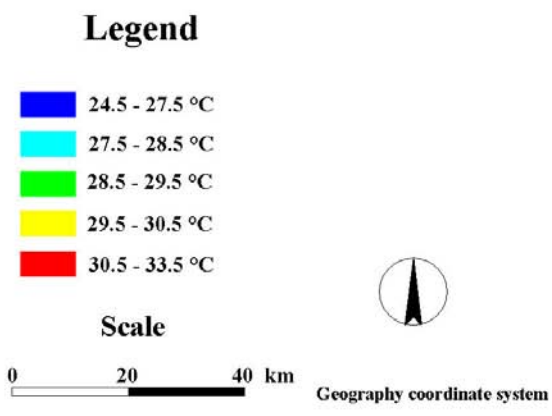

A2: Monthly sea surface temperatures in 1998

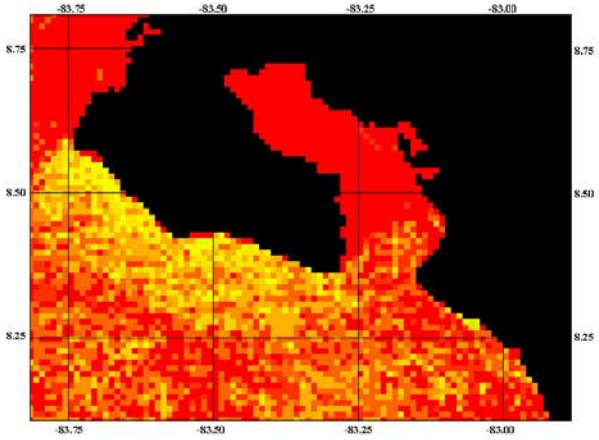

SST in January 1998

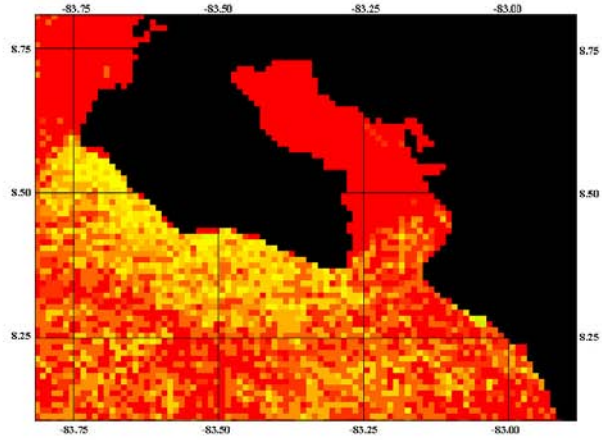

SST in February 1998

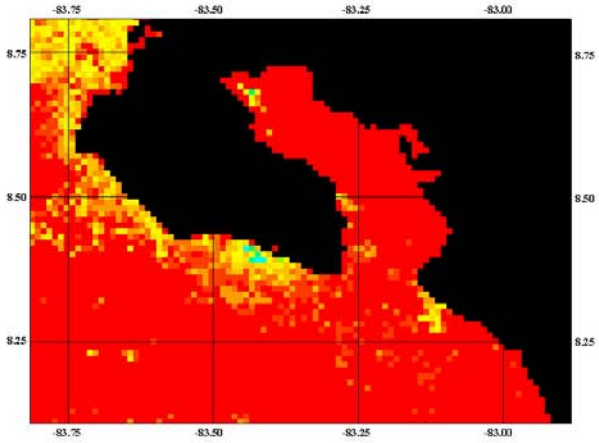

SST in March 1998

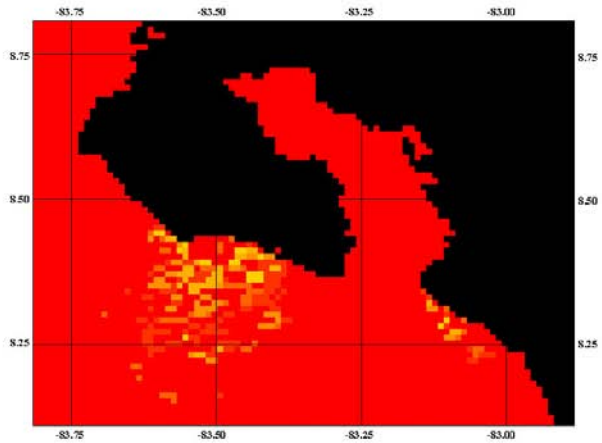

SST in April 1998

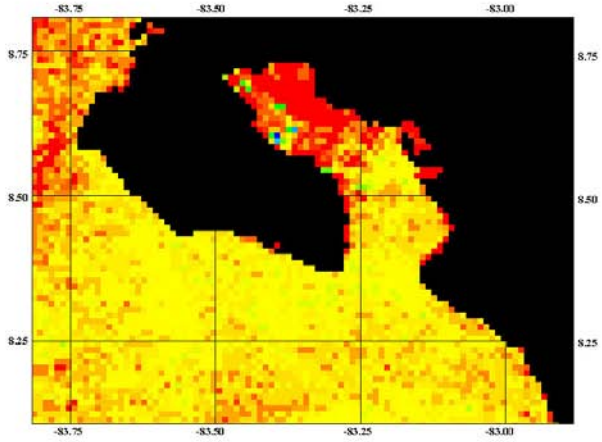

SST in May 1998

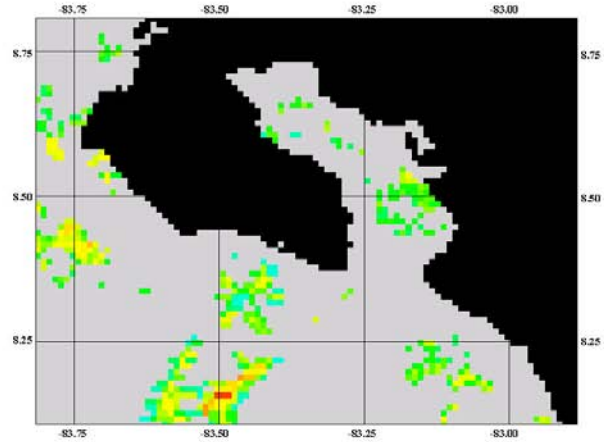

SST in June 1998

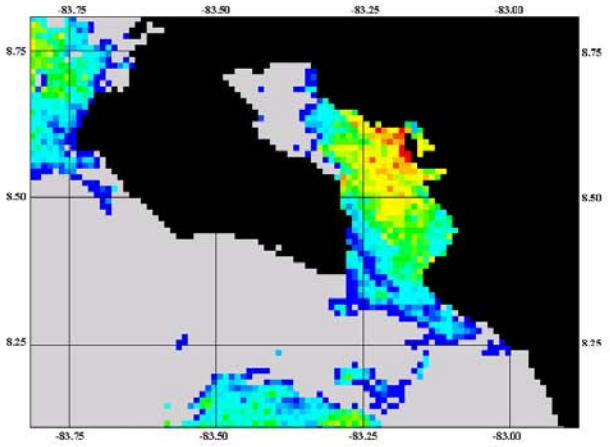

SST in July 1998

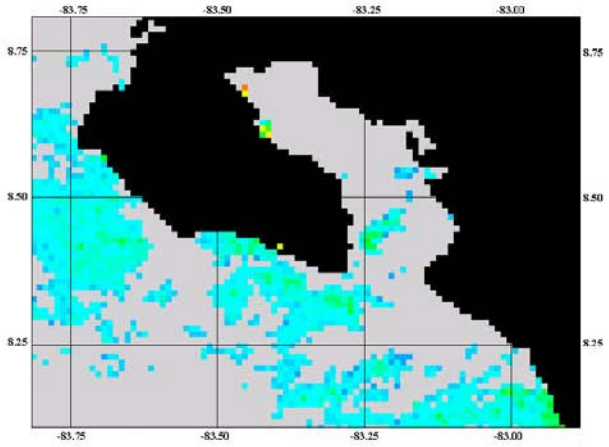

SST in August 1998

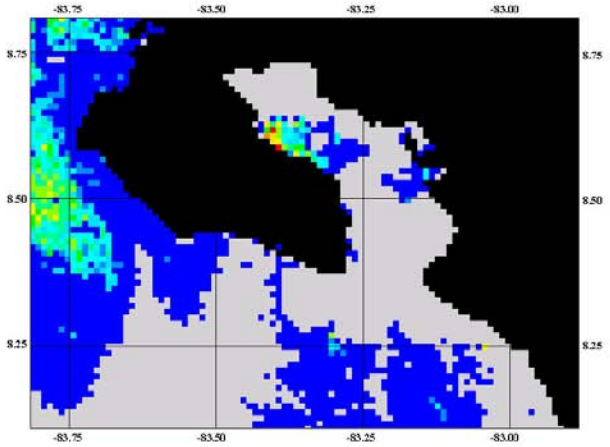

SST in October

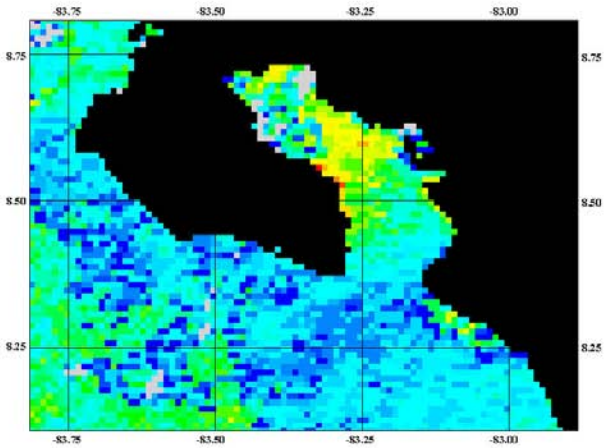

SST in November 1998

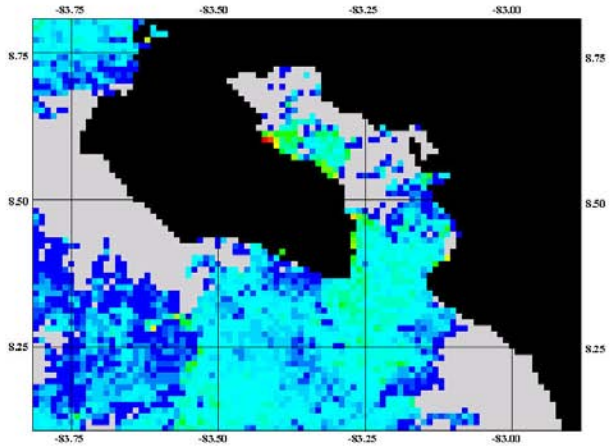

SST in December 1998

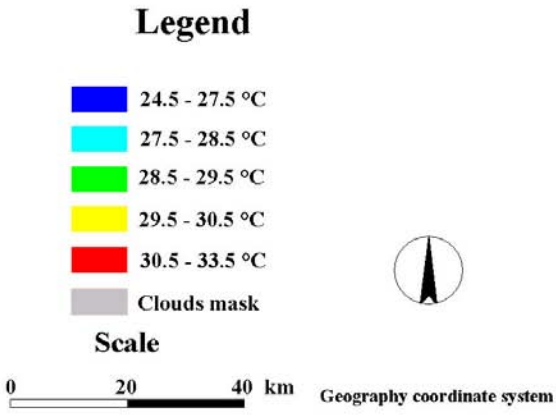

A3: Monthly Phytoplankton pigment concentration in 1998

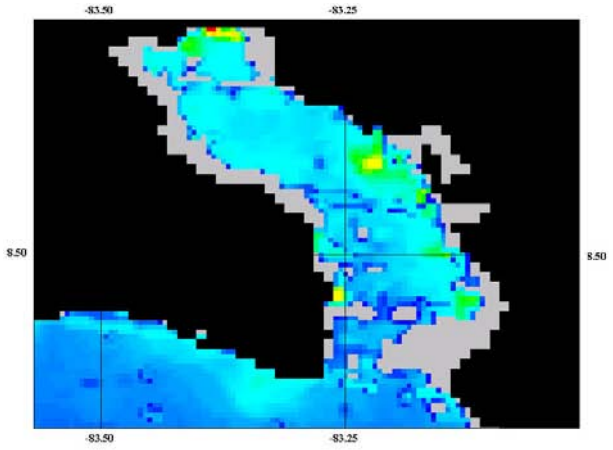

PPC in January 1998

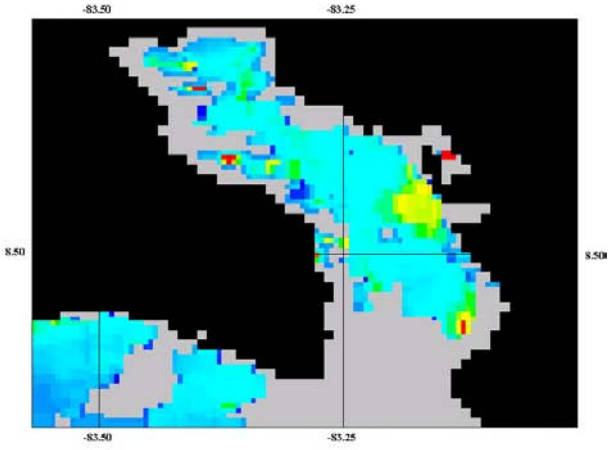

PPC in February 1998

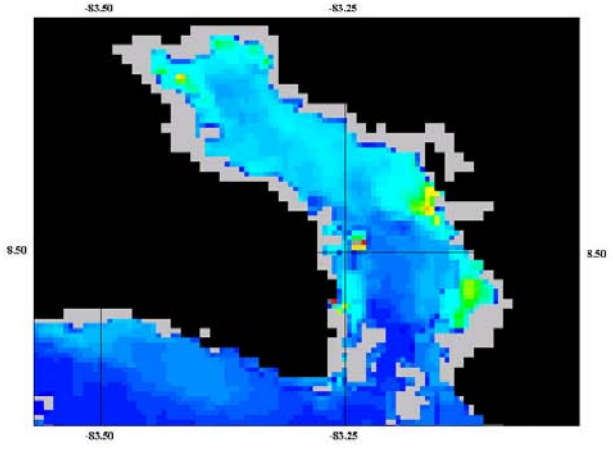

PPC in March 1998

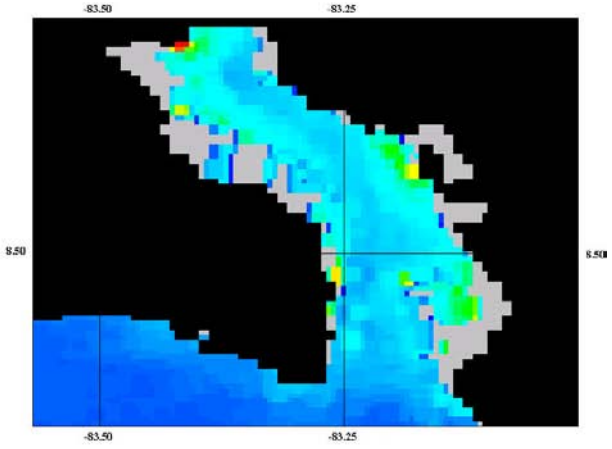

PPC in April 1998

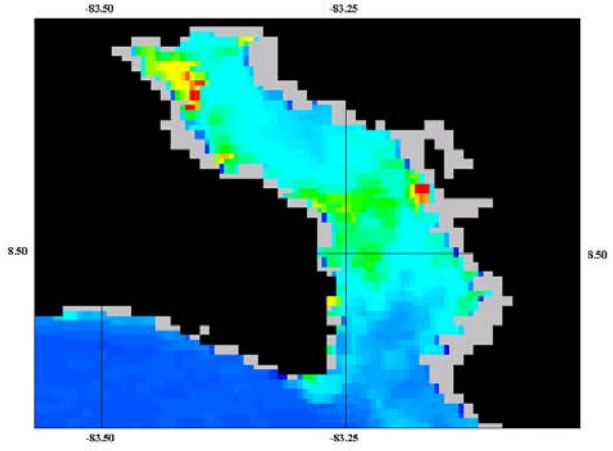

PPC in May 1998

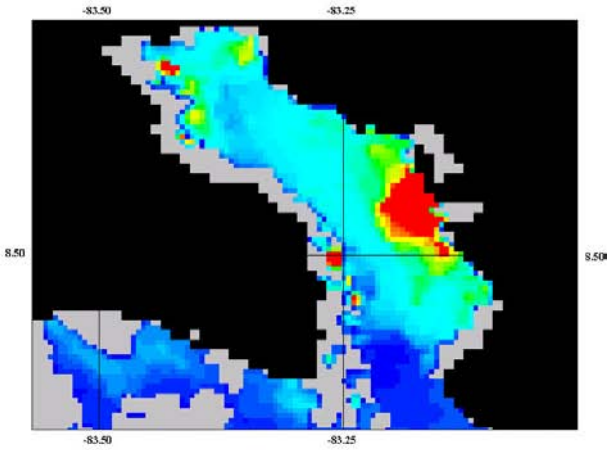

PPC in June 1998

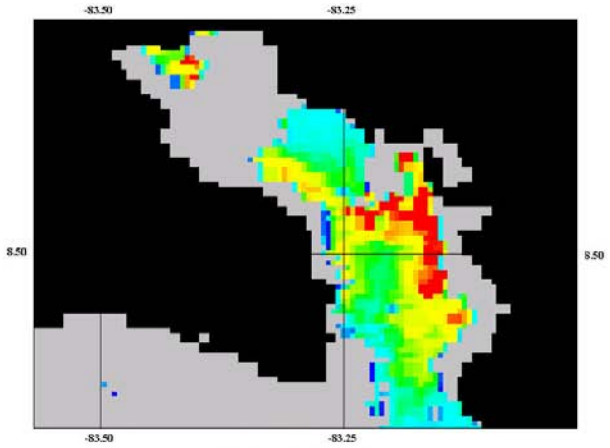

PPC in July 1998

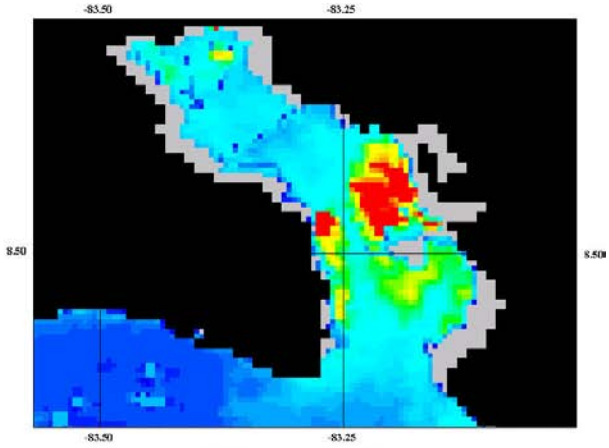

PPC in August 1998

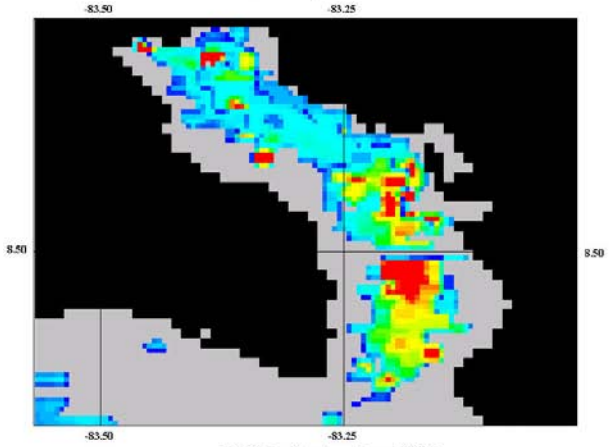

PPC in September 1998

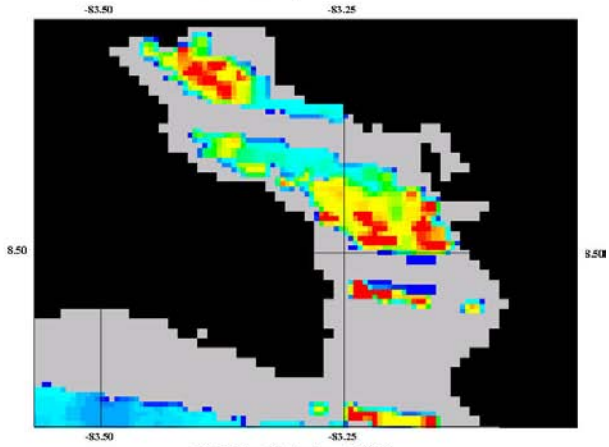

PPC in October 1998

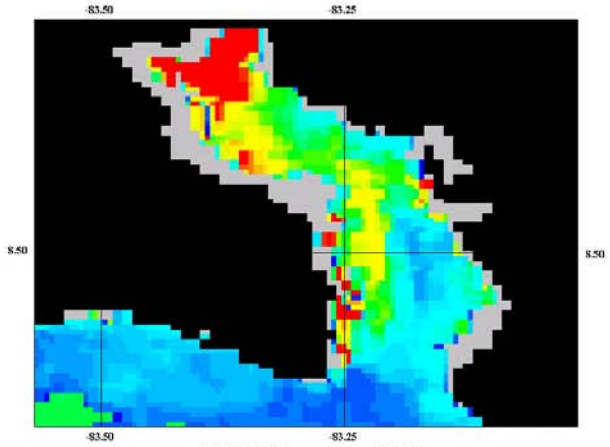

PPC in November 1998

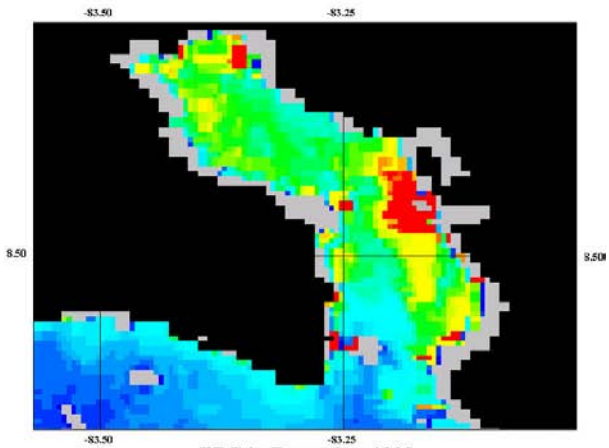

PPC in December 1998

Legend

- 0.0 - 0.5 mg/m3
- 0.5 - 1.5 mg/m3
- 1.5 - 2.5 mg/m3
- 2.5 - 3.5 mg/m3
- 3.5 - 20 mg/m3
- Clouds mask

Scale

0 20 40 km

Geography coordinate system

A4: Suspended sediment concetrations between 1998-2001

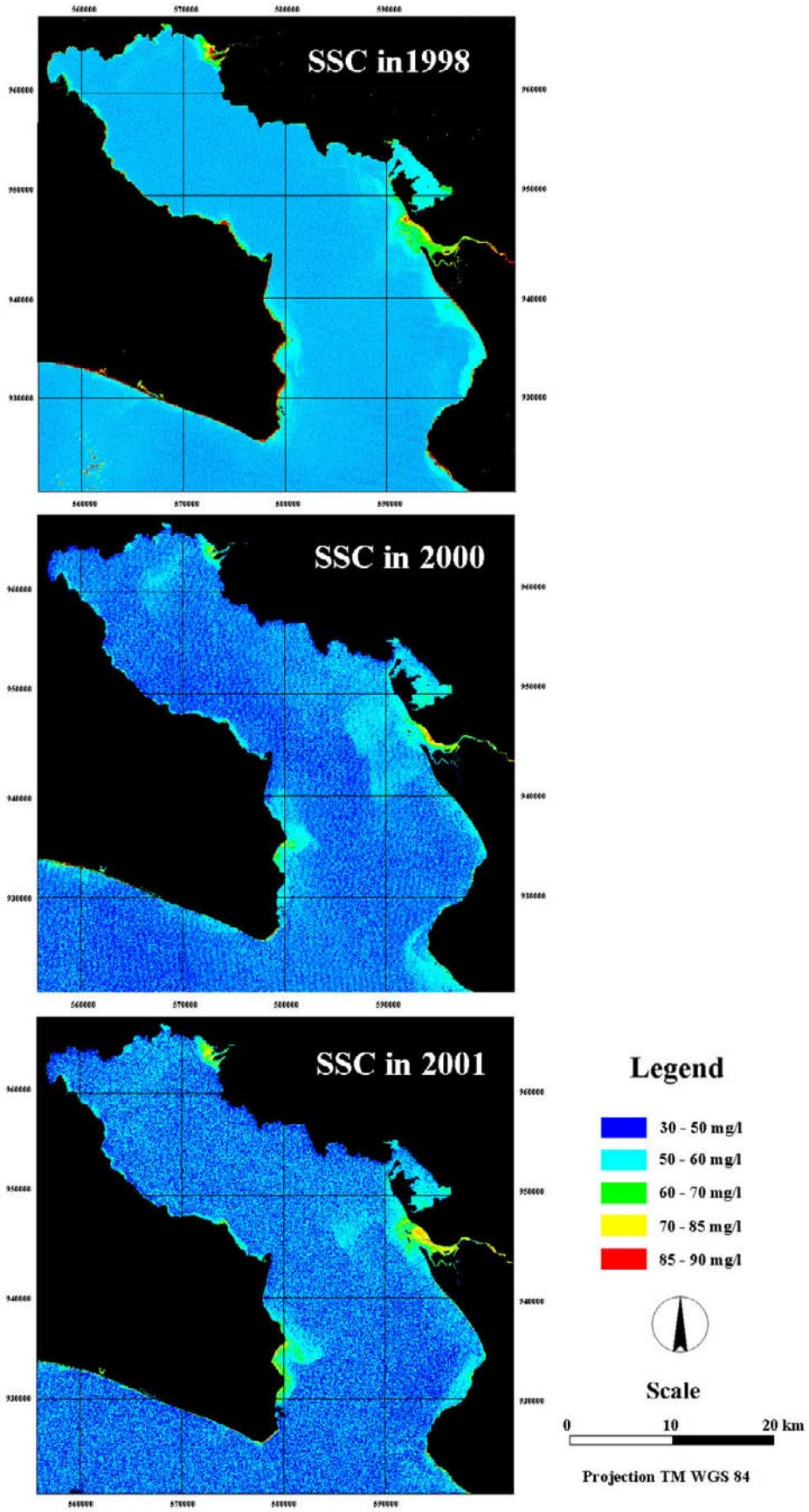

A5: Monthly sea wind directions and speeds in 2001

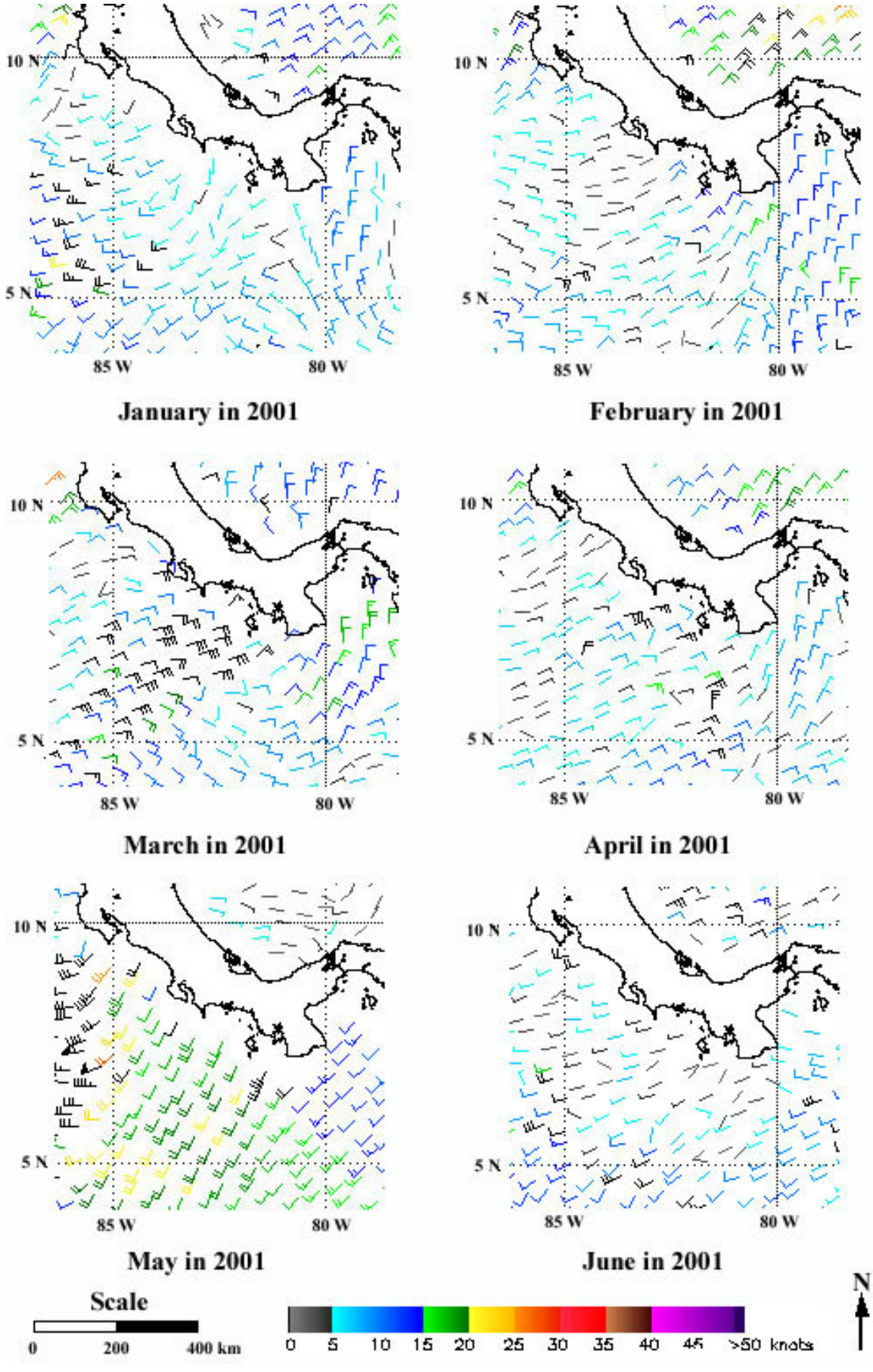

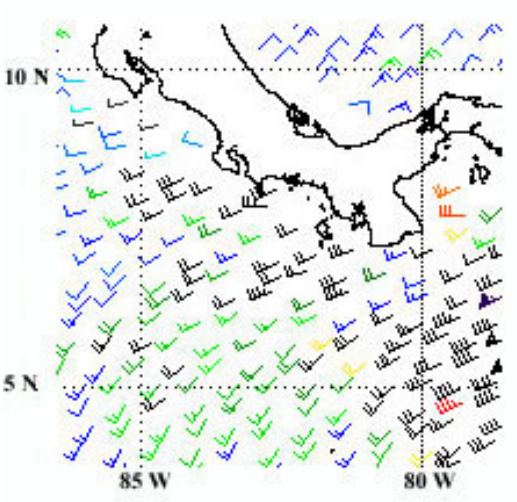

July in 2001

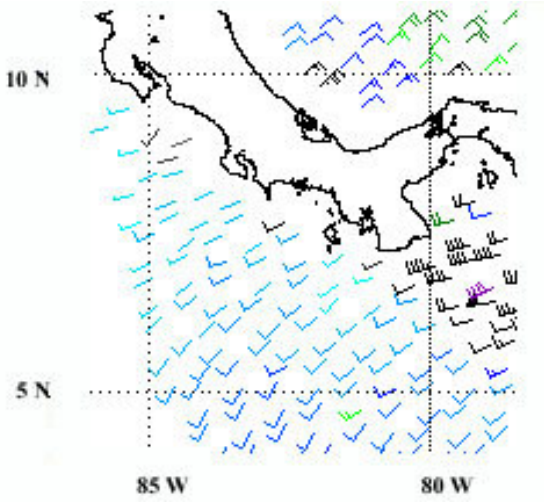

August in 2001

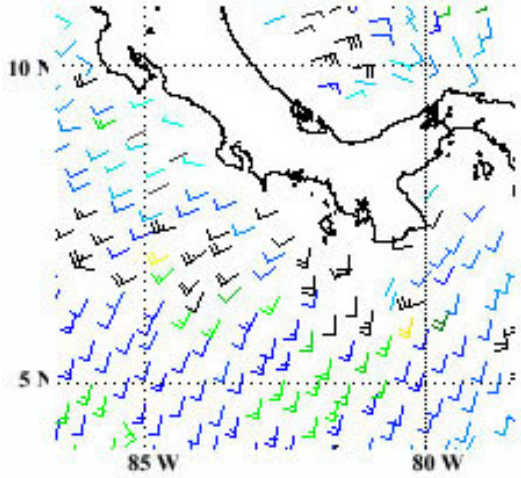

September in 2001

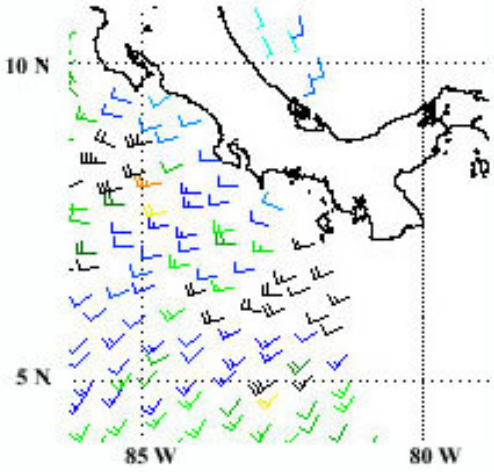

October in 2001

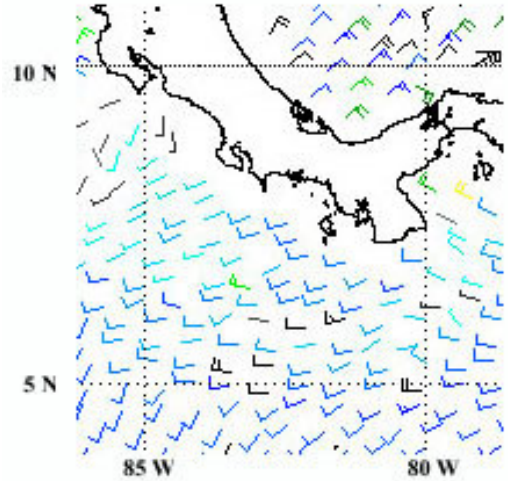

November in 2001

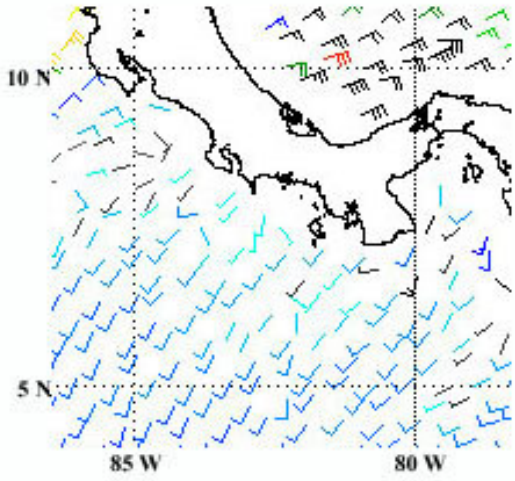

December in 2001

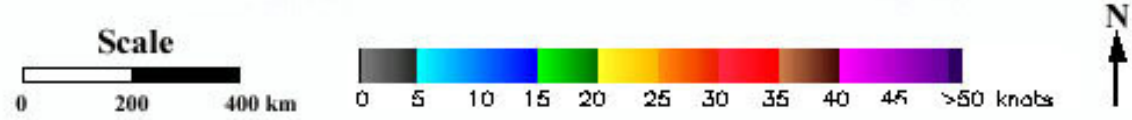

A6: Seawifs LAC database and quality

No.	Order name	Item ID	Begin date	End date	Vol. (kb)	Quality
1	LkD6611nMT1	S19980062100719_TOVS.OZONE	1/6/1998 21:00	1/7/1998 19:07	53	Missing line
2	LkD6611nMT1	S1998007174335.L1A_HCOS	1/7/1998 17:42	1/7/1998 17:49	23655	Missing line
3	LkD6611nMT1	S199800718_NCEP.MET	1/7/1998 18:00	1/7/1998 18:00	494	Missing line
4	LkD6611nMT1	S19980082100920_TOVS.OZONE	1/8/1998 21:00	1/9/1998 20:20	53	Excellent
5	LkD6611nMT1	S1998009173516.L1A_HCOS	1/9/1998 17:33	1/9/1998 17:41	27003	Excellent
6	LkD6611nMT1	S199800918_NCEP.MET	1/9/1998 18:00	1/9/1998 18:00	503	Excellent
7	BsvF61p4ce	S19980172101820_TOVS.OZONE	1/17/1998 21:00	1/18/1998 20:18	54	Excellent
8	BsvF61p4ce	S1998018174130.L1A_HCOS	1/18/1998 17:41	1/18/1998 17:48	29603	Excellent
9	BsvF61p4ce	S199801818_NCEP.MET	1/18/1998 18:00	1/18/1998 18:00	493	Excellent
10	BsvF61p4ce	S19980232102421_TOVS.OZONE	1/23/1998 21:00	1/24/1998 21:00	55	Miss navigation
11	BsvF61p4ce	S1998024171456.L1A_HCOS	1/24/1998 17:14	1/24/1998 17:21	24206	Miss navigation
12	BsvF61p4ce	S199802418_NCEP.MET	1/24/1998 18:00	1/24/1998 18:00	498	Miss navigation
13	EcvF61FvHc	S19980372103819_TOVS.OZONE	2/6/1998 21:00	2/7/1998 19:57	54	Cloud 90%
14	EcvF61FvHc	S1998038175016.L1A_HCOS	2/7/1998 17:48	2/7/1998 17:55	24080	Cloud 90%
15	EcvF61FvHc	S199803818_NCEP.MET	2/7/1998 18:00	2/7/1998 18:00	487	Cloud 90%
16	EcvF61FvHc	S19980392104019_TOVS.OZONE	2/8/1998 21:00	2/9/1998 19:36	54	Cloud 70%
17	EcvF61FvHc	S1998040173924.L1A_HCOS	2/9/1998 17:39	2/9/1998 17:45	22547	Cloud 70%
18	EcvF61FvHc	S199804018_NCEP.MET	2/9/1998 18:00	2/9/1998 18:00	490	Cloud 70%
19	EcvF61FvHc	S19980502105121_TOVS.OZONE	2/19/1998 21:00	2/20/1998 21:00	55	Miss navigation
20	EcvF61FvHc	S1998051173739.L1A_HCOS	2/20/1998 17:37	2/20/1998 17:45	18265	Miss navigation
21	EcvF61FvHc	S199805118_NCEP.MET	2/20/1998 18:00	2/20/1998 18:00	486	Miss navigation
22	GqD661uFgI1	S19980462104719_TOVS.OZONE	2/15/1998 21:00	2/16/1998 19:59	55	Heavy Missing line
23	GqD661uFgI1	S1998047175631.L1A_HCOS	2/16/1998 17:56	2/16/1998 18:03	14157	Heavy Missing line
24	GqD661uFgI1	S199804718_NCEP.MET	2/16/1998 18:00	2/16/1998 18:00	488	Heavy Missing line
25	GqD661uFgI1	S19980482104919_TOVS.OZONE	2/17/1998 21:00	2/18/1998 19:38	55	Missing line
26	GqD661uFgI1	S1998049174717.L1A_HCOS	2/18/1998 17:47	2/18/1998 17:53	16496	Missing line
27	GqD661uFgI1	S199804918_NCEP.MET	2/18/1998 18:00	2/18/1998 18:00	487	Missing line
28	GqD661uFgI1	S19980522105320_TOVS.OZONE	2/21/1998 21:00	2/22/1998 20:42	56	Cloud 10%
29	GqD661uFgI1	S1998053172830.L1A_HCOS	2/22/1998 17:28	2/22/1998 17:36	26436	Cloud 10%
30	GqD661uFgI1	S199805318_NCEP.MET	2/22/1998 18:00	2/22/1998 18:00	488	Cloud 10%
31	XxT66123GY1	S19980742107520_TOVS.OZONE	3/15/1998 21:00	3/16/1998 20:03	56	Excellent
32	XxT66123GY1	S1998075173033.L1A_HCOS	3/16/1998 17:30	3/16/1998 17:32	8156	Excellent
33	XxT66123GY1	S199807518_NCEP.MET	3/16/1998 18:00	3/16/1998 18:00	503	Excellent
34	XxT66123GY1	S19980762107721_TOVS.OZONE	3/17/1998 21:00	3/18/1998 21:00	56	Cloud 10%
35	XxT66123GY1	S1998077171755.L1A_HCOS	3/18/1998 17:17	3/18/1998 17:23	13636	Cloud 10%
36	XxT66123GY1	S199807718_NCEP.MET	3/18/1998 18:00	3/18/1998 18:00	492	Cloud 10%
37	XxT66123GY1	S19980832108419_TOVS.OZONE	3/24/1998 21:00	3/25/1998 19:53	57	Cloud 60%
38	XxT66123GY1	S1998084173439.L1A_HCOS	3/25/1998 17:34	3/25/1998 17:41	21721	Cloud 60%
39	XxT66123GY1	S199808418_NCEP.MET	3/25/1998 18:00	3/25/1998 18:00	494	Cloud 60%
40	83v661wTRd1	S19980942109521_TOVS.OZONE	4/4/1998 21:00	4/5/1998 21:00	55	Missing line
41	83v661wTRd1	S1998095173431.L1A_HCOS	4/5/1998 17:34	4/5/1998 17:38	12549	Missing line
42	83v661wTRd1	S199809518_NCEP.MET	4/5/1998 18:00	4/5/1998 18:00	490	Missing line
43	83v661wTRd1	S19981072110820_TOVS.OZONE	4/17/1998 21:00	4/18/1998 20:40	56	Excellent

44	83v661wTRd1	S1998108172150.L1A_HCOS	4/18/1998 17:21	4/18/1998 17:29	26140	Excellent
45	83v661wTRd1	S199810818_NCEP.MET	4/18/1998 18:00	4/18/1998 18:00	495	Excellent
46	C5v661Qdvd1	S19981382113919_TOVS.OZONE	5/18/1998 21:00	5/19/1998 19:51	57	Excellent
47	C5v661Qdvd1	S1998139172521.L1A_HCOS	5/19/1998 17:25	5/19/1998 17:35	35630	Excellent
48	C5v661Qdvd1	S199813918_NCEP.MET	5/19/1998 18:00	5/19/1998 18:00	500	Excellent
49	XZL861MnCo1	S19981522115320_TOVS.OZONE	6/1/1998 21:00	6/2/1998 20:38	55	Cloud 40%
50	XZL861MnCo1	S1998153175937.L1A_HCOS	6/2/1998 17:59	6/2/1998 18:08	34858	Cloud 40%
51	XZL861MnCo1	S199815318_NCEP.MET	6/2/1998 18:00	6/2/1998 18:00	494	Cloud 40%
52	XZL861MnCo1	S199817712_EPTOMS.OZONE	6/26/1998 0:00	6/26/1998 23:59	42	Excellent
53	XZL861MnCo1	S1998177174621.L1A_HCOS	6/26/1998 17:46	6/26/1998 17:56	31793	Excellent
54	XZL861MnCo1	S199817718_NCEP.MET	6/26/1998 18:00	6/26/1998 18:00	500	Excellent
55	VxWD611x22	S199819012_EPTOMS.OZONE	7/9/1998 0:00	7/9/1998 23:59	42	Cloud 30%
56	VxWD611x22	S1998190173245.L1A_HUPR	7/9/1998 17:32	7/9/1998 17:42	38492	Cloud 30%
57	VxWD611x22	S199819018_NCEP.MET	7/9/1998 18:00	7/9/1998 18:00	497	Cloud 30%
58	O4AE615hZ9	S199820112_EPTOMS.OZONE	7/20/1998 0:00	7/20/1998 23:59	42	Cloud 90%
59	O4AE615hZ9	S1998201172746.L1A_HNAV	7/20/1998 17:27	7/20/1998 17:39	45055	Cloud 90%
60	O4AE615hZ9	S199820118_NCEP.MET	7/20/1998 18:00	7/20/1998 18:00	494	Cloud 90%
61	PAAE614bc9	S199820312_EPTOMS.OZONE	7/22/1998 0:00	7/22/1998 23:59	41	Cloud 20%
62	PAAE614bc9	S1998203171819.L1A_HUSF	7/22/1998 17:18	7/22/1998 17:30	52315	Cloud 20%
63	PAAE614bc9	S199820318_NCEP.MET	7/22/1998 18:00	7/22/1998 18:00	489	Cloud 20%
64	21XD61ic32	S199822112_EPTOMS.OZONE	8/9/1998 0:00	8/9/1998 23:59	41	Cloud 20%
65	21XD61ic32	S1998221173618.L1A_HUPR	8/9/1998 17:36	8/9/1998 17:45	44319	Cloud 20%
66	21XD61ic32	S199822118_NCEP.MET	8/9/1998 18:00	8/9/1998 18:00	498	Cloud 20%
67	21XD61ic32	S199823612_EPTOMS.OZONE	8/24/1998 0:00	8/24/1998 23:59	43	Cloud 30%
68	21XD61ic32	S1998236171458.L1A_HUPR	8/24/1998 17:14	8/24/1998 17:26	48750	Cloud 30%
69	21XD61ic32	S199823618_NCEP.MET	8/24/1998 18:00	8/24/1998 18:00	490	Cloud 30%
70	6OBE61zMB8	S199825912_EPTOMS.OZONE	9/16/1998 0:00	9/16/1998 23:59	46	Cloud 20%, edge
71	6OBE61zMB8	S1998259175255.L1A_HUSF	9/16/1998 17:52	9/16/1998 18:05	50754	Cloud 20%, edge
72	6OBE61zMB8	S199825918_NCEP.MET	9/16/1998 18:00	9/16/1998 18:00	490	Cloud 20%, edge
73	RqBE61VK69	S199826512_EPTOMS.OZONE	9/22/1998 0:00	9/22/1998 23:59	47	Cloud 30%
74	RqBE61VK69	S1998265172447.L1A_HUSF	9/22/1998 17:24	9/22/1998 17:37	53004	Cloud 30%
75	RqBE61VK69	S199826518_NCEP.MET	9/22/1998 18:00	9/22/1998 18:00	492	Cloud 30%
76	RqBE61VK69	S199827012_EPTOMS.OZONE	9/27/1998 0:00	9/27/1998 23:59	47	Cloud 10%, edge
77	RqBE61VK69	S1998270175035.L1A_HUSF	9/27/1998 17:50	9/27/1998 18:03	51406	Cloud 10%, edge
78	RqBE61VK69	S199827018_NCEP.MET	9/27/1998 18:00	9/27/1998 18:00	487	Cloud 10%, edge
79	QjAE61vnj9	S199828812_EPTOMS.OZONE	10/15/1998 0:00	10/15/1998 23:59	47	Cloud 90%
80	QjAE61vnj9	S199828818_NCEP.MET	10/15/1998 18:00	10/15/1998 18:00	506	Cloud 90%
81	QjAE61vnj9	S1998288180729.L1A_HUMX	10/15/1998 18:07	10/15/1998 18:18	43570	Cloud 90%
82	RqBE61VK69	S199828912_EPTOMS.OZONE	10/16/1998 0:00	10/16/1998 23:59	47	Missing line
83	RqBE61VK69	S1998289171057.L1A_HUSF	10/16/1998 17:10	10/16/1998 17:23	49939	Missing line
84	RqBE61VK69	S199828918_NCEP.MET	10/16/1998 18:00	10/16/1998 18:00	490	Missing line
85	V5XD61OU52	S199832712_EPTOMS.OZONE	11/23/1998 0:00	11/23/1998 23:59	44	Cloud 60%
86	V5XD61OU52	S1998327173058.L1A_HUPR	11/23/1998 17:30	11/23/1998 17:41	47416	Cloud 60%
87	V5XD61OU52	S199832718_NCEP.MET	11/23/1998 18:00	11/23/1998 18:00	493	Cloud 60%
88	HuWD61Ed12	S199833112_EPTOMS.OZONE	11/27/1998 0:00	11/27/1998 23:59	44	Cloud 10%
89	HuWD61Ed12	S1998331171548.L1A_HVEN	11/27/1998 17:15	11/27/1998 17:23	33798	Cloud 10%
90	HuWD61Ed12	S199833118_NCEP.MET	11/27/1998 18:00	11/27/1998 18:00	487	Cloud 10%
91	ZgL8610Vxn1	S19983580035823_TOVS.OZONE	12/24/1998 0:00	12/24/1998 23:00	50	Cloud 5%

92	ZgL8610Vxn1	S1998358173530.L1A_HCOS	12/24/1998 17:35	12/24/1998 17:43	36522	Cloud 5%
93	ZgL8610Vxn1	S199835818_NCEP.MET	12/24/1998 18:00	12/24/1998 18:00	487	Cloud 5%
94	ZgL8610Vxn1	S19983630036323_TOVS.OZONE	12/29/1998 0:00	12/29/1998 23:00	50	Cloud 10%, edge
95	ZgL8610Vxn1	S199836318_NCEP.MET	12/29/1998 18:00	12/29/1998 18:00	483	Cloud 10%, edge
96	ZgL8610Vxn1	S1998363180053.L1A_HCOS	12/29/1998 18:00	12/29/1998 18:08	35168	Cloud 10%, edge
97	BUnG61XJ3v	S20000560005623_TOVS.OZONE	2/25/2000 0:00	2/25/2000 23:00	50	Cloud 10%
98	BUnG61XJ3v	S2000056175839.L1A_HCOS	2/25/2000 17:58	2/25/2000 18:05	16529	Cloud 10%
99	BUnG61XJ3v	S200005618_NCEP.MET	2/25/2000 18:00	2/25/2000 18:00	500	Cloud 10%
100	BUnG61XJ3v	S20000580005823_TOVS.OZONE	2/27/2000 0:00	2/27/2000 23:00	50	Cloud 30%
101	BUnG61XJ3v	S2000058174724.L1A_HCOS	2/27/2000 17:47	2/27/2000 17:53	17820	Cloud 30%
102	BUnG61XJ3v	S200005818_NCEP.MET	2/27/2000 18:00	2/27/2000 18:00	498	Cloud 30%
103	R2FV618lwV1	S2001025173258.L1A_HCOS	1/25/2001 17:32	1/25/2001 17:41	27133	
104	R2FV618lwV2	S2001030175110.L1A_HCOS	1/30/2001 17:51	1/30/2001 17:58	28505	
105	R2FV618lwV3	S200103018_NCEP.MET	1/30/2001 18:00	1/30/2001 18:00	513	
106	R2FV618lwV4	S20010300003023_TOVS.OZONE	1/30/2001 0:00	1/30/2001 23:00	51	
107	R2FV618lwV5	S200102518_NCEP.MET	1/25/2001 18:00	1/25/2001 18:00	486	
108	R2FV618lwV6	S20010250002523_TOVS.OZONE	1/25/2001 0:00	1/25/2001 23:00	50	

Description:

(1) Order name: SeaWIFS LAC file order name on internet
(2) Item ID: HCOS (HUPR, HUSF) extension file is HDF of image, TOVS.OZONE extension file is ozone on-line correction file, NCEP.MET extension file is Rayleigh scattering on-line correction file
(3) Begin date: SeaWIFS image scene first line scan time
(4) End date: SeaWIFS image scene last line scan time
(5) Vol. (kb): SeaWIFS image scene size
(6) Quality: cloud coverage, the gulf position on image, scanning line loss, navigation information (Latitude, longitude)

A 7: NOAA LAC image and SST calculation coefficients

No.	Start data	Start time	During sec	Satellite ID	Order file	Quality	B4 slope	B4 inter-cept	B5 slope	B5 inter-cept	T_4-T_5 > 0.7		
											a_0	b_0	c_0
1	1/3/91	19:24:37	665	N11	L1667968	Cloud 05	-0.1729	171.693	-0.18029	179.694	1.388	0.955	0.08
2	1/11/91	19:36:17	669	N11	L1651195	Cloud 10	-0.17286	171.654	-0.18027	179.679	1.388	0.955	0.08
3	1/12/91	19:24:54	673	N11	L1651194	Cloud 30	-0.17277	171.566	-0.18023	179.636	1.388	0.955	0.08
4	1/3/92	20:05:53	674	N11	L1651204	Cloud 20	-0.17789	176.652	-0.18192	181.332	1.682	0.971	0.081
5	1/9/92	20:36:23	672	N11	L1651200	Cloud 20	-0.17773	176.495	-0.18189	181.3	1.682	0.971	0.081
6	1/11/92	20:12:33	672	N11	L1651199	Cloud 10	-0.17777	176.528	-0.18195	181.36	1.682	0.971	0.081
7	1/2/93	21:05:17	462	N11	L1651212	Cloud 20	-0.17983	178.575	-0.18283	182.248	2.2	0.933	0.076
8	1/11/93	20:56:49	464	N11	L1651205	Cloud 0	-0.17952	178.273	-0.18267	182.096	2.2	0.933	0.076
9	1/5/94	21:51:20	464	N11	L1652838	Cloud 10	-0.18476	183.466	-0.18416	183.574	2.064	0.919	0.082
10	1/6/94	21:38:56	464	N11	L1652837	Cloud 20	-0.18464	183.357	-0.18412	183.532	2.064	0.919	0.082
11	1/7/94	21:26:32	464	N11	L1652836	Cloud 50	-0.18467	183.383	-0.18412	183.535	2.064	0.919	0.082
12	1/8/94	21:14:07	464	N11	L1652835	Cloud 10	-0.18469	183.406	-0.18411	183.529	2.064	0.919	0.082
13	1/29/95	19:15:29	480	N14	L1652841	Cloud 0	-0.16157	156.285	-0.17964	175.332	1.251	0.952	0.074
14	1/30/95	19:04:32	480	N14	L1652840	Cloud 20	-0.16161	156.321	-0.17964	175.338	1.251	0.952	0.074
15	12/29/95	19:29:15	465	N14	L1683738	Cloud 10	-0.16315	157.812	-0.18085	176.612	1.338	0.946	0.074
16	1/2/96	18:45:18	480	N14	L1653873	Edge	-0.16351	158.174	-0.18115	176.908	1.305	0.95	0.073
17	1/7/96	19:32:21	480	N14	L1653871	Cloud 10	-0.16315	157.815	-0.18087	176.627	1.305	0.95	0.073
18	1/11/96	18:47:21	457	N14	L1653868	Cloud10	-0.16335	158.021	-0.18102	176.778	1.305	0.95	0.073
19	12/31/96	19:50:38	660	N14	L1683741	Cloud 10	-0.16387	158.544	-0.18184	177.614	1.286	0.957	0.07
20	1/4/97	19:06:16	660	N14	L1653882	Cloud 10	-0.16401	158.675	-0.18196	177.725	1.265	0.957	0.071
21	1/10/97	19:41:49	720	N14	L1653878	Cloud 30	-0.16386	158.537	-0.18182	177.59	1.265	0.957	0.071
22	1/13/97	19:08:42	660	N14	L1653876	Cloud 20	-0.16388	158.559	-0.18182	177.585	1.265	0.957	0.071
23	1/1/98	20:04:39	345	N14	L1654401	Cloud 05	-0.16475	159.42	-0.18285	178.635	1.321	0.95	0.074
24	1/2/98	19:53:27	345	N14	L1654400	Cloud 05	-0.16476	159.431	-0.18286	178.639	1.321	0.95	0.074

25	1/3/98	19:42:18	347	N14	L1654399	Cloud 10	-0.16471	159.384	-0.18284	178.606	1.321	0.95	0.074
26	1/4/98	19:31:15	339	N14	L1654398	Cloud 10	-0.16477	159.436	-0.18287	178.651	1.321	0.95	0.074
27	1/12/98	19:43:50	343	N14	L1654394	Cloud 0	-0.16478	159.452	-0.1829	178.675	1.321	0.95	0.074
28	1/19/98	20:07:49	338	N14	L1679176	Cloud 10	-0.16459	159.267	-0.18279	178.566	1.321	0.95	0.074
29	2/16/98	20:00:45	346	N14	L1679178	Cloud 0	-0.16459	159.268	-0.18288	178.655	1.301	0.95	0.074
30	3/15/98	20:04:57	339	N14	L1679183	Cloud 10	-0.1647	159.375	-0.18302	178.795	1.338	0.949	0.074
31	3/16/98	19:53:40	345	N14	L1679184	Cloud 10	-0.16476	159.433	-0.18298	178.748	1.338	0.949	0.074
32	4/2/98	20:07:30	343	N14	L1718673	Fog 5	-0.16484	159.51	-0.18303	178.801	1.394	0.946	0.074
33	4/3/98	19:56:18	343	N14	L1718672	Cloud 20	-0.1647	159.374	-0.18291	178.685	1.394	0.946	0.074
34	4/5/98	19:33:51	346	N14	L1718670	Fog 10	-0.16479	159.462	-0.18301	178.786	1.394	0.946	0.074
35	5/9/98	20:01:06	346	N14	L1679192	Cloud 10	-0.16455	159.228	-0.18286	178.635	1.486	0.943	0.074
36	5/10/98	19:49:57	343	N14	L1679193	Cloud 10	-0.16465	159.331	-0.18301	178.783	1.486	0.943	0.074
37	6/6/98	19:53:11	342	N14	L1718678	Cloud 30	-0.16421	158.902	-0.18278	178.555	1.557	0.94	0.073
38	6/25/98	19:44:09	337	N14	L1718688	Fog 50	-0.16419	158.878	-0.18274	178.519	1.557	0.94	0.073
39	7/20/98	20:09:15	346	N14	L1679216	Cloud 25	-0.16442	159.097	-0.183	178.775	1.597	0.939	0.073
40	7/30/98	19:59:04	340	N14	L1718694	Fog 30	-0.1644	159.088	-0.18288	178.658	1.597	0.939	0.073
41	8/24/98	20:24:10	341	N14	L1718723	Cloud 60	-0.16485	159.523	-0.18314	178.907	1.557	0.942	0.072
42	10/9/98	20:16:21	343	N14	L1718740	Cloud 60	-0.16555	160.238	-0.18354	179.316	1.4	0.947	0.073
43	11/16/98	19:55:44	343	N14	L1679200	Cloud10	-0.16552	160.202	-0.18358	179.352	1.334	0.949	0.073
44	11/23/98	20:18:41	345	N14	L1718762	Cloud 20	-0.16544	160.121	-0.18368	179.454	1.334	0.949	0.073
45	12/20/98	20:19:32	341	N14	L1718768	Cloud 70	-0.16521	159.902	-0.18357	179.338	1.294	0.95	0.074
46	12/28/98	20:31:00	346	N14	L1718765	Cloud 50	-0.16518	159.859	-0.18355	179.318	1.294	0.95	0.074
47	1/7/99	20:19:53	340	N14	L1654407	Cloud 30	-0.16531	160.002	-0.18358	179.349	1.36	0.95	0.072
48	1/9/99	19:57:10	344	N14	L1654405	Edge	-0.16525	159.943	-0.18364	179.403	1.36	0.95	0.072
49	1/15/99	20:31:10	347	N14	L1654410	Cloud 10	-0.16524	159.93	-0.1836	179.376	1.36	0.95	0.072
50	1/11/00	21:22:03	339	N14	L1654413	Cloud 30	-0.16568	160.39	-0.1842	179.984	1.36	0.95	0.072
51	1/12/00	21:10:30	334	N14	L1654412	Cloud 20	-0.16564	160.357	-0.18422	180	1.36	0.95	0.072
52	1/5/01	21:56:51	357	N14	L1654423	Cloud 40	-0.16572	160.463	-0.18458	180.379	1.36	0.95	0.072
53	1/13/01	22:02:40	354	N14	L1654420	Cloud 50	-0.16566	160.39	-0.18447	180.258	1.36	0.95	0.072
54	1/15/01	21:38:42	350	N14	L1654419	Cloud 20	-0.16565	160.382	-0.18444	180.232	1.36	0.95	0.072

Description:

(1) Start data: NOAA image acquisition start date
(2) Start time: NOAA image acquisition start time
(3) During sec: the duration of NOAA image overpass the study area
(4) Satellite ID: NOAA satellite series number
(5) Order file: NOAA LAC file name
(6) Quality: corresponding to the cloud coverage, fog coverage, position of study area on image
(7) B4 slope: NOAA AVHRR band 4 slope for radiance calculation
(8) B4 intercept: NOAA AVHRR band 4 intercept for radiance calculation
(9) B5 slope: NOAA AVHRR band 5 slope for radiance calculation
(10) B5 intercept: NOAA AVHRR band 5 intercept for radiance calculation
(11) a_c, b_c, c_c, d_c : the coefficients of SST calculation as T_4-$T_5 > 0.7$, to eliminate the impact of water vapour in t
(12) a_1, b_1, c_1, d_1: the coefficients of SST calculation when T_4-$T_5 < 0.7$, to eliminate the impact of water vapour i
(13) T guess: SST in *situ* buoy measurement and interpolation